12-2014

Structure, Aboveground Biomass, and Soil Characterization of Avicennia marina in Eastern Mangrove Lagoon National Park, Abu Dhabi

Tareefa Alsumaiti
University of Arkansas, Fayetteville

Structure, Aboveground Biomass, and Soil Characterization of *Avicennia marina* in Eastern Mangrove Lagoon National Park, Abu Dhabi

Structure, Aboveground Biomass, and Soil Characterization of *Avicennia marina* in Eastern Mangrove Lagoon National Park, Abu Dhabi

A dissertation submitted in partial fulfillment
of the requirements for the degree of
Doctor of Philosophy in Environmental Dynamics

by

Tareefa Saad Sultan Alsumaiti
United Arab Emirates University
Bachelor of Geography, 2008
Arizona State University
Master of Advanced Study in Geographic Information Systems, 2010

December 2014
University of Arkansas

This dissertation is approved for recommendation to the Graduate Council.

Dr. Jason A. Tullis
Dissertation Director

Dr. Thomas R. Paradise
Committee Member

Dr. Fred Limp
Committee Member

Abstract

Mangrove forests are national treasures of the United Arab Emirates (UAE) and other arid countries with limited forested areas. Mangroves form a crucial part of the coastal ecosystem and provide numerous benefits to society, economy, and especially the environment. Mangrove trees, specifically *Avicennia marina,* are studied in their native habitat in order to characterize their population structure, aboveground biomass, and soil properties. This study focused on Eastern Mangrove Lagoon National Park in Abu Dhabi, which was the first mangrove protected area to be designated in UAE. *In situ* measurements were collected to estimate *Avicennia marina* status, mortality rate (%), height (m), crown spread (m), stem number, diameter at breast height (cm), basal area (m), and aboveground biomass (t ha^{-1}). Small-footprint aerial light detection and ranging (LIDAR) data acquired by UAE were processed to characterize mangrove canopy height and aboveground biomass density. This included extraction of LIDAR-derived height percentile statistics, segmentation of the forest into structurally homogenous units, and development of regression relationships between *in situ* reference and remote sensing data using a machine learning approach. An *in situ* soil survey was conducted to examine the soils' physical and chemical properties, fertility status, and organic matter. The data of soil survey were used to create soil maps to evaluate key characteristics of soils, and their influence on *Avicennia marina* in Eastern Mangrove Lagoon National Park. The results of this study provide new insights into *Avicennia marina* canopy population, structure, aboveground biomass, and soil properties in Abu Dhabi, as data in such arid environments is lacking. This valuable information can help in managing and preserving this unique ecosystem.

Acknowledgments

Firstly, I would like to sincerely thank my advisor Dr. Jason Tullis for his guidance, advice and insight during my time in graduate school at University of Arkansas. Appreciation is also extended to my advising committee, Dr. Thomas Paradise and Dr. Fred Limp. I would also like to thank Dr. Shabbir Shahid at the Dubai based International Center of Biosaline Agriculture (ICBA) for his guidance and advice throughout the soil research work, Dr. Henda Mahmoudi and Mr. Kaleem ul Hassan Naeem for their assistance in analyzing the soil samples at the Central Analytical Laboratory of ICBA. I'm grateful for the National Teaching Assistants Office at UAE University for their financial support to cover the cost of soil analysis tests, especially Dr. Mohamed Al-Hosani. I would further like to thank the Environment Information Management Sector and Marine Biodiversity Sector at the Environment Agency in Abu Dhabi (EAD) for their assistance in providing water transportation and facilitating both forest and soil surveys. I extend my thanks to General Enterprises Co. Engineering Division (GECO) in Abu Dhabi for providing GPS receivers and assistance in collecting sampling plots' locations. I'm especially grateful for Mr. Yousef Al-Marzouqi from Bayanat Company and Mr. Jorge Merrit from Abu Dhabi Systems and Information Company (ADSIC) for their assistance in providing remote sensing data including LIDAR and WorldView-2 satellite images of the study area. I extend my sincere thanks to Mr. Khalfan Al-Meherbi from EAD, Mr. Zia Rehman from GECO, and Mr. Abdulla Al-Marzouqi from ADSIC for their great assistance in gathering *in situ* data. Finally, I would like to thank my friend and colleague Bowei Xue for his time and effort in helping with LIDAR processing and biomass modeling.

Dedication

I dedicate this doctoral dissertation to my parents, Saad Alsumaiti and Aisha Aljumaa for their endless love, prayers, sacrifices, and encouragement throughout my life. I also dedicate this dissertation to my husband Abdulla Almarzouqi for his love, support, and motivation.

Table of Contents

I. Introduction

Mangroves are one of various types of littoral trees that mostly inhabit sheltered coastlines within the intertidal zone of tropical and subtropical regions near the equator. Mangrove forests are exceedingly important in forming a crucial part of coastal ecosystems, and are among the most productive ecosystems worldwide (Food and Agricultural Organization, 2007). They provide numerous benefits to the environment and to society, from sources of food for animals and human beings to rich natural habitat and safe breeding grounds for marine and terrestrial animals. Mangroves prevent coastline erosion, provide a barrier to storm surge, and control water and air pollution. Fauna and flora associated with the mangroves foster tourism as well as recreational, educational, and research opportunities (Ashton & Macintosh, 2002; Aspinall, 2001; Marshall, 1994).

A. Mangroves Worldwide

Mangrove forests can be found along the shoreline of over 118 countries and territories (Giri et. al., 2011). This global distribution of mangrove forests is determined by several factors. For instance, climatic factors such as moisture and temperature play a major role in the distribution of these forests. However, coastal processes like coastal currents, tidal mixing, tidal fluctuation, wave energy, salinity, and sedimentation influences the distribution of mangroves in some regions. This occurs through affecting propagate dispersion (McLeod & Salm, 2006). Reflecting on a latitudinal perspective, it is clear that mangroves are dispersed throughout the subtropics and tropics. Through this distribution, mangroves reach their utmost growth between 25°00' S and 25°00' N (Gilman et. al., 2008). Estimations of global mangrove area vary from 12 million hectares to 20 million hectares. However, recent estimates by Food and Agriculture

Organization (FAO) of the United Nation (2007) suggest that the overall global mangrove forest coverage is approximately 15.2 million hectares. According to FAO's study entitled The World's Mangroves 1980-2005, "the world has lost around 3.6 million hectares of mangroves since 1980, equivalent to an alarming 20 percent loss of total mangrove area" (FAO, 2007).

With biodiversity threatened in many habitats worldwide, the mangroves are threatened by both anthropogenic and natural forces. Mangroves once occupied three-quarters of tropical and subtropical coastlines throughout the world. However, only about one-half of mangrove forests remain today (Upadhyay et. al., 2002). It is estimated that mangrove ecosystems are reduced by 2% annually due to eutrophication, toxic-chemical pollution, agricultural expansion, and adverse water quality and quantity (Valiela et. al., 2001). Furthermore, climate change poses additional threats to mangrove ecosystems. According to Houghton et al. (2001), human reclamation of wetland will represent a 37% loss of global wetlands by 2080. This does not include the impacts of the sea level rising, which has boosted this percentage an additional 25%. At this rate, Houghton estimates that over 60% of the total wetlands in the world will be lost by 2080.

Mangroves are an important resource for carbon sequestration, and have been a topic of discussion in world forums concerned with global climate change especially in regards to Reduced Emissions from Forest Degradation and Deforestation Plus ($REDD^{+}$) (McLeod & Salm, 2006). The forests absorb carbon and although they form only 3% of the earth's forest cover, their per-area capacity to absorb and store carbon is greater than that of tropical forests (Alongi, 2002; Lucas et al, 2007). Furthermore, the quantity of mangrove carbon transferred into water bodies from fallen litter, such as leaves, is immense. Globally, more than 10% of the total organic carbon integrated into oceans originates from mangroves (Dittmar et al, 2006).

Having a strong knowledge of the various mangroves' physical and biological distinguishing properties such as height, trunk diameter, crown spread, and biomass is important for proper coordination, preservation, conservation, and change monitoring (Wannasiri et al, 2013; White et al., 2013). For example, by establishing the weight of the aboveground and belowground biomass and subsequently the carbon stored in mangrove forests, approximation of carbon removal, release into the atmosphere and retention in the ecosystem can be estimated. Determining the size and extent of mangrove forests, the structure and biomass, is of significance in resolving issues concerning change of climate and adaptation to a particular ecosystem or to anthropogenic forces (Bombelli et. al., 2009).

B. Mangrove Forest Observation

Mangrove physical and biological characteristics of the forest may be assembled via *in situ* observation. A series of sampling plots are typically established and then the characteristics of each tree are determined manually, thus requiring considerable effort for monitoring over space and time. Given the resource-intensive nature of *in situ* data collection, this approach by itself may not deliver realistic results when the area of study is extensive. Furthermore, navigation in mangrove forests is particularly difficult due to the presence of mud, large root-like mangrove structures on the marshy ground, and the rise and fall of tidal waters. It is therefore unpractical to monitor the forests using *in situ* data alone (Aschbacher et al., 1995; Ramsey and Jensen, 1996; Laba et al., 1997; Rasolofoharinoro et al., 1998). Remote sensing and other geospatial disciplines have been extensively applied in a plethora of access-prohibitive environmental scenarios.

In recent years, improved techniques have been developed to map structural characteristics of forests such as height, density, and biomass. These are most commonly

executed in two distinct remote sensing methodologies. First, there is the use of optical data and subsequent estimates of spatially-averaged biomass values. Optical remote sensing typically makes use of visible and near-infrared reflectance from the surface of the earth to produce images. This lays a foundation for contemporary global-scale vegetation monitoring through numerous sensor systems such as Landsat, ASTER, IKONOS, MODIS, WorldView-3 and others (Jensen, 2005). Such tools find wide application in research aimed at linking forest biomass measurements from *in situ* data to those obtained from aerial or satellite images. Major obstacles include persistent cloud cover and the presence of ubiquitous sun shadows. Furthermore, most satellite images obtained through optical sensors do not provide important vegetation characteristics such as canopy height. While this information can be derived via stereo analysis of overlapping imagery, the stereo imagery may be costly, have a limited spatial coverage, and demand a huge allocation of time to analyze (Lucas et al., 2000; Geotz et al., 2009).

In a second remote sensing methodology, researchers may determine values of characteristics such as volume or height using laser-based airborne light detection and ranging or LIDAR (Fatoyinbo & Armstrong, 2010) which captures a large number of unevenly arranged x, y and z positions within the volume of the forest structure (NOAA Coastal Services Center, 2012). The sensor in a LIDAR system continuously records the amplitude of the pulse registered as initiated by reflectance from laser targets of the forest canopy. Through this system, the vertical structure of vegetation can be estimated in remarkable detail, thus providing a clear advantage compared with optical imagery. Airborne LIDAR systems are capable of detecting objects with a horizontal accuracy of few meters and a vertical accuracy of a few centimeters (Simard et al., 2006; Aguilar & Mills, 2008). The structural form of mangrove forests (in terms of height and density) may be extracted from LIDAR and is very applicable in the derivation of

forest biomass (Wannasiri et al, 2013). However, due to costs of data collection and processing, LIDAR systems are often limited to measurements across only a small portion of forest area; thus, its use may be confined to calibrating datasets collected via other technologies (Fatoyinbo & Armstrong, 2010).

Both optical (passive) remote sensing data and LIDAR (active) data find useful application in research involving coastal ecosystem, such as mangrove forests, that are difficult to access and analyze (Proisy et al, 2009; Gillespie et al, 2004). Various datasets and techniques obtained from multiple remote sensing approaches can be used with *in situ* measurements to form a convenient spatial analysis and mapping framework to map and measure the biophysical characteristics of the mangrove forests discussed above (Chadwick, 2011).

Researchers who measure and map the biophysical characteristics of the mangrove forests observe that forcing functions such as tides and stressors such as hurricanes, droughts, and accumulation of salt are important factors that influence the structural features of a mangrove forest. Notably, the effect of these factors varies widely across geographic regions, and consequently, the structural characteristics of mangrove forests show a wide variation both regionally and locally (English et al., 1997; Tam & Wong, 1998). According to Cintron et al. (1985), the local morphology of a region coupled with the associated environmental factors such as tidal range and climate conditions is the element that influences the growth and distribution of mangrove trees. In addition, soil characteristics including soil texture, salinity, nutrient availability, and organic matter have a direct influence on mangrove structure, and distribution (McKee, 1993; Feller et al., 2002). Over any geographical region, significant variations in environmental factors are often evident. These variations are the key elements that cause

regional and local disparities with regard to the structural or physical characteristics of mangrove stands.

In their report, Zenner and Hibbs (2000) argue that forest structure and biomass are the most important factors in the analysis and management of any forest ecosystem. Indeed, structural characteristics have proven to be fundamental elements in defining and examining spatial heterogeneity as well as temporal dynamics of understory vegetation. In relation to this, a clear understanding of such descriptive parameters as tree height and trunk diameter is crucial in studying structural attributes. In particular, diameter-at-breast height, which is denoted by DBH, is closely associated with mangrove stand development. Therefore, such parameters as crown spread, basal area, and the biomass of a mangrove can be estimated (White et al., 2013). Comley and McGuinness (2005) observe that an accurate estimate of biomass is of particular importance in describing the present state of mangrove forests, in addition to predicting the effects of change.

By measuring several structural parameters of individual trees in a forest, allometric relationships can be developed and utilized to estimate other parameters that are much difficult to measure *in situ*. Several research projects have developed allometric relationships to estimate trees volume and aboveground biomass based on DBH values collected *in situ* (Dahle & Grabosky, 2009; Parvaresh et al., 2012). Still, no allometric equations have been developed for *Avicennia marina* trees in Abu Dhabi, United Arab Emirates (UAE).

C. Mangrove Forests in Abu Dhabi, UAE

While mangrove forests are natural resources of global importance, they are of special significance to UAE where they are the only coastal forests that link land and sea. In UAE, Mangrove forests cover thousands of hectares of land along the shoreline. The forests occur

naturally along several eastern coastal areas and islands in the country. The UAE eastern coast stretches for more than 400 miles along the southern shore of the Arabian Gulf (Al-Habshi et. al., 2007). Abu Dhabi city is located at approximately 23°00' north latitude and 52°00' east longitude. More than 70% of the Mangrove forests in UAE are present along the near shore islands, such as Futaisi, Saadiyat, Al Reem, Bisrat Fahid, Sas Al Nakhal and the islands of Khor Faridah, and lagoons of Abu Dhabi covering thousands of hectares (Tamaei, 1999). Even though there are more than fifty different species of mangroves found worldwide, the only mangrove species that grow widely in Abu Dhabi are the *Avicennia marina* or grey mangroves (Figure1). *Avicennia marina* trees are named after the great Muslim philosopher Ibn Sina (Avicennia) 981-1037 CE, and they are locally referred to as Al-Qurm (Boer and Aspinall, 2009). However, historical records show that one other mangrove species, *Rhizopohra Mucronata*, once grew in Abu Dhabi. This species has become extinct in the entire Arabian Gulf region due to wood cutting and over-exploitation (Vistro, 2010).

Major changes have occurred in the growth and spatial distribution of mangrove forests in Abu Dhabi in the last 50 years due to increased anthropogenic activities which jeopardize the integrity of mangrove forests. Many mangrove swamps are now lost due to recent intense urbanization and industrialization projects (McKee, 2004; Al Ashram, 2008; Howari et al., 2009). Besides human activities that threaten mangrove ecosystems in Abu Dhabi, natural threats such as climate change have the capacity for significant destructive effects on the growth of mangroves and their environment. The primary climate factors that affect mangrove forests include changes in sea level, temperature, precipitation, CO_2 concentration, and frequency of storms and hurricanes (Gilman et al., 2008).

Figure 1. *Avicennia marina* on the coast of Abu Dhabi, United Arab Emirates.

Evaluating the spatial distribution and areal extent of mangrove forests in coastal areas has been and continues to be a research priority in UAE due to the significant reduction of mangrove forests as a result of human and natural disturbances. Optical remote sensing and geographic information system (GIS) technology are being utilized to establish spatial mangrove patterns and to detect changes in the forests' growth and extent over time (Yagoub & Kolan, 2006). However, studies that estimate forest structural and biophysical parameters have been lacking for mangrove forests in Abu Dhabi and UAE. Such studies can estimate parameters related to tree height, tree density, basal area, biomass, diameter at breast height (DBH), age, and their distributions within forests at the landscape level in order to obtain a better understanding of mangrove forest to effectively study, manage, conserve, sustain, and enhance these valuable coastal ecosystems.

D. The Ecological Characteristics of *Avicennia marina* in Abu Dhabi, UAE

Avicennia marina is one of the most habitat-tolerant mangrove species (Boer & Aspinall, 2009). It is capable of surviving the harsh arid climate conditions and high saline seawater environment of Abu Dhbai. *Avicennia marina* trees have mechanisms which help in salt uptake and extraction of water molecules thereby excreting the salt through the leaves (Howari et al., 2009). The trees have short and branchy stems and thick, salty-tasting leaves with pencil-like roots which develop above the soil surface. The *Avicennia marina* root system, which allows the tree to absorb oxygen, is generally shallow. Typically, the aerial roots grow up to a height of 30 cm, and to a diameter of 1 cm.

Furthermore, the grey mangrove possesses other ecological characteristics that improve its ability to populate the Abu Dhabi region. From early life stages, mangroves are adaptable. They can adjust to new conditions as well as propagate and survive in changing water environments. Every mangrove yields buoyant seeds which can float and spread in water. Different from land plants, many mangrove species are viviparous and their seeds can germinate while attached to the parent plant. Their healthy seedlings can drop into water once mature after they have germinated and grown within or outside the fruit. Then, their journey to find a suitable flourishing location begins. Water currents transport the seedlings over long distances. Desiccation is not a problem to the propagules as they can remain dormant for a couple of months to a year, till they can find a suitable environment. In order for the propagule to take root, its density must lessen so it can float vertically instead of horizontally, improving its ability to lodge within the mud or roots. If it fails to take root in one specific area, it changes its density again and floats away to continue searching for a more suitable home (Environmental Atlas of

Abu Dhabi Emirate, 2011). These ecological characteristics allow *Avicennia Marina* to survive the harsh arid environment of Abu Dhabi.

E. Study Objectives

The primary objective of this study is to characterize mangrove population and biophysical parameters specific to Eastern Mangrove Lagoon National Park in Abu Dhabi (a mangrove treasure to UAE) using both *in situ* measurements and remote sensing. *In situ* measurements are used to estimate *Avicennia marina* status, height, crown spread, stem number, DBH, basal area, mortality rate, and aboveground biomass within the sampling plots as well as indicating the relationships among tree attributes. On the other hand, small-footprint aerial LIDAR observations are used to estimate canopy height and aboveground biomass density across the whole study area. Using LIDAR-derived height percentile statistics and object-based segmentation of the forest into structurally homogenous units, the study develops regression relationships between remote sensor and *in situ* reference data using a machine learning approach. A secondary objective of the study is to better understand key characteristics, and influence on mangroves, of soils in Eastern Mangrove Lagoon National Park. An *in situ* soil survey examines the soils' physical and chemical properties, fertility (nutrient) status, and organic matter. The results of the soil survey are used to create soil maps specific to the study area so that soil variation effects on the distribution of the mangrove trees can be evaluated.

F. Research Questions and Hypotheses

This study aims to provide a better understanding Abu Dhabi's mangrove population structure, aboveground biomass, and soil by answering the following three questions:

1. What are the structural characteristics and the current status of mangrove vegetation in Eastern Mangrove Lagoon National Park?
2. How applicable is the only available airborne LIDAR (collected in January 2013) for characterization of mangrove forests, including canopy height and stand biomass?
3. What are the key characteristics of mangrove forest soils, and how do soil properties influence the spatial distribution of mangrove trees?

The above questions are addressed by the following research hypotheses:

1. There are strong positive correlations among mangrove structural parameters including DBH, basal area, height, crown spread, and above ground biomass.
2. The available airborne LIDAR data can derive high resolution 3D map products of mangrove canopy height.
3. Image segmentation of LIDAR canopy height metrics can be used in a machine learning environment to accurately estimate and map aboveground biomass density of *Avicennia marina*.
4. Variations in soil characteristics play a major role in the spatial distribution of *Avicennia marina*.
5. The soil conditions of the study area are ideal to the growth of mangrove trees, and no urgent actions are needed to increase soil fertility.

G. Study Site

The study site is found in Eastern Mangrove Lagoon National Park, Abu Dhabi, UAE. The main vegetation cover in the study area includes *Avicennia marina* (grey mangrove) and salt marshes dominant by *Arthrocnemum macrostachyum*. The study area has warm arid climate conditions, a high saline seawater environment, nearly flat topography, and several interconnected tidal creeks through the forest. The mangrove stand in the forest is usually inundated by tides twice daily. The soil surface is completely covered by sea water during high tide. The 1.7 km² study area is contained within a rectangle defined by latitude and longitude of an upper left hand corner at 24°27'20"N and 54°25'18"E and a lower right hand corner at 24°26'52"N and 54°26'24"E (Figure 2).

Figure 2. The location of the study area (red box) within Eastern Mangrove Lagoon National Park (green polygon) in Abu Dhabi, UAE.

H. Study Value

This study provides valuable information about the *Avicennia marina* forest canopy population and structure in Abu Dhabi since data about mangrove structural properties in such arid environments has been lacking. The study also utilizes *in situ* data to estimate mangroves' aboveground biomass, which is one of the most important measures of forest ecosystem structure and function. A better understanding of *Avicennia marina* forest structure and growth characteristics is important for the management of this unique ecosystem. Furthermore, the results of this study are useful for evaluating the capabilities of available LIDAR remote sensing to estimate aboveground biomass of mangrove forests in Abu Dhabi. Additionally, the results will indicate the possibilities and limitations of mangrove attribute acquisition from existing LIDAR by comparing the attribute values with *in situ* measurements. This study further supports evaluation of soil variation effects on the spatial distribution of the mangrove trees by both understanding the key characteristics of soils in Eastern Mangrove Lagoon National Park in Abu Dhabi and by creating soil maps of the physical and chemical properties, fertility status, and organic matter specific to the study area.

This research is critical for understanding and therefore preserving the valuable mangroves of Abu Dhabi. The analysis of the airborne LIDAR generates new high spatial resolution geodata that characterize the structure and aboveground biomass of mangroves in Eastern Mangrove Lagoon National Park. The aboveground biomass estimation can be used in future research related to climate change concerns. This research also develops a 3D structural characterization of mangroves in their native habitat throughout the study area. Incorporation of these results will lead to continued studies of UAE's mangroves and will contribute to ongoing research opportunities for monitoring and protecting this national treasure.

II. An Assessment of *Avicennia marina* Forest Structure and Aboveground Biomass in Eastern Mangrove Lagoon National Park, Abu Dhabi

A. Summary

Remnant *Avicennia marina* forests are national treasures of UAE and other arid countries with limited natural forest resources. In order to better understand their current status, this study reports on the population structure and aboveground biomass of *Avicennia marina* in Eastern Mangrove Lagoon National Park, Abu Dhabi. *In situ* data include twenty randomly established circular ground plots and measurements recorded from 2,216 trees. Direct measurements include tree status, stem number, diameter at breast height (DBH), and height; while derived measurements include density, basal area, average crown spread, plot height, mortality rate, and aboveground biomass. The results show a significant variation of mangrove tree density in the sampling plots. Total basal area in all plots is 20.58 m^2 ha^{-1}, while the basal area mortality rate is very low (0.2%) with only 5 dead trees in all sites. Overall this indicates that the mangroves in Abu Dhabi are healthy. The percentage of seedlings and saplings is 51%, while the percentage of adult trees is 49%. The frequency distribution for trees height is positively skewed, showing the existence of many small and few large individuals. The mean height of trees with DBH > 5 cm is 2.47 ± 0.02 m, whereas the mean height of all trees is 1.97 ± 0.02 m. The distribution of the tree-diameter and average crown spread indicates a reverse-J-shaped pattern which is typical of naturally regenerating forest with a high population of saplings and young trees. The mean DBH of the trees is only 5.38 ± 0.14 cm and their average crown spread is 0.79 ± 0.02 m. Additionally, aboveground biomass, calculated from DBH measurements, in all sites is 265.66 t ha^{-1}. Linear regression analysis reveals relationships among several variables including height,

DBH, basal area, crown spread, and aboveground biomass. Both Pearson correlation coefficients (ranging from 0.518 to 0.981) and coefficients of determination (ranging from 0.268 to 0.963) indicate strong, positive correlations between the variables. A high number of regeneration trees can be a result of land-protection policies by authorities. However, more studies should be conducted to monitor changes in the floristic structure of *Avicennia marina* over time.

B. Introduction

Mangrove forests are among the most productive coastal ecosystems and they are associated with various environmental benefits (FAO, 2007). The importance of mangroves has resulted in increased research attention from different perspectives (Inoue et al., 2011; Fry & Cormier, 2011). Early research studies on mangroves were mostly aimed at understanding mangroves and their uses in coastal regions (Hutchings & Saenger, 1987; Kogo, 1988; Blasco et. al., 2001). Human population has been on the increase, which has had major implications for the ecosystem. Therefore, several research studies on mangroves have focused on the interaction between human population and mangrove forests. Increased human activities in the last decades and global warming arising from these activities pose major threats on mangroves and their environment, which puts mangroves at a risk of extinction (FAO, 2007). Consequently, most recent research studies have concentrated on management of mangrove ecosystems, efforts aimed at rehabilitating mangroves, while other studies have aimed at contributing towards mangroves' sustainability (Chong, 2006; Powel & Osbeck, 2010).

Although there are many papers that have been published on the various aspects of mangrove ecosystems, only a few of them have sufficiently explored the mangrove forest population structure, which is a vital element in studies concerning the ecological dynamics of mangrove forests (Cintron et al. 1985; English et al. 1997; Fromard et al., 1998; Aheto et al.,

2011). In fact, structural characteristics such a tree height, diameter at breast height (DBH), basal area, crown spread, and aboveground biomass (AGB) are extremely important to assess the status and stand development of the forest. Few researchers have developed allometric relations to estimate structural parameters that are difficult to measure *in situ* such as trees aboveground biomass and volume based on other parameters such as height and DBH (Dahle & Grabosky, 2009; Parvaresh et al., 2012).

Such studies about mangrove population structure are necessary since mangrove conservation and management efforts highly depend on a deep understanding of the dynamics of mangrove vegetation structure. A clear understanding of the origin and the ecological dynamics of mangrove vegetation in a given area is vital before embarking on protection and conservation efforts such as afforestation and re-afforestation. Therefore, the main objective of this work is to assess mangrove population and vegetation structure specific to Eastern Mangrove Lagoon National Park, Abu Dhabi (a mangrove treasure to UAE). The only mangrove species that grows widely in the park is the *Avicennia marina*, because it is the only species capable of surviving the harsh arid climate conditions and high saline seawater environment of Abu Dhabi (Boer & Aspinall, 2009). Data about mangrove structural properties in such environment has been lacking; therefore, the study will provide valuable information about the forest canopy status, mortality rate, height, density, crown spread, stem number, and DBH. Moreover, it will utilize *in situ* data to estimate aboveground biomass and basal area of mangrove forest. A better understanding of *Avicennia marina* forest structure and growth characteristics of this species is important for the management of this unique ecosystem.

C. Materials and Methods

1. Plot Design and *In situ* Survey

The first step in studying forest structural properties is to establish sampling plots. An assessment of the available literature indicates that sizes of the sampling plots range from 50 m² (8 m diameter) to 2500 m² (56 m diameter) (Naesset & Okland, 2002; Thomas et al., 2008). However, these studies do not explain the choice of plot size. Although there is no universal optimum plot size for studying forest attributes (Frazer et al. 2011; Gobakken & Næsset, 2009), White et al. (2013) recommended that a minimum ground plot should have an area of 200 m² and a radius of 8 m². They recommended such plot size to minimize edge effects and planimetric co-registration errors in modeled outcomes associated with ground data that does not capture a full range of the forest structural variability as captured by LIDAR data. Furthermore, this plot size increases both the efficiency of sampling and the accuracy of target and explanatory variables.

In the present study, *in situ* sampling was conducted in the study area from January to April, 2014. Fixed area circular plots with an area of 154 m² (14 m diameter) were established. Circular plots were selected and not square plots because it is easier to establish them *in situ*. This ease of establishment emanates from the fact that the centers of circular plots are registered unlike those of square plots that have four corners. Besides, this research opts for circular plots because they have 13% less perimeter compared to square plots of an equal area (White et al., 2013). This difference in perimeter is helpful in eliminating the negative impact of edge effects such as the error in metric calculation (Wulder et al., 2012).

It is recommended to have a minimum of one sampling plot per every 4 hectares according to Natural Resource Information System (NRIS) of the United States Department of Agriculture (USDA). Ideally, because the study area covers 170 hectares (1.7 km²), 42 plots

should be established. However, only 20 plots were established due to several factors: 1) working in mangrove swamps is challenging due to the presence of mud, large root-like mangrove structures on the marshy ground, and the rise and fall of tidal waters; 2) a large portion of the study area consists of very dense forest that is impractical to walk through to collect tree attributes; and 3) dangerously high temperatures during the summer limit the collection of tree attributes to the winter season. The 20 plots covered a clear range of forest structural variability present in the study area. The plots' locations were randomly distributed, within very accessible forested areas near the main water creek, and not clustered in one area to ensure that different conditions available in the area under focus were captured with ground plot measurements (Figure3).

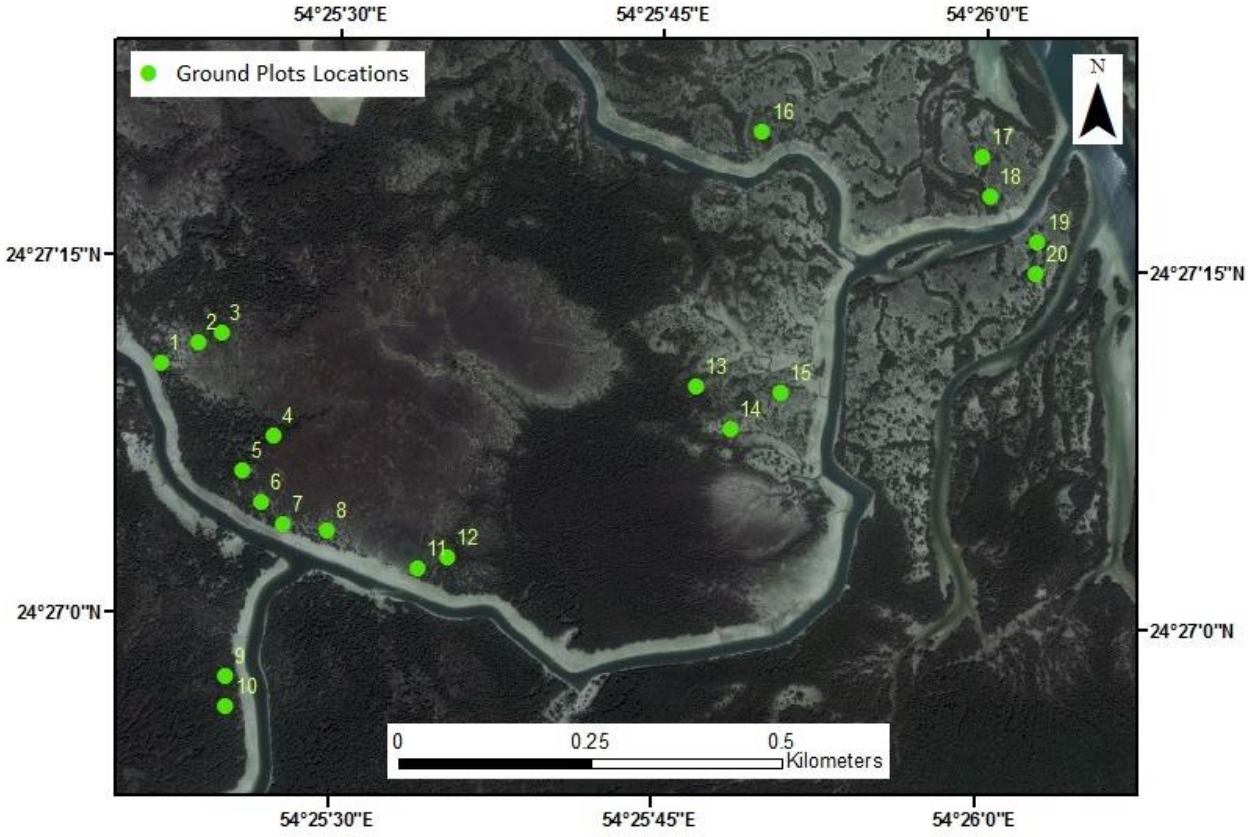

Figure 3. The locations of ground plots in the study area.

The coordinates of each plot were determined using a GNSS GPS System. To record accurate GPS positions, factors were taken into consideration such as the satellites' geometry, atmospheric conditions, multipath problem, number of location measurements at each point, and quality of GPS receiver. A Leica Viva GS14 GNSS RTK receiver was used to ensure the highest degree of quality and reliability, and a real-time differential correction was applied using a technique called real-time kinematic (RTK) GPS to enhance the accuracy of location data gathered (Figure 4). The estimated average accuracy of the location data is 7 ± 4 cm.

Figure 4. Determining the locations of ground plots using Leica Viva GS14 GNSS RTK receiver in January, 2014.

2. Tree Attributes

Accurate tree attributes were gathered from direct measurements at the ground plot level; then they were used to calculate derived measurements (Figure 5).

Figure 5. Collecting tree attributes in Mangrove National Park during the winter season of 2014.

Direct measurements were used to quantify aspects such as:

a) Status of the tree (e.g., live or dead).

b) Stem number, which quantifies the total number of measured trees in a plot. The total stem number of each plot was recorded regardless to the tree status.

c) Tree height, which is the distance between the top and the base of the tree. The height of the individual trees was measured using a height stick.

d) Diameter at breast height (DBH), which is the trunk diameter of a tree. This diameter was measured at 1.3 m above the ground using a diameter tape. Usually, a minimum threshold for measurement is specified (ranging from 5 to 10 cm) and all trees with a DBH greater than this minimum threshold should be measured, regardless of the tree status (live or dead) (McGarrigle et al., 2011). However, the majority of *Avicennia marina* trees (about 69%) in the sampling plots have a DBH value of ≤ 5 cm. Therefore, all trees with DBH ≥ 1 cm in diameter were measured and recorded. For trees with multiple trunks, each trunk was measured individually.

Derived measurements were used to quantify the following:

a) Absolute density, which is the number of trees per hectare, where the hectare is 10, 000 m². Tree density was calculated using this formula:

$$\text{Tree density} = \frac{\text{no. trees}}{\text{area of plot in m}^2} \times 10{,}000 \text{ m}^2$$

b) Average crown spread. Two direct measurements of the crown length and width were taken perpendicular to each other. Average crown spread was calculated using this formula:

$$\text{Average crown spread} = \frac{(\text{Wide spread} + \text{narrow spread})}{2}$$

c) Basal area, which is the area of earth occupied by tree trunks and stems, usually measured in square meters. Because *Avicennia marina* trees have multiple trunks, the basal area of each trunk was computed separately. Only trees higher than 1.3 m were included in the estimation. The basal area was calculated from DBH, measured in centimeters, using this formula (Bettinger et. al., 2009):

$$\text{Basal area (Unit}^2\text{)} = \pi\left(\frac{\text{DBH}}{2}\right)^2 \text{ or } \pi\left(\frac{\text{DBH}^2}{4}\right)$$

Since basal area in UAE is usually measured in m^2, the equation is divided by 10,000, which is the number of square meters in a hectare.

$$\frac{\left(\frac{\text{DBH}^2}{4}\right)}{10{,}000}$$

The condensed version of the basal area equation then becomes:

$$\text{Basal area (m}^2\text{)} = 0.00007854 \times \text{DBH}^2$$

In addition, mean basal area can be computed as:

$$\text{mean basal area} = \frac{G}{N}$$

Where *G* is the plot basal area measured and *N* is the total number of trees in the plot.

d) Aboveground biomass, which is the quantity of vegetation matter per unit of area. It is calculated as the dry weight of tree elements above ground; this includes leaves, branches, and stems (Hougton, 2005). Aboveground biomass was obtained from DBH ground measurements using the following allometric equation:

$$\text{M} = aD^b$$

M is the total aboveground tree dry biomass (kg), D is diameter at breast height (DBH) (cm), "a" and "b" are constants. According to Kirui's study (2006), in calculating aboveground biomass of *Avicennia marina* using this allometric equation, "a" and "b" constants are estimated to be 0.5317 and 1.7476, respectively. Kirui's allometric equation was used in this study since no allometric equations have been developed for *Avicennia marina* in Abu Dhabi, UAE. However, a better estimation of AGB in Eastern Mangrove Lagoon National Park can only be obtained by measuring the oven-dry-weight of different trees of all sizes in the park, and then allometric equations can be developed for accurate AGB estimation.

e) Mean plot height, a calculation of plot-level variations of height, is obtained from measurement of each tree height.

f) Trees mortality rate, which was calculated using this formula:

$$\text{Mortality rate (\%)} = \frac{Total\ number\ dead\ trees}{Total\ number\ of\ trees} \times 100$$

D. Results

Statistical analysis of trees' attributes was used to study the population structure of *Avicennia marina* and a linear regression analysis was performed to evaluate the relationships between the structural characteristics and aboveground biomass. A summary of the trees' structural characteristics measured for each plot is shown in Table 1.

This study found that the total number of *Avicennia marina* trees in all plots is 2,216, with only 5 dead trees in all sites (Figure 6). The number of adult trees with DBH $\geq$ 2 cm is 1,077 (49%), whereas the number of saplings and seedlings with DBH < 2 cm is 1,139 (51%; Figure 7). The stem number varied in the ground plots (Figure 8). Plot 10 has the highest stem number (390) and density (25,324 trees ha^{-1}), while plot 6 has the lowest stem number (14) and density (909 trees ha^{-1}). This indicates a significant variation of the tree density in the sampling plots.

The total basal area in all plots is 20.58 m^2, while the basal area mortality rate is very low (0.02%), which shows that the mangrove forest in Abu Dhabi is generally healthy. Plot 7 has the highest basal area (3.05m^2), while plot 18 has the lowest basal area (0.07m^2) (Figure 9). Even though plots 9 and 10 have the highest numbers of trees (highest density) compared to the other plots, they have relatively low basal areas: 1.48m^2 and 1.55m^2 respectively. This is due to the high population of young trees and saplings with small diameter at breast height (DBH $\leq$ 5cm). A comparison of tree density and basal area is shown in Table 2.

The frequency distribution for tree height is positively skewed (Figure 10a), indicating the presence of many small and few large stems. About 83% of the measured trees are $\leq$ 3 m in height, whereas only 17% of the trees are between 3.1 to 5.0 m in height, with only one tree over

5m in height in all sites. The mean height of the trees in all sampling plots is 1.97 ± 0.02 m, while the mean height of trees with DBH > 5cm is 2.47 ± 0.02 m.

The distribution of the trees' diameter (DBH) classes reveals a typical reverse-J-shaped pattern (Figure 10b), which indicates an uneven-aged stand structure: 69% of all trees with a minimum height of 1.3 m have a diameter of ≤ 5 cm, 15% of the trees have a diameter ranging from 6 to 10cm, 10% of trees have a diameter ranging from 11 to 15 cm, 4% of the trees have a diameter ranging from 16 to 20 cm, and only 2% of the trees have a diameter greater than 20 cm. The observed reverse-J-shaped diameter distribution illustrates a normal structure in the forest development, which means that many regeneration seedlings and young trees can be found in a normal mangrove forest area. The mean DBH of the trees is 5.38 ± 0.14 cm.

The distribution of the trees' average crown spread classes also reveals a typical reverse-J-shaped pattern very similar to DBH classes (Figure 10c). This shows a strong correlation between DBH and crown spread measurements. Over 65% of the trees have an average crown spread of ≤ 1 m, 26% of the trees have an average crown spread ranging from 1.1 to 2 m, 6% of the trees have an average crown spread ranging from 2.1 to 3 m, 1.5% of the trees have an average crown spread ranging from 3.1 to 4 m, and less than 1% of the trees have an average crown spread of > 4 m. The average crown spread of all the trees is 0.79 ± 0.02 m, while the average crown spread of adult trees is 0.99 ± 0.02 m.

Aboveground biomass can be estimated using different variables such as DBH, height, or DBH and height. However, Kirui (2006) determined that the best estimate of *Avicennia marina* biomass can be obtained using only DBH values. In his study, he found a significant relationship between DBH and dry weight of *Avicennia marina*, where $r^2 = 0.9638$. Since no allometric equation has been developed for *Avicennia marina* in the study area, his equation was used to

estimate AGB of *Avicennia marina* in the present study. The total aboveground biomass in the study sites is 265.66 t ha^{-1}. Plot 7 has the highest values of aboveground biomass estimation (42.79 t ha^{-1}) as well as basal area and DBH, while plot 18 has the lowest values of aboveground biomass (1.03 t ha^{-1}), basal area, and DBH. This is predictable because AGB and basal area were both calculated from DBH measurements.

Pearson correlation coefficients and coefficients of determination were calculated between mangrove aboveground biomass and the measurements of structural parameters including height, diameter at breast height, basal area, and crown spread (Table 3 and Figure 11). The correlation coefficients vary from 0.518 to 0.981, which indicates positive to strong positive correlations between the structural variables. Aboveground biomass has the strongest correlation with basal area explaining 96% of the variance. On the other hand, aboveground biomass has the weakest correlation with height accounting for 26% of the variance. Indeed, height has the weakest correlation with all parameters.

Table 1. Mangrove Vegetation Structural Attributes of the Study Area.

Plot Number	Trees Number	Trees Number H>1.3m	Absolute Density (ha^{-1})	Mean Height (m) Mean ± SE	* Mean Height (m) Mean ± SE	Average Crown Spread (m) Mean ± SE	* Average Crown Spread (m) Mean ± SE	* Mean DBH (cm) Mean ± SE	* Total Basal Area (m^2)	*Total AGB ($t\ ha^{-1}$)
1	98	75	6,363	2.16 ± 0.11	2.57 ± 0.09	1.05 ± 0.06	1.22 ± 0.07	9.30 ± 0.80	1.77	23.01
2	32	25	2,077	1.94 ± 0.13	2.23 ± 0.10	1.40 ± 0.12	1.58 ± 0.14	9.08 ± 1.15	1.23	15.59
3	57	50	3,701	2.29 ± 0.06	2.48 ± 0.05	1.39 ± 0.10	1.51 ± 0.11	11.24 ± 0.87	1.75	22.54
4	19	19	1,233	3.02 ± 0.25	3.02 ± 0.25	1.98 ± 0.30	1.98 ± 0.30	9.15 ± 2.44	0.54	6.10
5	23	23	1,493	2.70 ± 0.20	2.70 ± 0.20	1.80 ± 0.31	1.80 ± 0.31	11.60 ± 2.98	1.35	14.95
6	14	14	909	2.67 ± 0.20	2.67 ± 0.20	1.72 ± 0.25	1.72 ± 0.25	12.14 ± 2.35	0.78	8.82
7	98	93	6,363	2.66 ± 0.09	2.74 ± 0.09	1.38 ± 0.09	1.43 ± 0.09	10.47 ± 0.69	3.05	42.79
8	30	28	1,948	2.49 ± 0.05	2.59 ± 0.06	1.71 ± 0.19	1.77 ± 0.19	10.42 ± 1.67	1.58	14.75
9	378	326	24,545	2.33 ± 0.05	2.57 ± 0.09	0.68 ± 0.03	0.75 ± 0.03	3.75 ± 0.22	1.48	20.53
10	390	338	25,324	2.34 ± 0.05	2.58 ± 0.05	0.69 ± 0.03	0.75 ± 0.03	3.50 ± 0.21	1.55	20.61
11	92	89	5,974	2.42 ± 0.06	2.47 ± 0.05	1.11 ± 0.06	1.12 ± 0.06	8.23 ± 0.46	1.70	22.62
12	58	55	3,766	2.49 ± 0.08	2.57 ± 0.06	1.36 ± 0.07	1.41 ± 0.07	10.10 ± 0.54	1.75	25.27
13	204	79	13,246	1.23 ± 0.05	1.95 ± 0.06	0.47 ± 0.09	0.79 ± 0.07	2.89 ± 0.40	0.29	4.59
14	243	104	15,779	1.32 ± 0.06	2.18 ± 0.07	0.58 ± 0.12	0.92 ± 0.09	2.57 ± 0.26	0.26	4.07
15	38	14	2.467	1.52 ± 0.14	2.44 ± 0.35	0.84 ± 0.13	1.61 ± 0.32	6.85 ± 2.04	0.23	3.06
16	39	29	2,532	1.83 ± 0.16	2.15 ± 0.17	0.80 ± 0.17	0.99 ± 0.22	3.93 ± 1.41	0.35	4.17
17	132	87	8,571	1.82 ± 0.08	2.43 ± 0.07	0.66 ± 0.07	0.86 ± 0.07	1.88 ± 0.17	0.11	2.18
18	41	13	2,662	1.13 ± 0.16	2.22 ± 0.35	0.50 ± 0.10	0.96 ± 0.28	3.46 ± 1.25	0.07	1.03
19	53	31	3,441	1.59 ± 0.13	2.11 ± 0.15	0.80 ± 0.13	1.16 ± 0.19	2.96 ± 0.76	0.18	2.53
20	177	77	11,493	1.32 ± 0.07	2.05 ± 0.09	0.50 ± 0.12	0.78 ± 0.15	3.01 ± 0.71	0.56	6.45
Total Plots	Total Trees	Total Trees H>1.3m	Total Density (ha^{-1})	Mean Height (m)	* Mean Height (m)	Average Crown Spread (m)	* Average Crown Spread (m)	* Mean DBH (cm)	* Total Basal Area (m^2)	*Total AGB ($t\ ha^{-1}$)
20	2216	1569	1,438,960	1.97 ± 0.02	2.47 ± 0.02	0.79 ± 0.02	0.99 ± 0.02	5.38 ± 0.14	20.58	265.66

* Measurements collected for trees >1.3 m in height

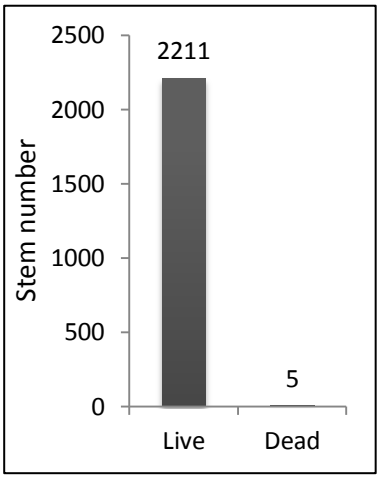

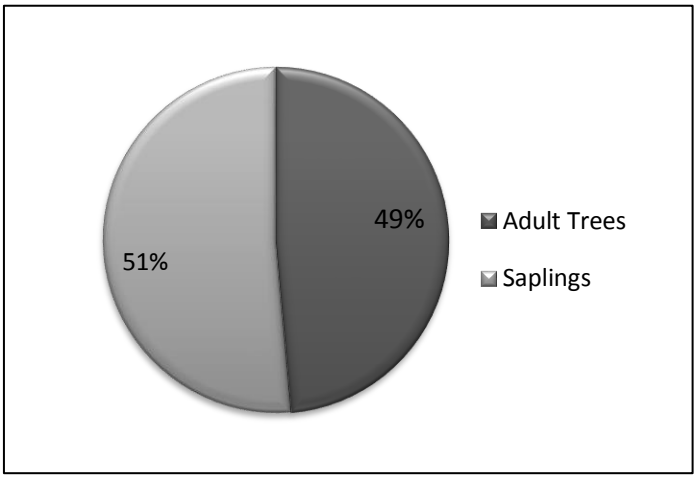

Figure 6. Status of trees in all plots. Figure 7. Percentage of saplings vs. adult trees in all plots.

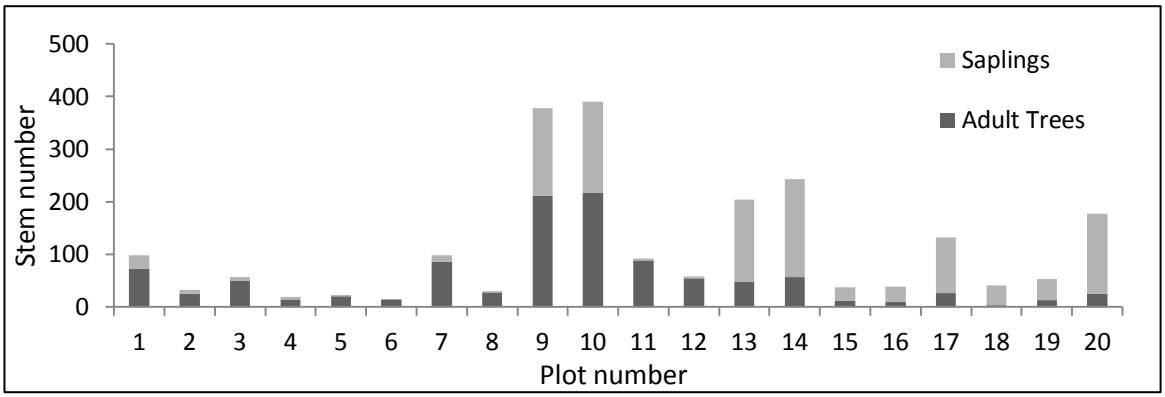

Figure 8. Total number of trees in each plot.

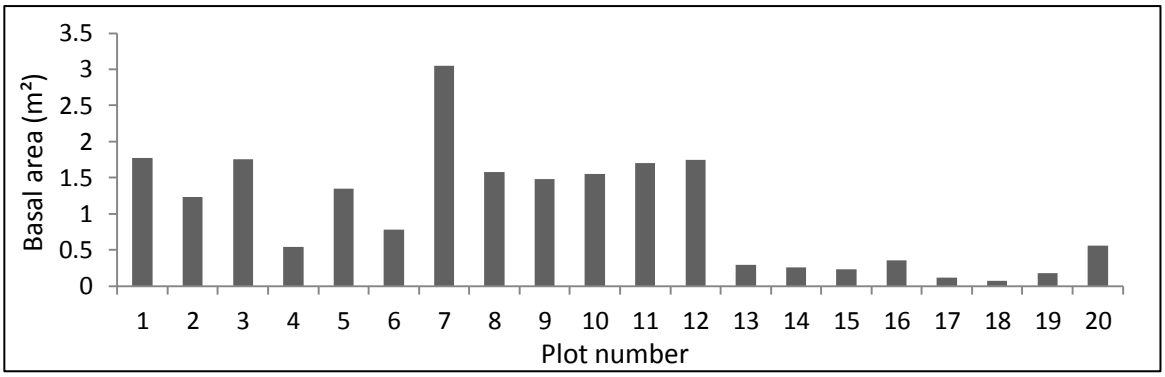

Figure 9. Total basal area in each plot.

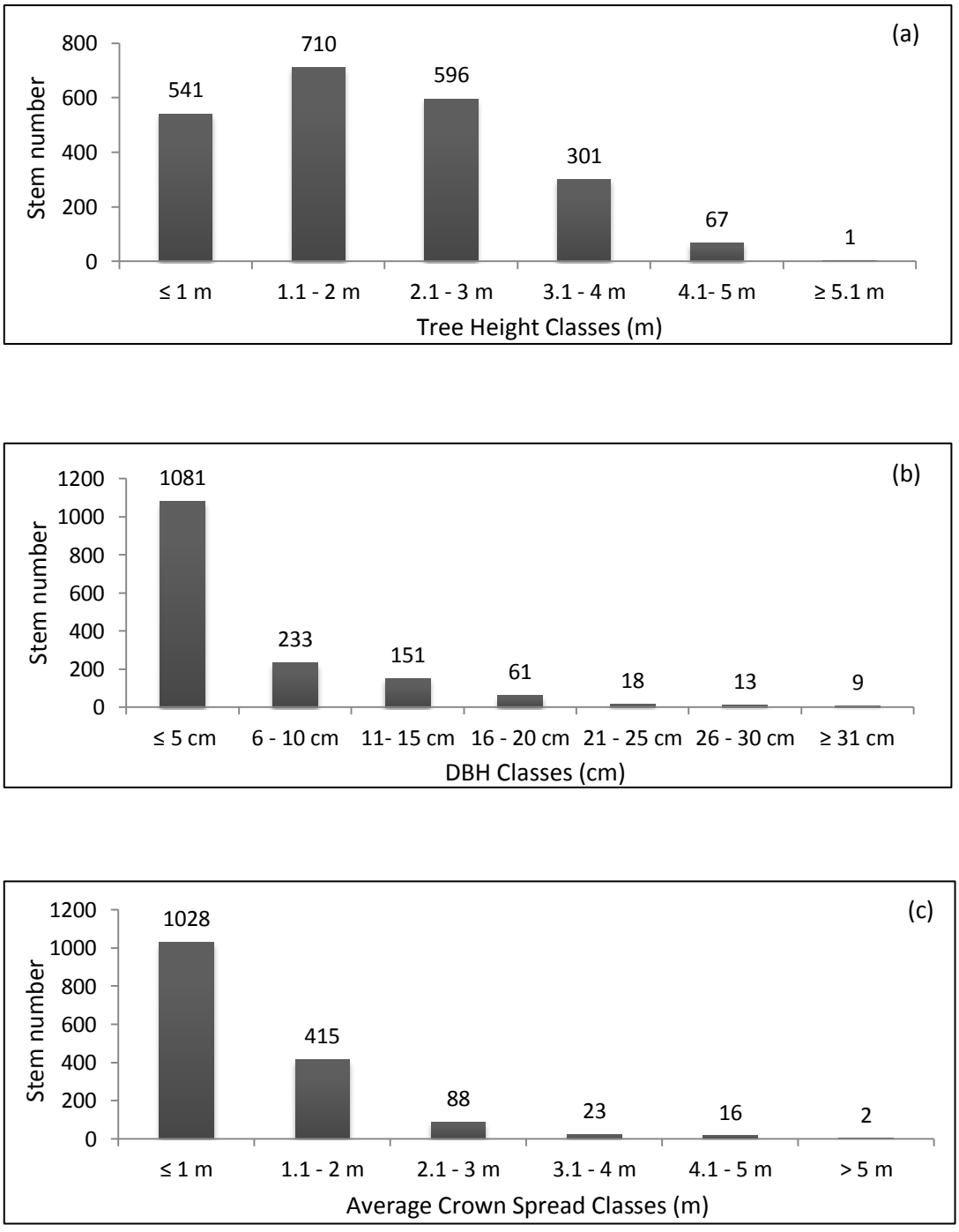

Figure 10. Frequency distributions of trees height (a), DBH (b) and average crown spread (c) classes in all sampled plots.

Table 2. Comparison of trees density and basal area in the study sites.

Plot Number	Total Basal Area (m^2)	Basal Area%	Density (ha^1)	Density%
1	1.77	8.6	6,363	4.4
2	1.23	6	2,077	1.4
3	1.75	8.5	3,701	2.6
4	0.54	2.6	1,233	0.9
5	1.35	6.6	1,493	1
6	0.78	3.8	909	0.6
7	3.05	14.9	6,363	4.4
8	1.58	7.7	1,948	1.4
9	1.48	7.2	24,545	17
10	1.55	7.5	25,324	17.6
11	1.70	8.2	5,974	4.1
12	1.75	8.5	3,766	2.6
13	0.29	1.4	13,246	9.2
14	0.26	1.3	15,779	11
15	0.23	1.1	2.467	1.7
16	0.35	1.7	2,532	1.8
17	0.11	0.5	8,571	6
18	0.07	0.3	2,662	1.9
19	0.18	0.9	3,441	2.4
20	0.56	2.7	11,493	8
		Total		
20	20.58	100%	143,896	100%

Table3. Correlation coefficient (r) among forest structural parameters and biomass.

Parameters	Height	DBH	Basal Area	Crown Spread	AGB
Height	1.000	0.594	0.520	0.627	0.518
DBH	0.594	1.000	0.912	0.850	0.940
Basal Area	0.520	0.912	1.000	0.852	0.981
Crown Spread	0.627	0.850	0.852	1.000	0.840
AGB	0.518	0.940	0.981	0.840	1.000

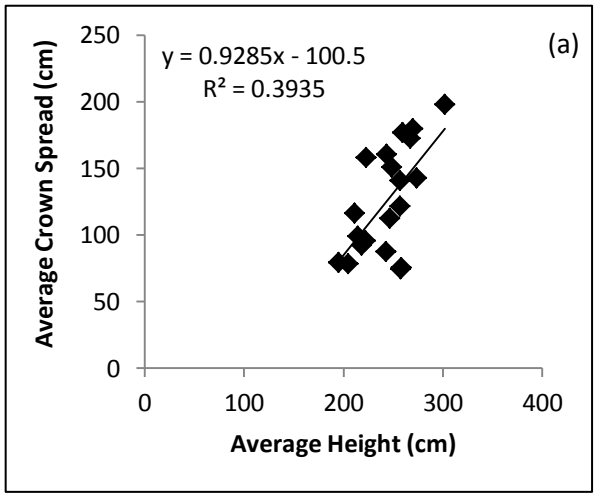
(a)
y = 0.9285x - 100.5
R² = 0.3935
Average Crown Spread (cm)
Average Height (cm)
0
50
100
150
200
250
0
100
200
300
400

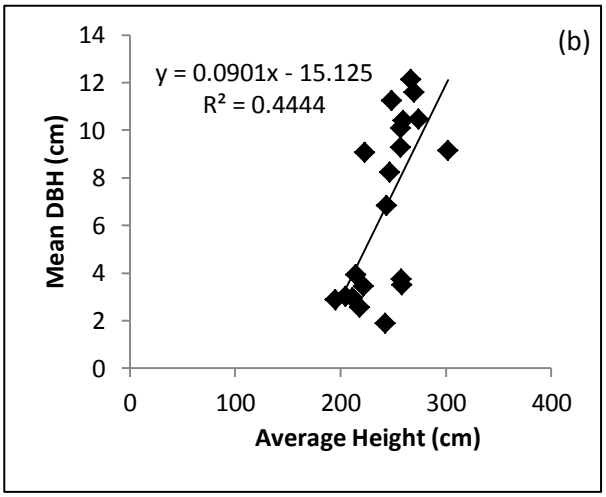
(b)
y = 0.0901x - 15.125
R² = 0.4444
Mean DBH (cm)
Average Height (cm)
0
2
4
6
8
10
12
14
0
100
200
300
400

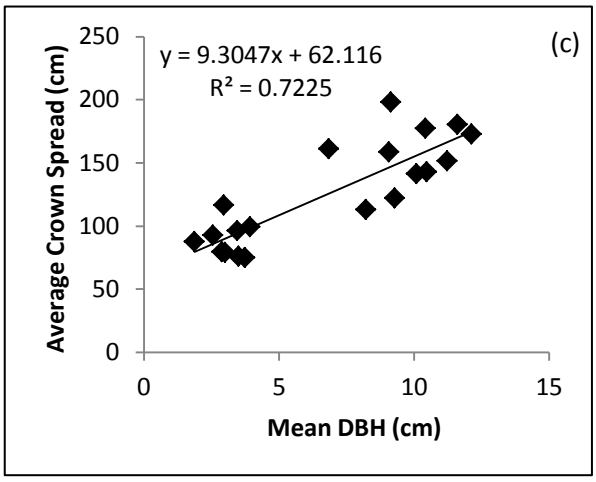
(c)
y = 9.3047x + 62.116
R² = 0.7225
Average Crown Spread (cm)
Mean DBH (cm)
0
50
100
150
200
250
0
5
10
15

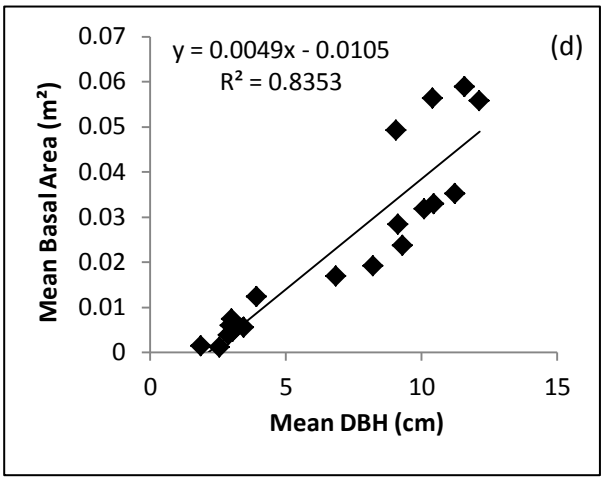
(d)
y = 0.0049x - 0.0105
R² = 0.8353
Mean Basal Area (m²)
Mean DBH (cm)
0
0.01
0.02
0.03
0.04
0.05
0.06
0.07
0
5
10
15

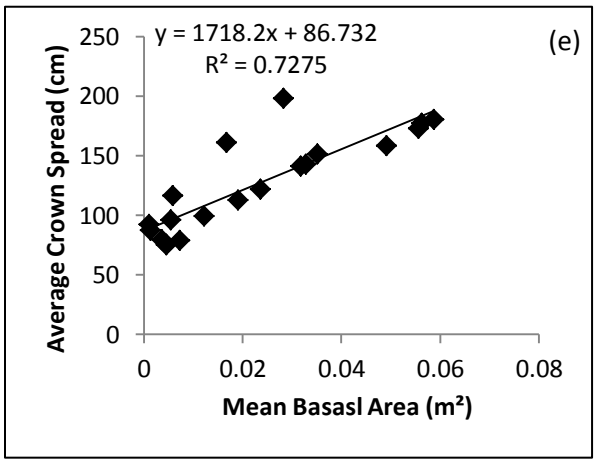
(e)
y = 1718.2x + 86.732
R² = 0.7275
Average Crown Spread (cm)
Mean Basasl Area (m²)
0
50
100
150
200
250
0
0.02
0.04
0.06
0.08

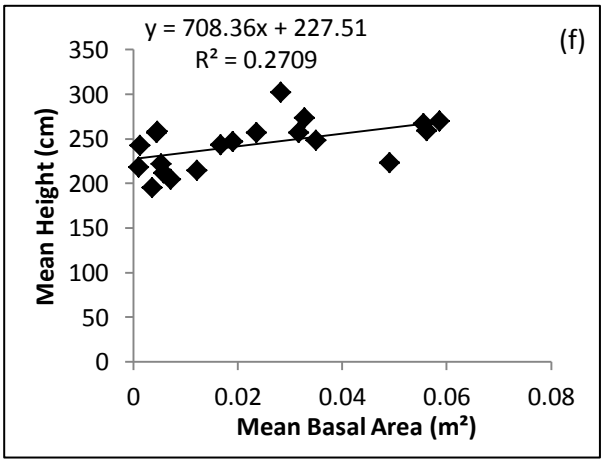
(f)
y = 708.36x + 227.51
R² = 0.2709
Mean Height (cm)
Mean Basal Area (m²)
0
50
100
150
200
250
300
350
0
0.02
0.04
0.06
0.08

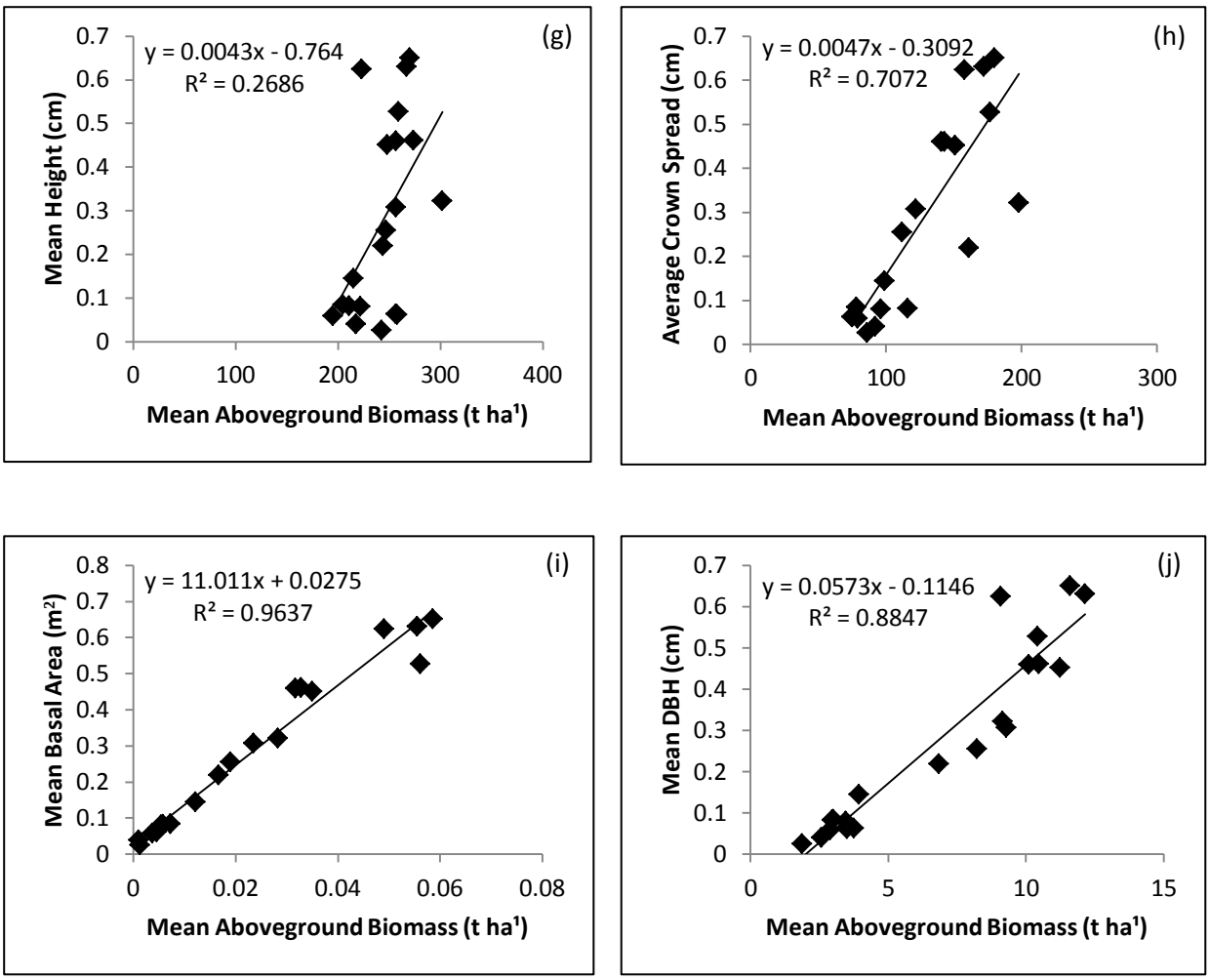

Figure 11. Relationships between DBH, basal area, height, crown spread, and aboveground biomass of *Avicennia marina*.

E. Discussion and Conclusion

Mangrove structure and biomass are important components to studies related to their environmental dynamics. This research studies *Avicennia marina* population structure and aboveground biomass in Eastern Mangrove Lagoon National Park, Abu Dhabi. The *in situ* survey shows that the forest is generally healthy with a very low mortality rate. There is a high population of young trees and seedlings, which is typical for a naturally regenerating forest. The distribution of the trees' diameter classes indicates an uneven-aged stand structure. This study also finds a significant variation between tree density and basal area in the sampling plots. The height of the trees is generally short where the majority of trees are less than three meters. The low height of the trees allows seedling to colonize the area as there is more light and space available for them to grow. According to Snedaker and Snedaker (1984), both basal area and tree height can determine the maturity of the forest trees. Higher mangrove basal area, height, diameters, and lower densities indicate more mature trees. While lower mangrove basal area, height, diameters, and higher densities indicate that the forest is in early development phases, which is characterized by high seedling density. This study also calculated aboveground biomass of all sites from DBH values, and it is estimated to be 265.66 t ha^{-1}. Finally, this study indicates a strong, positive correlation between structural variables including height, basal area, DBH, crown spread, and aboveground biomass. This research provides new data to evaluate the current health and status of *Avicennia marina* population structure and aboveground biomass in Eastern Mangrove Lagoon National Park, Abu Dhabi.

Land protection policies were established in the last few years by authorities, such as the Ministry of Environment and Water and the Federal Environment Agency of Abu Dhabi, to conserve the coastal and marine biodiversity and ecosystems, including the valuable mangroves.

An environmental protection and awareness plan at the Eastern Mangrove Forest was implemented. Actions and polices, including the monitoring of marine water quality, the treatment of water pollution, the establishment of urban and industrial economic development boundaries, the prevention of coastal erosion, and the regulation of dredging and landfills, all aim at preserving the coastal ecosystems and ensuring the long-term environment sustainability of Abu Dhabi.

As this study presents, the high population of mangrove seedlings and saplings could be a result of coastal land protection policies in the last few years. However, due to the lack of detailed information about previous mangrove population and structural characterization, it is strongly recommended that more studies should be conducted in the future to monitor changes in *Avicennia marina* floristic structure over time. For instance, by measuring numbers of individuals from different size classes of *Avicennia marina*, a baseline data can be created to estimate the species' future population structure and predict their fate. Such studies, on how the *Avicennia marina* population is regenerating, provide valuable data in order to better understand the forests' ecological dynamics, which is critical for the conservation and management of mangrove trees in Abu Dhabi.

III. Per-Segment Aboveground Biomass Estimation of *Avicennia marina* in Eastern Mangrove Lagoon National Park, Abu Dhabi Using LIDAR-derived Height Percentile Statistics

A. Summary

A biomass model of *Avicennia marina* forest was produced using LIDAR multiple percentile heights to estimate and map aboveground biomass density in Eastern Mangrove Lagoon National Park, Abu Dhabi. After processing small-footprint aerial LIDAR data, multiple percentile heights were calculated using a neighborhood algorithm. Then, image segmentation algorithm was employed to transform the 2D LIDAR-derived image into structurally homogeneous modeling units. However, the size of the neighborhood affects the calculation of LIDAR-derived height statistics, and thus two different neighborhood sizes, 3 m and 5 m radius, were tested to evaluate the best model performance. The models' performance indicates that the 5 m neighborhood resulted in higher accuracy (RMSE= 10.16713, R= 0.8722238, R^2= 0.7597432). Aboveground biomass of twenty sampling plots (154 m^2 each) calculated from *in situ* measurements were incorporated into a machine learning algorithm to produce a regression-tree model for aboveground biomass estimation per segment of the entire study area. A biomass map of the study area, with 715 image segments, was created. The segments' size ranges from 42.25 to 20,004.50 m^2 with an average of 2,445.37± 117.88 m^2, whereas biomass density per segment ranges from 0.234 to 13.178 (kg/m^2) with an average of 5.159 ± 0.144 and a total of 14,850.26 kg. Additionally, about 49% of the study area has relatively low biomass density (≤ 4.15 kg/m^2), 23% of the study area has a relatively moderate biomass density (from 4.16 to 8.01 kg/m^2), and 28% of the study area has a relatively high biomass density (from 8.02 to 13.17 kg/m^2). A canopy height model of the study area was also created with a maximum height of

7.86 m. This means that based on LIDAR observations no trees in the study area exceed 7.86 m in height. The average pixels height is 3.03 m, while the minimum pixels height is 0.12m.

B. Introduction

One of the most vital measures of mangrove forest ecosystem structure and function is aboveground biomass (AGB). The measurement of AGB is important for carbon storage and evaluating the forest response to climate change and anthropogenic disturbances (Houghton, 2009). Calculating AGB from forest inventory plots generally provides highly accurate data on the AGB of an area. This usually includes the measurement of the diameter at breast height (DBH), and ideally tree height. Then, AGB can be estimated from these measurements using allometric equations (White et al., 2013). However, it is impossible to have a sufficient number of plots in a large forested area due to restrictions in resources, time and access. Therefore, estimating AGB for a whole forest cannot be done directly. Several remote sensing technologies (e.g. optical and radar sensors) can be used to estimate the biomass of a large forested area (Song C., 2013; Mitchard et al., 2009).

Small-footprint LIDAR is considered to be a highly accurate method to estimate AGB because it provides detailed information on canopy structure in terms of density and height, typically within a few centimeters (Simard et al., 2006). To use LIDAR data for forest biomass estimation, statistical analysis is made to deduce a relationship between AGB calculated from *in situ* data (based on allometric equations) and LIDAR height metrics (White et al., 2013).

According to Zhao et al. (2012), several researchers approved the efficiency of utilizing LIDAR data to estimate forest biomass based on relationships between LIDAR canopy height metrics, such as mean canopy height and canopy height percentiles. However, recent studies attempt to predict AGB using image segmentation of LIDAR canopy height metrics, which

allows the estimate of AGB to be conducted on structurally homogeneous units of forested areas. The image segmentation method reduces the variability of subsequent AGB estimations. As mentioned by Riggins et al. (2009), the coefficient of determination values (R^2) of LIDAR, derived AGB estimates analyzed on a per-segment scale, is higher than the values of a plot level study in the same area. A higher accuracy in estimating biomass of various forest environments, especially the complex, heterogeneous ones, can be provided if multiple LIDAR derived canopy height metrics and image segmentations is used in a machine learning environment.

Various biomass models have been published for different types of forests worldwide (Simard et. al., 2006; Jan et. al., 2008; Zhao et. al., 2009; Lu et. al., 2012). However, none have been created to estimate biomass of *Avicennia marina* forests in Abu Dhabi. Therefore, the main objective of this study is to predict total AGB of mangrove forest in the study area by utilizing LIDAR derived height percentiles statistics, created using a neighborhood algorithm, to segment the forest into structurally homogenous units; using *in situ* reference data in a machine learning environment to estimate total AGB per unit area in each segment; and classify the biomass output into biomass density classes.

C. Materials and Methods

1. *In situ* Measurements

In situ survey was conducted in the winter of 2014 (January through April). As described in chapter 2, a total of 20 circular plots located in accessible areas were selected randomly. The coordinates of the sampling plots were determined using GNSS GPS System. Each plot covered an area of 154 m^2 (14 m diameter). A total of 2,216 trees (≥ 1cm DBH) were measured, and

their structural attributes were recorded including tree status, height (m), DBH (cm), basal area (m), average crown spread (m), mortality rate (%), plot height(m), and density (kg/m^2).

2. Plot-Level AGB Estimation

Aboveground biomass was estimated for each tree, then for each plot. As mentioned in chapter 2, AGB was obtained from DBH ground measurements using the following allometric equation:

$$M = aD^b$$

M is the total aboveground tree dry biomass (kg), D is diameter at breast height (cm), "a" and "b" are constants, which estimated to be 0.5317 and 1.7476, respectively (Kirui, 2006). Kirui's allometric equation was used to estimate AGB because no allometric equations have been developed for *Avicennia marina* in the study area. Nevertheless, a better estimation of AGB can only be obtained by measuring the oven-dry-weight of *Avicennia marina* of all sizes in the park, and then allometric equations can be developed for accurate AGB estimation.

3. LIDAR Data

Airborne LIDAR data (Figure 12) were collected on 21st January, 2013 using an Airborne Laser Terrain Mapper (ALTM) 3100 EA system mounted in a Beech Craft KING AIR 350 aircraft. The aircraft was operated by Bayanat Company, which provides high quality national level geospatial products and services, with a flight altitude of 5,000 feet above ground level (AGL), a flight speed of 90 m per second (175 knot), and a scan angle varying from -25 to 25° from nadir. The LIDAR system utilized a pulse rate of 100 kHz and recorded first and last returns of an emitted laser pulse. A 1,420 meter-wide swath of laser footprints spaced approximately every 2 m beneath the flight path was produced. LIDAR data was received in raw

LAS format, which is an American Society for Photogrammetry and Remote Sensing (ASPRS) standard file format for the interchange of LIDAR data. It maintains information related to LIDAR data and contains metadata of the survey. Most proprietary GIS software, such as ArcGIS and LP360, supports LIDAR data that is provided in LAS file format.

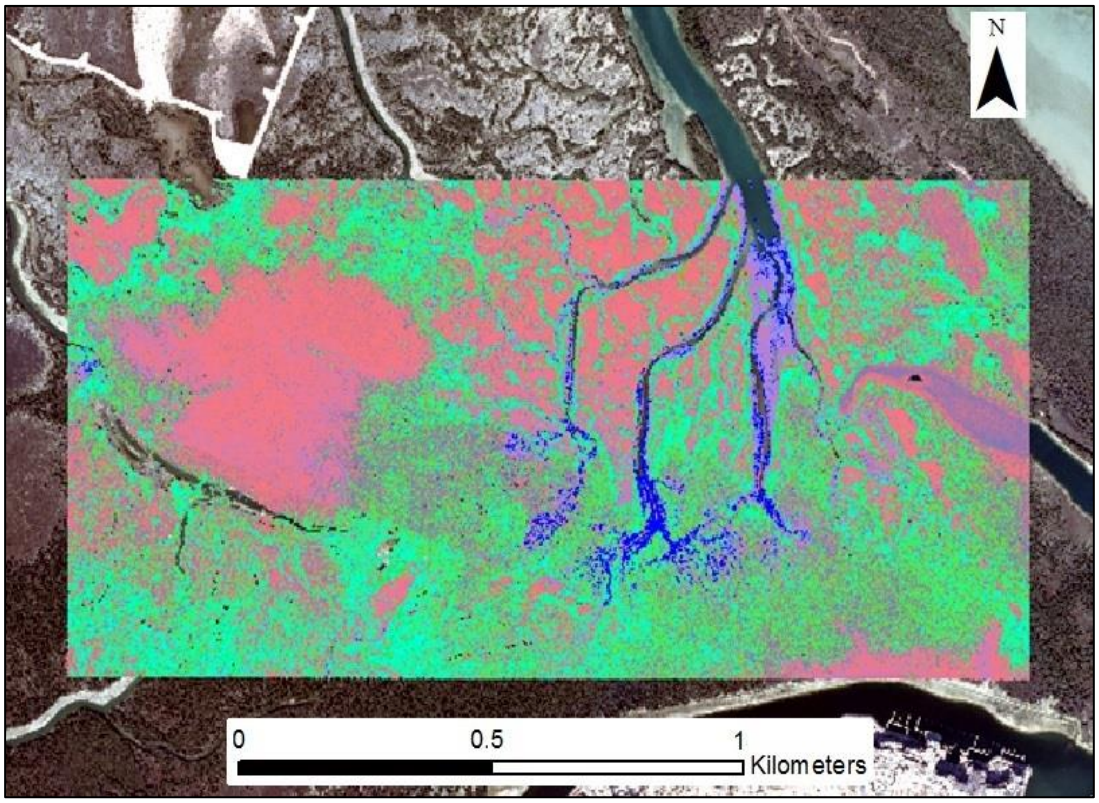

Figure 12. Digital surface model created using LIDAR data. Blue dots represent areas with lower elevation values. Green dots represent areas with higher elevation values.

4. LIDAR-derived statistics

The first step in processing LIDAR data is to classify LIDAR points according to ASPRS standard LIDAR point classes, as shown in Table 4. In the present study, LIDAR points were classified into three main categories: noise points (class 7), ground points (class 2), and high vegetation points (class 5). The noise points, identified as the very low or high points compared to the actual elevations of the study area, were identified and ignored. Usually, low points can be

a result of laser multipath. On the other hand, high points can be caused by aircraft flying at low levels, birds, and/or atmospheric aerosols (McGaughey, 2014). Several software programs can be used to filter or classify LIDAR points; however, LAS tools were used in the present study for this purpose. A total of 79 noise points were ignored out of 862, 015 total points. Furthermore, the classification results show that the total number of ground points is 208,430; while the total number of vegetation points is 653,506. Then, the LAS file was transformed to a text file to be used in R statistical software. This text file contains information about x, y, z values for each LIDAR point, as well as the return number and class number. With such information, LIDAR-derived metrics can be generated, and different statistics can be calculated.

Table 4. ASPRS Standard LIDAR Point Classes (ASPRS, 2013).

Classification Value	Meaning
0	Created, never classified
1	Unclassified
2	Ground
3	Low Vegetation
4	Medium Vegetation
5	High Vegetation
6	Building
7	Low Point (noise)
8	Model Key-point (mass point)
9	Water
10	Reserved for ASPRS Definition
11	Reserved for ASPRS Definition
12	Overlap Points
13-31	Reserved for ASPRS Definition

The next step is to create a grid points, separated by the pre-defined grid spacing, for the study area using the neighborhood technique. A neighborhood centering each grid point was generated, and LIDAR points within the neighborhood were extracted, so certain statistics can be calculated to describe the distribution of the points' z-value. Then, the statistics were assigned to

the grid points. This technique transforms discrete LIDAR points into 2D image layers showing the spatial distributions of LIDAR height metrics with user specified resolutions and generalization extents. The user specified resolutions, equals to the grid spacing, control the amount of details that could be revealed. While the generalization extents, the spatial area where LIDAR points are queried, are determined by the neighborhood size and shape. The neighborhood size should be large enough to include a sufficient number of LIDAR points to calculate statistics precisely, and to avoid local outliers. It should also be larger than the grid spacing to allow overlapping between adjacent neighborhoods. However, too large neighborhood may result in masking spatial details and creating very similar adjacent grid points. Additionally, too large of a neighborhood may include more LIDAR points falling outside the plots' boundaries, presenting unwanted information to the plots and making the regression models inaccurate. Furthermore, the pre-defined grid spacing affects the performance of the neighborhood method. For instance, large grid spacing results in coarse image resolutions, but decreases the computing time. On the other hand, small grid spacing results in fine image resolutions, but increases the computing time (Miyazaki et. al., 2014).

In the present study, grid points were created for the study area, including the 20 circular plots, and were separated by 0.5 m. The advantage of using such fine spatial resolution is to capture more spatial details and not to increase computing cost significantly due to the relatively small plot area. The spatial extents of the sampling plots were buffered by half of the neighborhood radius. In this way, a sufficient number of LIDAR points is included to calculate statistics for grid points located at the plot boundaries. Two neighborhood sizes, 3 and 5 m, were used as the neighborhood radius in order to test the effect of different neighborhood sizes, and to select the most feasible size to be used to calculate LIDAR-derived height percentile statistics for

the whole study area. For the 3 m neighborhood radius, a buffer of 1.5 m was used to clip the entire point cloud. While for the 5 m neighborhood radius, a buffer of 2.5 m was used. The combination of grid spacing and neighborhood size contributes to performance of the final regression models. Thus, the performance of the models was employed to decide the best neighborhood size to be applied for the entire study area.

An algorithm was prepared to create the circular neighborhood windows centering each of the grid points to extract LIDAR points falling within the neighborhood. This means that the window stopped at every point on the half meter grid and selected all LIDAR returns within its boundary. Certain statistics, including total number of points, ratio of high vegetation points, minimum elevation, and height above the minimum elevation on the 5^{th}, 15^{th}, 25^{th}, 35th, 45th, 55th, 65th, 75th, 85th, 95th, and 100^{th} percentiles, were calculated to describe the distribution of the z-value of these points and they were assigned to the grid point. The calculations resulted in a 0.5 × 0.5 m 2D raster images with 13 layers, each representing a continuous statistical surface. However, when the numbers of LIDAR points were not sufficient to calculate statistics of some pixels within the raster images, an Inverse Distance Weighted (IDW) method was used to estimate the values of these pixels. The grid was transformed to multilayer images showing spatial distributions of LIDAR height metrics after they were clipped by the plot polygons.

5. Biomass modeling

Forests AGB can be conducted at four scales: 1) individual tree level, 2) pixel level, 3) plot level, 4) and segment level. However, in this study the segment level was chosen because this approach avoids difficulties associated with predicting AGB at the individual tree or pixel scales. Image segmentation was used to group individual pixels, with similar attributes (color, texture, contextual information and other image features), into image objects that correspond to

real objects (Skurikhin, 2009). Different algorithms have been developed and used to find objects from given image layers including the multi-resolution image segmentation. This algorithm is widely used for segmenting canopy height models using eCognition software (Baatz & Schape, 2000). It employs a bottom-up process to connect similar pixels that represent a homogeneous forest structure in the study area. This process is a spatial clustering technique that would place each pixel in the image into a segment based on the degree of similarity to the neighboring pixels, so it becomes more spatially meaningful than an arbitrary 1 × 1 m pixel.

In order to perform the multi-resolution image segmentation, the algorithm requires some parameters to be fed as seen in Table 5. The estimation of the scale parameter tool (ESP), developed by Lucian et. al. (2010), was employed to automatically determine the scale parameter. Two sets of raster images, each with 13 bands, were created using the multi-resolution image segmentation algorithm. The first was generated using 3m neighborhood radius, while the second was generated using 5m neighborhood radius. The image objects, or polygons, of connected pixels that represent homogeneous forest units were created; and the mean value of all the height metric image pixels falling within the image object was taken as its attribute value. After assigning height metric attributes to all the image objects of the plots, they were stored as shapefiles to be processed in R in order to be used to build regression models. The known aboveground biomass of each plot, calculated based on *in situ* data and allometric equation, was included in the model as the dependent variable. Decision tree regression equations, employs rule-managed linear regression to predict the dependent variable, were developed from the LIDAR percentile height values of each image object. Using Cubist software, regression models to estimate AGB per square meter in the image segments were developed.

Table 5. Image segmentation parameters.

Parameter	**Value**
Use of Hierarchy	1
Starting scale level1	1
Step size level1	1
Starting scale level2	1
Step size level2	3
Starting scale level3	1
Step seize level3	5
Shape	0.5
Compactness	0.5
Number of loops	100

The size of the neighborhood affects the calculation of LIDAR derived height metrics statistics, and therefore it affects the performance of the regression model. It is important to determine which of the two neighborhood sizes (3 m or 5 m) is the most appropriate to be used to calculate LIDAR height metrics statistics in the study area. Thus, a 10-fold cross validation approach was applied to train models to evaluate the model performance. For each fold (10% of the data), regression models were generated using data outside this fold (90% of the data). Thus, a total of 10 models for each neighborhood size were built. As seen in Table 6 and 7, the following statistics were used to evaluate the model performance with the different neighborhood sizes: root mean square error (RMSE), correlation coefficient (R) between predicted target values and reference target values, and adjusted coefficient of determination (R^2). These statistics were calculated on the training set as well as the validation set. Furthermore, Table 8 and 9 show the statistics of the model performance using all the data with the two neighborhood sizes.

Table 6. The statistics of the 10-fold cross validation approach using the 3 m neighborhood size to evaluate the model performance.

	Training Set			Validation Set		
Fold#	**RMSE**	**R**	**R^2**	**RMSE**	**R**	**R^2**
1	13.83864	0.7054886	0.4954818	15.524623	0.5947681	0.32565117
2	14.38525	0.6379581	0.4043549	17.984837	0.3451831	0.08085361
3	13.71380	0.7259871	0.5249459	12.438358	0.4219661	0.14380768
4	14.72932	0.6588072	0.4315115	8.229039	0.8086516	0.63887035
5	13.38331	0.6871066	0.4697483	19.181549	0.5743643	0.30309010
6	15.12956	0.6143610	0.3746848	11.701434	0.5092722	0.22569258
7	11.44226	0.7815071	0.6090234	25.477416	0.5374108	0.25788911
8	11.26868	0.8276651	0.6836359	16.002185	0.4977096	0.21352001
9	13.08538	0.7415483	0.5478934	14.708022	0.5953108	0.32632518
10	15.15773	0.6203578	0.3820976	9.889388	0.5389714	0.26092721
Average	**13.61339**	**0.700079**	**0.492338**	**15.11369**	**0.542361**	**0.277663**

Table 7. The statistics of the 10-fold cross validation approach using the 5 m neighborhood size to evaluate the model performance.

	Training Set			Validation Set		
Fold#	**RMSE**	**R**	**R^2**	**RMSE**	**R**	**R^2**
1	9.877935	0.8870133	0.7857676	12.20700	0.6788549	0.4363369
2	9.883728	0.8667939	0.7501362	18.43174	0.7581887	0.5555251
3	9.993537	0.8764812	0.7671102	15.96126	0.5782398	0.3026642
4	9.331044	0.8920627	0.7947988	13.04494	0.6606591	0.4096358
5	9.918873	0.8885575	0.7885226	10.37690	0.6924297	0.4557979
6	9.769111	0.8895798	0.7903492	14.77400	0.6435909	0.3875824
7	10.756413	0.8439984	0.7109503	13.18081	0.6601536	0.4101575
8	9.597458	0.8953195	0.8006477	12.05046	0.8110344	0.6414804
9	9.947189	0.8710412	0.7575528	17.85925	0.8296321	0.6741207
10	10.449998	0.8661168	0.7489743	14.78610	0.6443782	0.3844455
Average	**9.952529**	**0.877696**	**0.769481**	**14.2672**	**0.695716**	**0.465775**

Table 8. The statistics to evaluate model performance using all data with the 3 m neighborhood size.

RMSE	**R**	**R^2**
14.09802	0.6613797	0.4351728

Table 9. The statistics to evaluate model performance using all data with the 5 m neighborhood size.

RMSE	**R**	**R^2**
10.16713	0.8722238	0.7597432

D. Results

As seen in Table 6 and 7, higher average R and R^2 values of the training and validation sets are observed with 5 m neighborhood (training R= 0.87, training R^2= 0.76, validation R= 0.69, validation R^2= 0.46) compared to the 3 m neighborhood (training R= 0.70, training R^2= 0.49 , validation R= 0.54 , validation R^2= 0.27). The average RMSE is lower with the 5 m neighborhood (training RMSE= 9.95, validation RMSR=14.26) compared to the 3 m neighborhood (training RMSE= 13.61, validation RMSR= 15.11). These statistics indicate that Cubist models performed much better on the 10-fold training and validation data (of the cross validation approach) generated using the 5 m neighborhood radius. It is noted that the model performance of the validation data is lower than the training data even with the 5 m neighborhood radius. In order to increase the performance on the validation data, a larger neighborhood size can be used. However, due to the relatively small plot size (7 m radius), it will not be reliable to used neighborhood size larger than the size of the training plots. This will present unwanted information outside the plots, and will affect the accuracy of the model.

Additionally, the model performance of all data using the 5 m neighborhood (RMSE= 10.16, R= 0.87, R^2= 0.75) is significantly better than the 3 m neighborhood (RMSE= 14.09, R= 0.66, R^2= 0.43). The R and R^2 values of the 5 m neighborhood are high enough to ensure the algorithms can provide reliable and accurate predictions on the data set. Since the 5 m neighborhood corresponded to the best model performance, it was selected to calculate LIDAR statistics in order to estimate biomass for the entire study area. The image of the study area was segmented and the model was applied to each segment. Plots of known AGB, calculated from ground reference DBH measurements using allometric equations, were then utilized as training data to generate a model for predicting AGB in the remainder of the image. Biomass density of

the 20 sampling plots ranges from 0.103 to 4.279 (kg/m²), with an average of 1.328 ± 0.243 (Table 10). The use of the Cubist model to utilize LIDAR percentile height statistics to image segmentation resulted in a segment-level aboveground biomass map of the study area as seen in Figure 13. The total number of the image segments is 715. While the size of the segments ranges from 42.25 m² to 20,004.50 m², with an average of 2,445.37 ± 117.88 m². The aboveground biomass density per segment ranges from 0.23 to 13.18 (kg/m²), with an average of 5.16 ± 0.14. While the total aboveground biomass per segment ranges from 0.90 to 76.89 kg, with an average of 29.88 and a total of 14,850.26 kg.

Table 10. Above ground biomass of the sampling plots estimated using *in situ* measurements and allometric equations.

Plot #	**AGB (kg/m²)**	**Plot #**	**AGB (kg/m²)**
1	2.301	**11**	2.262
2	1.559	**12**	2.527
3	2.254	**13**	0.459
4	0.610	**14**	0.407
5	1.495	**15**	0.306
6	0.882	**16**	0.417
7	4.279	**17**	0.218
8	1.475	**18**	0.103
9	2.053	**19**	0.253
10	2.061	**20**	0.645

Using Esri's ArcGIS for Desktop 10.2, biomass estimates are classified into 10 classes from the lowest to the highest. The results indicate that 49% of the study area has a relatively low biomass density with values less than 4.15 (kg/m²), 23% of the study area has a relatively moderate biomass density with values ranging from 4.16 to 8.01, and 28% of the study area has a relatively high biomass density with values ranging from 8.02 to 13.17(kg/m²). Furthermore, a canopy height model (CHM) was created of the whole study area using the classified LIDAR

points (class 5: high vegetation) as seen in Figure 14. The maximum height value of the canopy model pixels is 7.86 m, which means that no trees in the study area exceed this height. The average height value of the pixels is 3.03 m while the minimum height value is 0.12m.

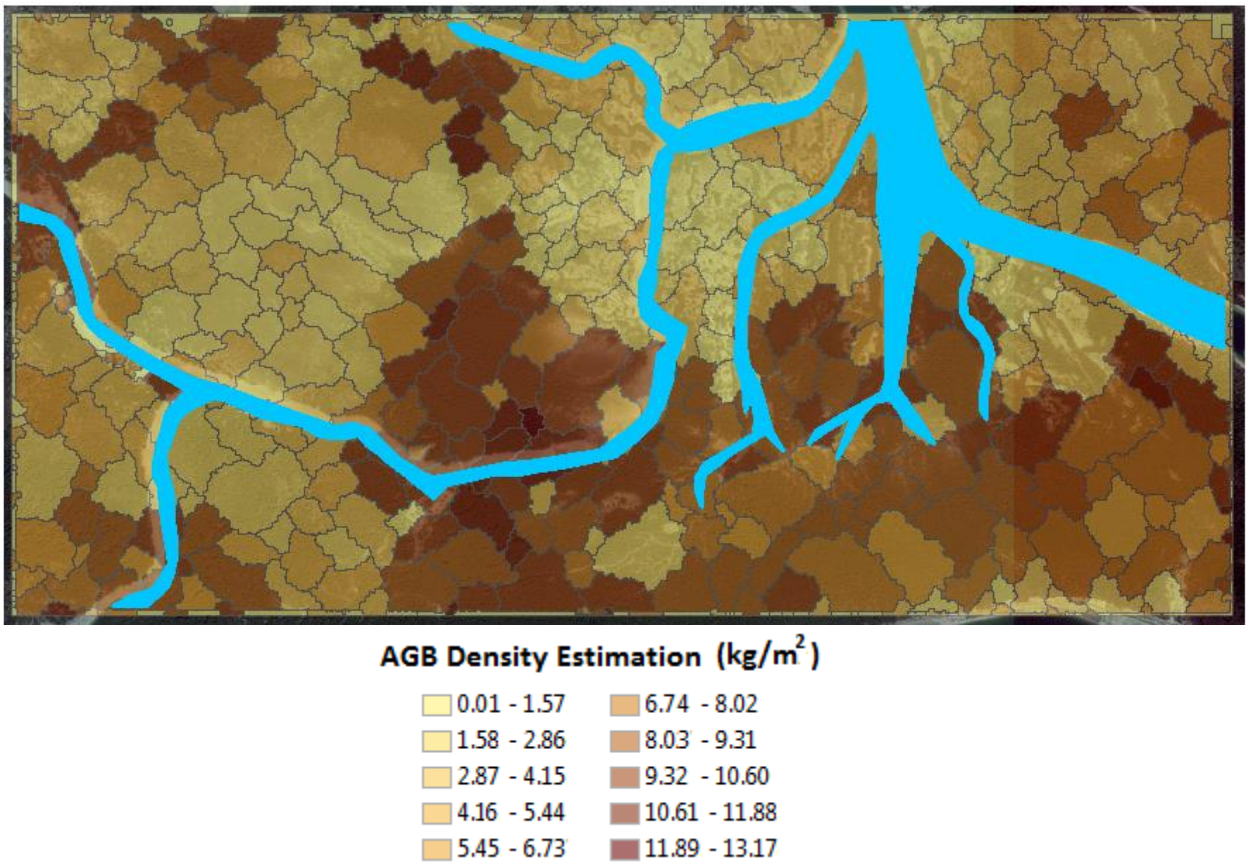

Figure 13. The map represents aboveground biomass density (kg/m²) of each segment in the entire study area. Biomass estimates are differentiates into 10 classes from the lowest to the highest.

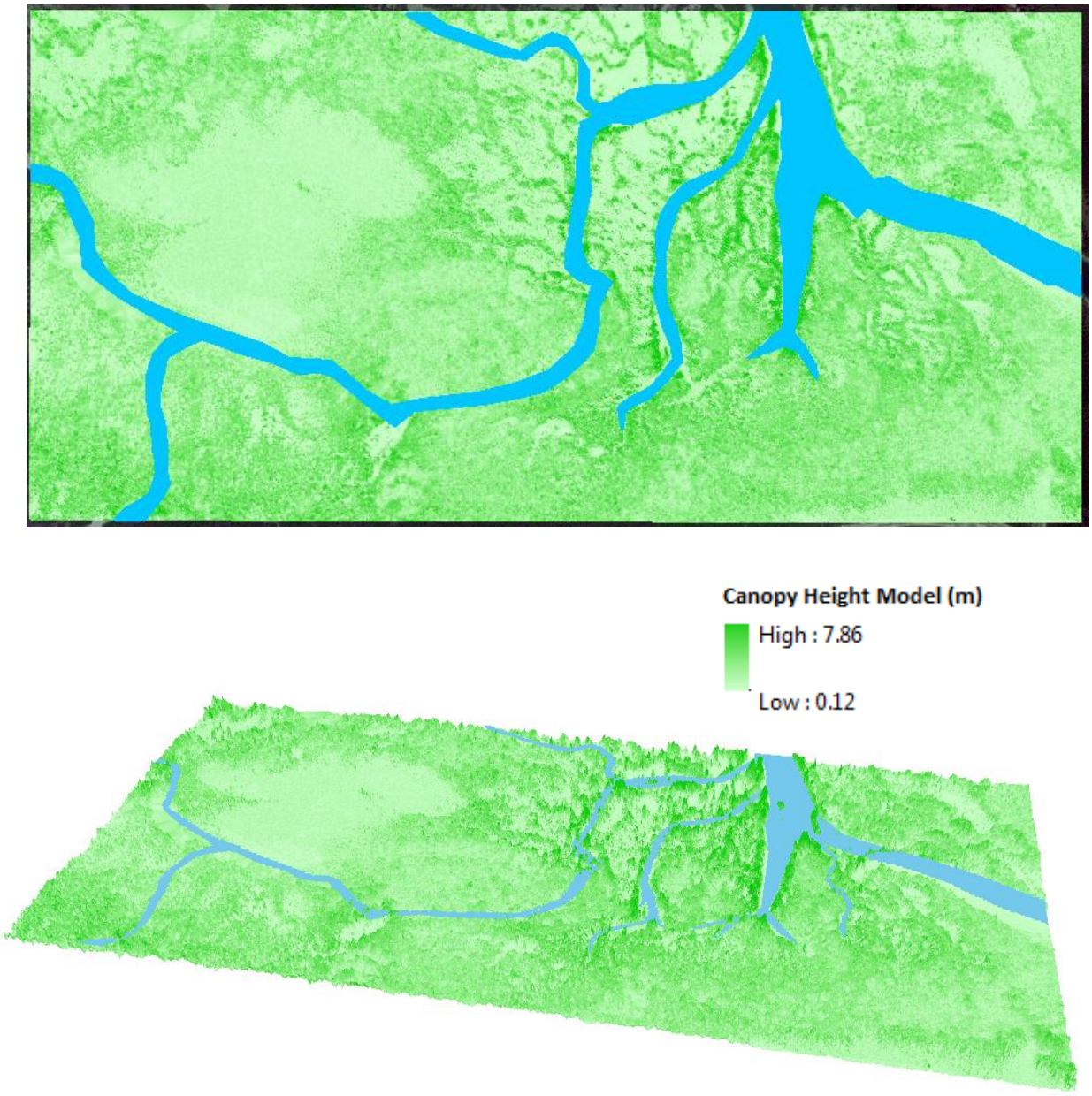

Figure 14. Canopy height model of the study area created in ArcMap and ArcScene (10.2). The darker green color indicates higher pixel values while the lighter green color indicates lower pixel values.

E. Discussion and Conclusion

Several studies attempted to estimate aboveground biomass for various types of forests using segmentation approach, while other studies attempted to estimate aboveground biomass using multiple percentile height statistics. The current study combined the two approaches with a machine learning environment and ground reference data. Riggins et al., (2013) research is considered one of the first attempts to combine these two methods together. According to Riggins et al., combing the two methods together provide a powerful approach for deriving forest biophysical variables from LIDAR data. Additionally, this study used spatial aggregation methods to estimate aboveground biomass from small foot-print airborne LIDAR data. Similar methods can be used to estimate other forest biophysical characteristics such as basal area or leaf area index of the whole study area. However, the collection of a limited number of ground sampling plots for training purposes is still required.

The present study is considered as the first attempt to estimate and map aboveground biomass of *Avicennia marina* forest in Eastern Mangrove Lagoon National Park, Abu Dhabi. By utilizing LIDAR percentile canopy height and image segmentation in a machine-learning algorithm and *in situ* reference data, a map of aboveground biomass density per segments was successfully produced. Segments- level processing divides the data into homogenous forested units according to the values of the neighboring pixels. Therefore, selecting the best neighborhood size is critical for calculating LIDAR height metrics, and it influences the accuracy of the regression model. Due to the small size of the circular sampling plots (7 m radius each), the choice of neighborhood size is limited. In this study two sizes were tested, a 3 m radius and a 5 m radius. The latest resulted in the highest model accuracy (RMSE= 10.16713, R= 0.8722238,

R^2= 0.7597432). However, if the training plots were larger in size, larger neighborhood sizes could be tested in order to increase the model performance.

The number of the percentiles height layers affects the accuracy of the model performance as well. The fewer number of percentile heights means that less information about a canopy structure is taken into account. Some studies used 5 or 6 percentiles heights (Lim and Treitz, 2004; Mariappan et. al., 2012); however, this study used 11 percentiles heights (0, 5, 15, 25, 35, 45, 55, 65, 75, 85,100th) to provide better information about the canopy structure at more elevations. Although creating more percentiles layers increase the computing time, the small study area and the small LIDAR point cloud data (less than a million points) did not lead to any computing disadvantages.

The biomass model presented in this study can be very useful in monitoring mangrove status and biomass conditions, leading to a better management of the forested areas in Abu Dhabi. Landscape mangrove biomass estimates are needed because of the importance of mangrove in the carbon cycle. By quantifying the amount of forest biomass, carbon emission and storage can be easily estimated. Thus, measuring mangrove extent, structure and biomass is vital for addressing climate change mitigation and adaptation.

IV. Soil Characteristics in Eastern Mangrove Lagoon National Park, Abu Dhabi

A. Summary

Soils serve as a medium for plants' growth and provide nutrients, water, and minerals to them. Understanding soil properties is essential to a proper management of soil for maintaining plants health. Thus, soils in Eastern Mangrove Lagoon National Park were tested for their physical and chemical properties, fertility status, and organic matter content (OM). A total of 72 soil samples were collected from 36 sites at two depths. The results show that the soils are clayey on the surface and sandy beneath. The salinity test indicates highly saline soils with ECe values ranging from 48.60 to 85.70 dSm^{-1}, which exceeds seawater salinity. The pH test indicates values ranging from 6.78 to 7.72, with 86% of the soil samples being neutral, while 14% are slightly alkaline. The high values of SAR and ESP (ranging from 53.57 to 80.69 $(mmoles/\mathrm{L})^{0.5}$ and 43.74 to 54.08%, respectively) indicate high Na due to the effect of seawater. The high $CaCO_3$ amounts (ranging from 68.40 to 88.30%) increase the soil buffering capacity causing pH to stabilize above the optimal range and limiting the amounts of available nutrients. Additionally, the rich OM content (ranging from 2.06 to 6.8%) associated with soft mud sediments of fine silt and clay supports forest development. The total nitrogen values (N) are high (ranging from 34 to 1330 mg kg^{-1}) compared to the values of available phosphorus (P) (ranging from 11 to 74 mg kg^{-1}). The low P availability and efficiency to the plants is attributed to P fixation with high amounts of $CaCO_3$ in the soil. The soil tests show higher concentration of ammonium acetate extractable K (ranging from 245 to 799 mg kg^{-1}) compared to soluble K from soil saturation extract (ranging from 156 to 198 mg kg^{-1}). The high amounts of K and N can be attributed to organic rich mud and decomposed OM accumulated over years by the mangrove

root system, which releases K and N into the soil to keep mangroves healthy even in harsh environments. The saline-sodic soil conditions are not ideal to mangrove growth. Therefore, actions should be taken to enhance the soil conditions.

B. Introduction

Evaluating the spatial distribution and the areal extent of mangrove forests has been a research priority in UAE due to the significant reduction in the forest area as a result of human and natural disturbances. Various environmental factors including geomorphology, tidal range, and climate conditions tend to influence mangrove forests' productivity and distribution; some types of mangrove trees are more tolerant than others to variations in these environmental factors (Cintron et al., 1985; English et al., 1997; Tam & Wong, 1998). Notably, soil characteristics are one of the most important environmental factors that have a direct influence on mangrove structure, productivity, and distribution. Several researchers have examined the link between mangroves structure and various soil conditions. They found that the variation in trees' height and productivity are due to the temporal and spatial variation of soil properties such as soil salinity, soil nutrient availability, and soil fertility (McKee, 1993; Feller et al., 2002). Therefore, it is salient to comprehend the soils' physical and chemical characteristics from mangrove plantation to evaluate vegetation structure (Boto & Wellington, 1984).

In the last few years, researchers have conducted extensive studies regarding UAE soils (Shahid et al., 2014; Abdelfattah & Shahid, 2006; 2007). However, there is a lack of detailed research of the mangrove soils with an impetus to assess or explore mangrove forests' distribution and status. Data about soil properties and characteristics such as soil fertility can help in planning the best action of governing the ideal ecosystem and enhancing the soil quality. Scientifically, as a medium of growth, soil requires supplying sufficient nutrients and possessing

good characteristics in order to increase the performance of a tree and in turn establish better forest ecology for wildlife while at the same time balancing the environmental condition (Rambok et al., 2010).

The main objective of the present work is to understand the key characteristics of soils in Eastern Mangrove Lagoon National Park in Abu Dhabi. This is achievable through testing the physical and chemical properties, fertility (nutrient) status, and organic matter contents. Another objective of this work is to create soil maps, using inverse distance weighted (IDW) interpolation in ArcGIS software, specific to the area of study. These maps will show the spatial variation of soil characteristics at different sites and different depths in order to indicate whether or not soils' characteristics effect the spatial distribution of *Avicennia marina*.

In conducting the soil tests, four steps were involved: 1) collection of a representative soil samples, 2) analysis of the samples in a soil testing laboratory, 3) interpretation and understanding the analysis results, and 4) management recommendations to enhance the soil. The results of three months of study (from February until April, 2014) were summarized, and the important or interesting indications and trends were discussed.

C. Materials and Methods

1. Soil Investigation

Ideally, sampling involves selection of individuals from a population to estimate the entire population's properties. A sampling design entails the most effective and efficient method of choosing samples, which will in turn aid in estimating the population properties. Therefore, the first salient step in the soil testing is the collection of soil samples (Carter & Gregorich, 2006). Several methods of soil sampling are applicable including stratified sampling, stratified

systematic unaligned sampling, random sampling, as well as stratified random sampling. In the current study, the stratified systematic unaligned sampling method was used. This method combines randomness and stratification with a systematic interval. In this way, it introduces more randomness than just starting with x, y coordinate for the first sample in each stratum (Jensen, 2005).

The soil investigation was successfully conducted (from February to April 2014), despite the difficulties experienced in getting deep sub-surface soil samples in mangrove swamps. The extensive root system and the high water table limited the sampling depth to around one meter. The holes dug in the swamps tended to fill with water in seconds because of the considerably high water table. Mostly, mangrove soil occurs as a very soft liquid mass (slaked mud) and shows modest profile differentiation up to this depth.

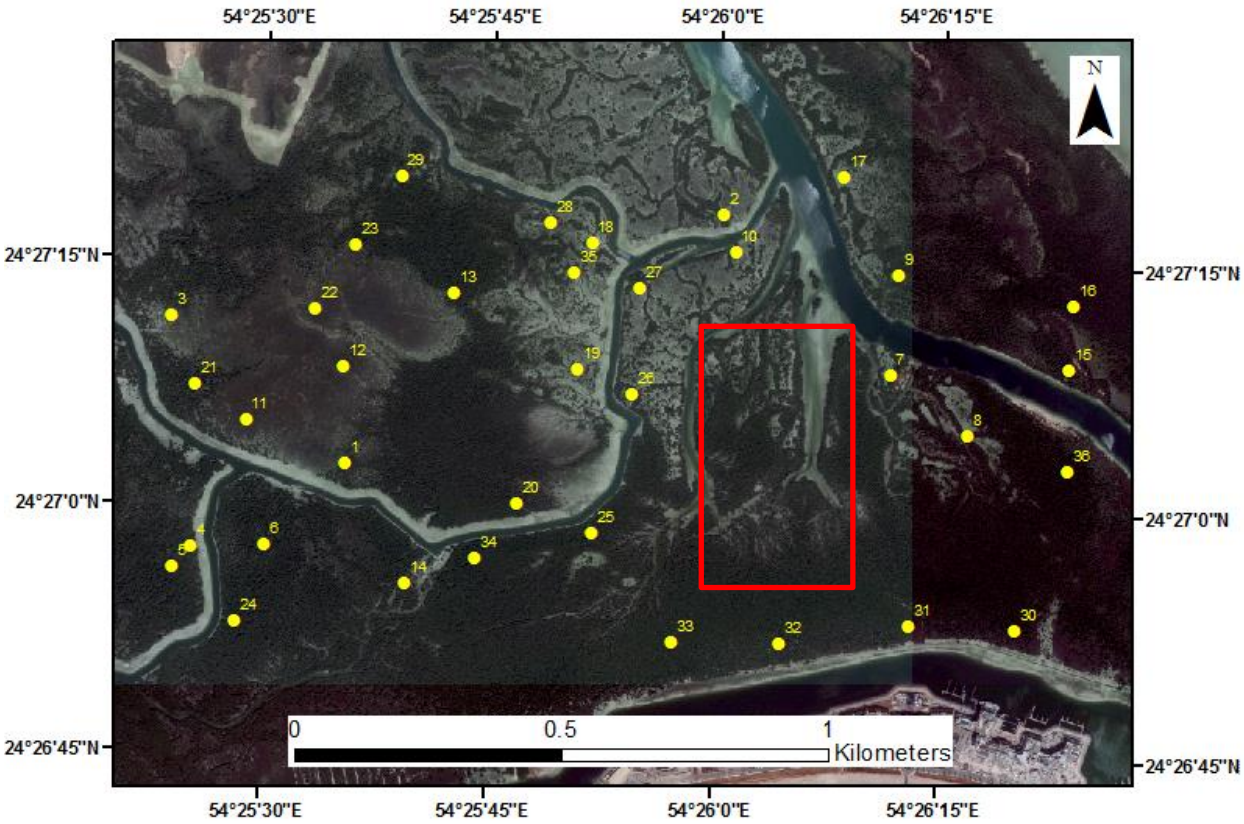

Figure 15: The locations of soil sampling sites in the study area.

As shown in Figure 15, a total of 36 sites were located in the study area using Global Positioning System (GPS) equipment. However, the red box indicates the area where no soil samples could be collected due to the high water level. Accordingly, for each accessible site, soil samples were collected using standard soil sampling augers (Figure 16) at depths of 0-50 cm and 50-100 cm. Thus, a total of 72 soil samples were collected from 36 locations. About one kilogram of soil sample from each location was obtained, and then placed in a clean plastic bag. Subsequently, the samples were sent to the laboratory for analysis to determine their important physical and chemical characteristics.

Figure 16: Collecting soil samples using augers in February 2014.

2. Laboratory Analysis of Soil Samples

Laboratory analysis of the soils is necessary to verify the collected data in order to determine soil characteristics that cannot be estimated accurately based on *in situ* observation. The laboratory analysis of the 72 samples was conducted at the Central Analytical Laboratory (CAL) of the Dubai based International Center of Biosaline Agriculture (ICBA). The analysis

was performed using the standard procedures from the United States Department of Agriculture-Natural Resources Conservation Service (USDA-NRCS) as described in the Soil Survey Laboratory Methods Manual (Burt 2004). The soil analysis included the testing of soil physical and chemical characteristics, nutrient status, and organic matter content. Prior to soil analyses in the laboratory, soil samples were air-dried, and then ground to pass a 2 mm sieve. The material retained (gravels, shells, roots) on 2 mm sieve was discarded. Below is a brief description of the soil analysis procedures used in this soil investigation.

2.1. Soil Texture

Soil texture is the percent distribution of sand (2-0.05 mm), silt (0.05-0.002 mm) and clay (<0.002 mm) in a soil samples (< 2mm). Prior to soil texture analyses, the materials which pose a problem in achieving soil dispersion (organic matter, gypsum, soluble salts, and calcium carbonates) should be removed. Since the soil samples from mangrove sites are extremely rich in $CaCO_3$, removing the high amounts of $CaCO_3$ will cause the soil texture to not be representative. Under such conditions, feel test method is used in order to have an apparent soil texture. In this test, a small volume of water is added into a small handful of soil, and then mixed to form a ball until it starts sticking to the analyst hand. The ball is transformed to different shapes to confirm soil texture. Moist soil is rubbed between fingers and observations are made, such as sand feels gritty, silt feels smooth and clay feels sticky. Other soil textures can be determined through finger test as described in Table 11.

2.2.Soil Chemical Analysis

A soil analysis was performed on air-dried soil samples and the results were presented on oven-dried soil basis. The following tests were performed to estimate soil chemical properties:

- Soil Reaction or Hydrogen Ion Activity (pH): Soil pH measures the level of soil alkalinity or acidity, which plays an essential role in controlling the nutrient availability and fixation in the soil (Shahid et al., 2014). A standard pH meter calibrated using buffer solutions was used to measure the pH of saturated soil paste (pHs). The USDA-NRCS classifies soil pH ranges as shown in Table 12.
- Electrical Conductivity of the Saturated Soil Paste Extract (ECe): The electrical conductivity is a standard representation of an indirect measurement of soil salinity, which is an important indicator of the health of the soil (Shahid et al., 2014). Electrical conductivity is related to the amount of salts which are more soluble than gypsum in the soil, although it may contain a small contribution from dissolved gypsum (up to 2 dS/m) (Soil Survey Division 1993). A standard EC meter was used to measure ECe, which is reported as deciSiemens per meter ($dS\ m^{-1}$). Soil salinity classes are given in Table 13.
- Soil Solution Chemistry: This is determined by measuring the ionic composition of soil saturation extract. Using standard titration procedures and equipment such as Flame photometer, the major concentration of cations and anions are determined (Shahid et al., 2014).
- Calcium Carbonate Equivalents (CCE): CCE refers to the calcium carbonates and its equivalent ($MgCO_3$, etc.) in soil. Calcium carbonate, a common substance found in rocks, is the main component of marine organisms shells (Keller, 2007). Calcium carbonate equivalents are vital in controlling the buffering capacity (resistance in soil pH change) of soil as well as nutrients availability. To measure the carbonate level in the soil, the sample was treated with hydrochloride acid (HCl). The evolved carbon dioxide (CO_2) was measured manometrically using a calcimeter. Then, the carbonate amount

was calculated as percent calcium carbonate equivalent regardless of the carbonate's form in the soil sample (e.g. dolomite, sodium carbonate, magnesium carbonate, etc.) (Shahid et al., 2014).

- Sodium Adsorption Ratio (SAR): SAR, which indicates the relative concentration of sodium to calcium and magnesium in the soil saturation extract, expresses the relative activity of sodium ions in the exchange reactions with the soil (Stahl & Ramadan, 2011). SAR indicates the balance between the amount of sodium in saline solution and exchangeable sodium, which adheres to the soil exchange complex (Shahid et al., 2014). The SAR was calculated using the following standard formula:

$$SAR = \frac{Na^{+}}{\sqrt{\frac{1}{2}(Ca^{2+} + Mg^{2+})}}$$

Using inputs for the water soluble cations expressed as milliequivalents per liter ($meq\ L^{-1}$), and SAR expressed as $(mmoles\ L^{-1})^{0.5}$

- Exchangeable Sodium Percentage (ESP): ESP is the amount of saturation of the soil exchange complex with sodium (Soil Survey Staff, 1966). ESP was calculated using SAR values in the following equation:

ESP = [100(-0.0126+0.01475SAR)]/[1+(-0.0126+0.01475 SAR)]

Table 11: Soil texture classes based on shape criteria (Herweg, 1996; Hurni, 1986).

Soil texture	Shape Criteria
Sand	The soil remains loose and single-grained; it can only be heaped into a pyramid.
Loamy sand	The soil contains sufficient silt and clay to become somewhat expensive; it can be shaped into a ball that easily falls apart.
Silt loam	The sample can be rolled into a short, thick cylinder approximately the diameter of a pencil.
Loam	The cylinder can be rolled into a thinner cylinder about 15 cm long.
Clay loam	The thinner cylinder can be bent into U-shape.
Light clay	The U-shaped cylinder can be bent to form a circle that shows cracks.
Heavy clay	The U-shaped cylinder can be bent to form a circle without showing cracks.

Table 12: Soil pH classes (Soil Survey Division Staff, 1993).

Denomination	pH range
Ultra acid	< 3.5
Extreme acid	3.5–4.4
Very strong acid	4.5–5.0
Strong acid	5.1–5.5
Moderate acid	5.6–6.0
Slight acid	6.1–6.5
Neutral	6.6–7.3
Slightly alkaline	7.4–7.8
Moderately alkaline	7.9–8.4
Strongly alkaline	8.5–9.0
Very strongly alkaline	> 9.0

Table 13: Soil Salinity Classes and effects on crops (Soil Survey Division Staff, 1993; Richards, 1954).

Soil Salinity Class	ECe (dS/m)	Effect on Crop Plants
Non saline	0 - 2	Salinity effects negligible.
Very slightly saline	2 - 4	Yields of sensitive crops may be restricted.
Slightly saline	4 - 8	Yields of many crops are restricted.
Moderately saline	8 - 16	Only tolerant crops yield satisfactorily.
Strongly saline	16 - 40	Only a few tolerant crops yield satisfactorily.
Very strongly saline	> 40	Only a few very salt-tolerance grasses and trees will grow.

2.3. Soil Fertility

Soil fertility refers to the amount of major nutrients in the soil including nitrogen, phosphorus, and potassium.

- Nitrogen (N): Standard Kjeldahl equipment was used to measure the amount of nitrogen. The sample was digested at high temperature and then the nitrogen is absorbed in acid which was measured through standard titration (Burt, 2004).
- Phosphorous (P): The amount of phosphorous was determined colorimetrically after using a standard sample preparation procedure (Burt, 2004).
- Potassium (K): The amount of potassium was measured in 1N ammonium acetate extract by a Flame photometer (Burt, 2004).

2.4. Soil Organic Matter

Plant and animal remains at different decomposition states in addition to the products of root exudation and cells and tissues of soil organisms, make up soil organic matter. Soil organic matter has several positive impacts on soil's physical and chemical properties, and on soil's capacity to regulate the ecosystem (Brady & Weil, 1999). The presence of organic matter is important for the quality and function of the soil. For upland soils, the amount of organic matter content normally ranges from 1% to 6% of the total topsoil mass. While for desert soils, the total topsoil mass contain less than 1% organic matter (Troeh & Thompson, 2005). Soil organic matter acts as a major sink and source of soil carbon. Organic carbon capacity to affect plant growth, both as an energy source and as a catalyst to make nutrients available, makes organic carbon an important constituent of the soil (Edwards et al., 1999).

Soil organic matter was determined by igniting the samples at 450°C after they have been dried at 105°C in order to remove the moisture. The amount of weight loss after ignition was then determined to estimate organic matter contents (Storer, 1984). The following formula was used to calculate the percentage of organic matter (OM %).

$$OM\% = 100 \times \frac{weight\ of\ dried\ soil\ at\ 105°C - weight\ of\ soil\ at\ 450°C}{weight\ of\ dried\ soil\ at\ 105°C}$$

This formula estimates OM by the loss of weight in the soil sample heated at a temperature high enough to burn OM but not so high to decompose carbonates.

D. Results and Discussions

1. Soil Texture

The results indicate that there are seven soil textures in the study area, which are loamy sand (21.6%), silt loam (21.6%), light clay (17.6%), sand (12.1%), clay loam (10.8%), heavy clay (9.5%), and loam (6.8%) (Figure 17). There are significant differences in soil texture among the sites and at different layer depths. At 0 – 50 cm depth, light clay soil and clay loam are the most dominant soil texture types; while at 50 – 100 cm depth, loamy sand, sand, and silt loam are the main types of soil texture (Figure 18). According to Lacerda (2002), soils in mangrove swamps are usually clayey on the surface (fine in texture) and sandy beneath (coarse in texture). This is due to the development of mud in mangroves area over a long period of time in different phases under tidal affects and deposition of wind borne material. Perhaps at an earlier stage, there was a high contribution of sand deposits (from sea and wind), and then the coarser material transformed to finer material through physical weathering. The maps in Figure 19, created using inverse distance weighted (IDW) interpolation, show the spatial distribution of soil texture in the study area.

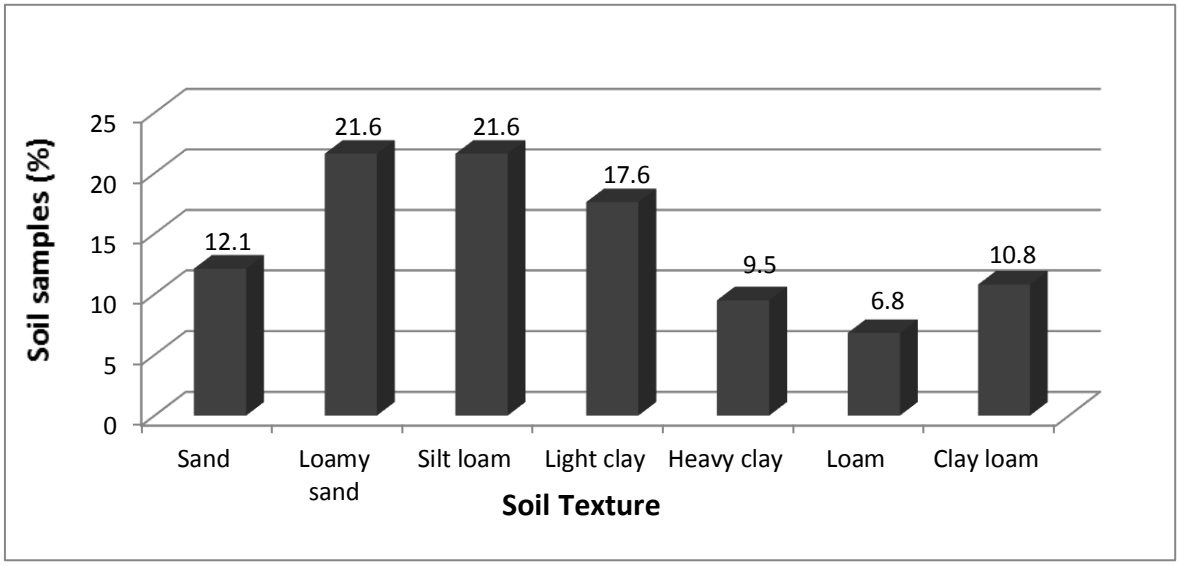

Figure 17: The frequency distribution of soil sample into different types of soil texture.

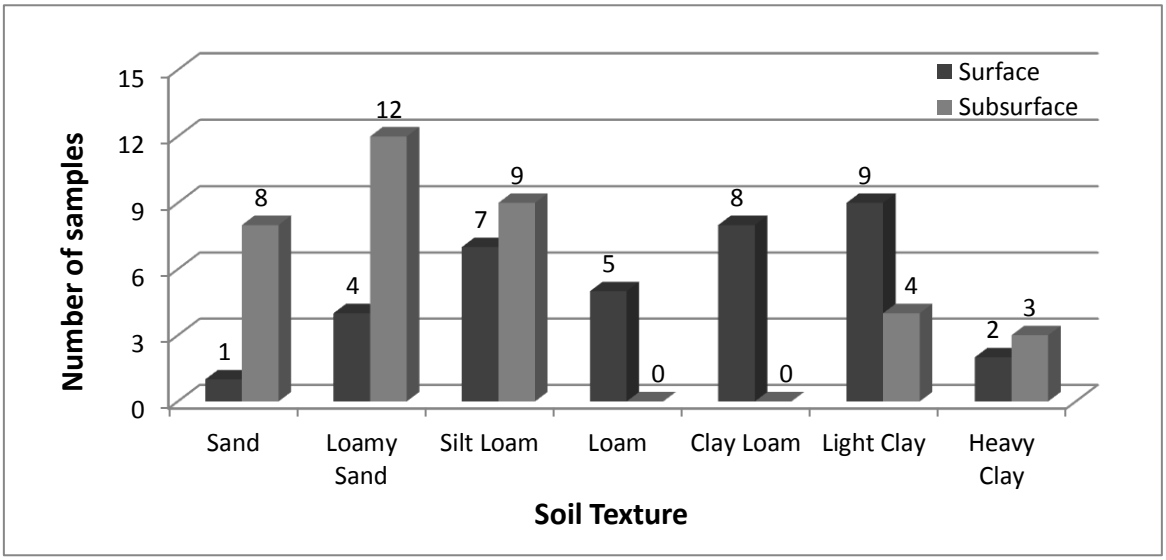

Figure 18: The frequency distribution of soil texture at surface and subsurface.

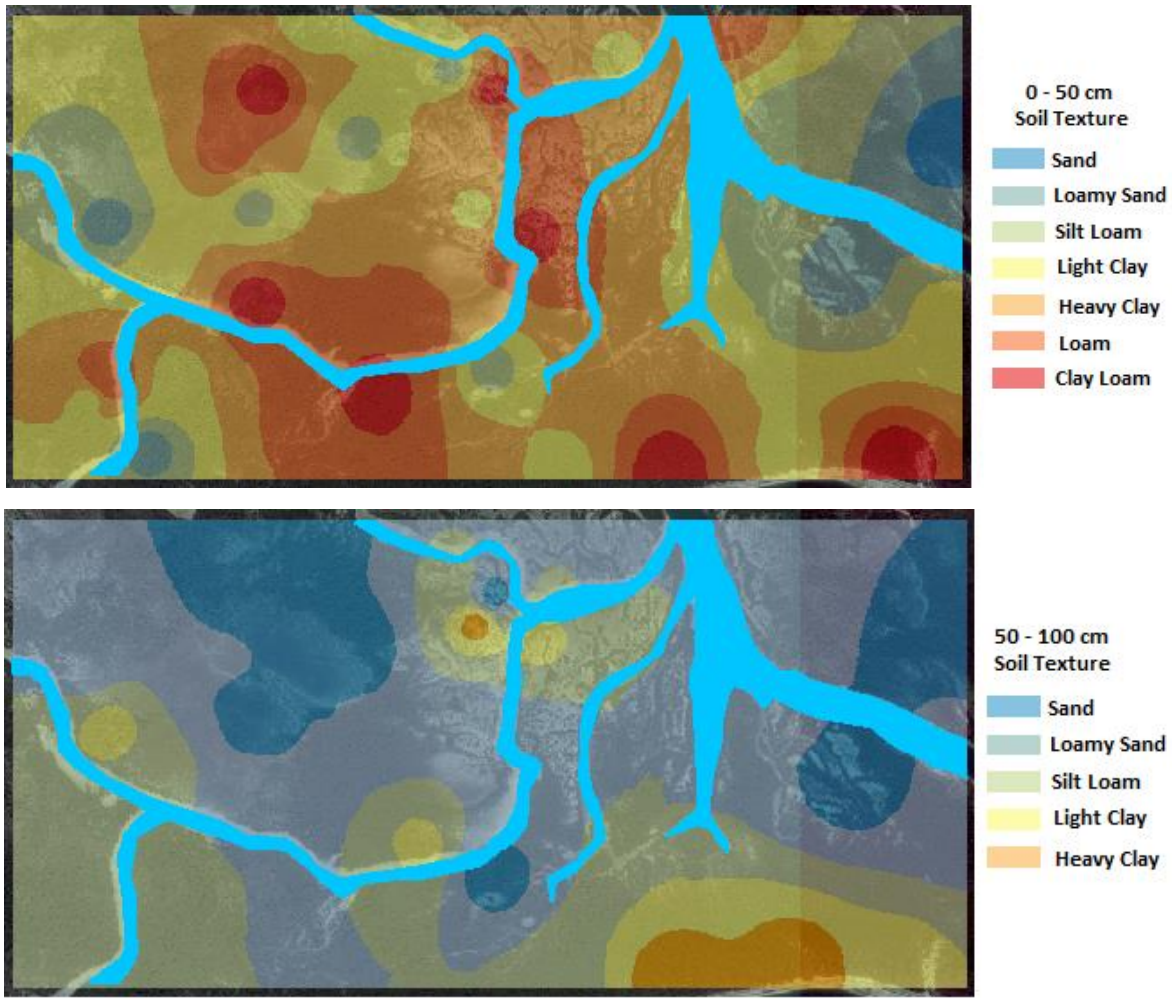

Figure 19: Soil texture maps at 0- 50 cm and 50 – 100 cm depths created using IDW interpolation.

2. Soil Salinity

The results of the analysis indicate that 100% of soil samples in the study area are very strongly saline (> 40 dSm^{-1}) as shown in Figure 20. The actual ECe values range from 48.60 to 85.70 dSm^{-1} with an average of 63.20 ± 0.90 dSm^{-1}. There are significant differences in soil salinity among the sites, while salinity levels slightly vary in different layer depths as seen in the maps of Figure 21. Some of the soils have higher salinity values near the surface (0-50 cm),

while other soils have higher salinity values at greater depths (50-100cm). This shows a heterogeneous trend of soil salinity at depth.

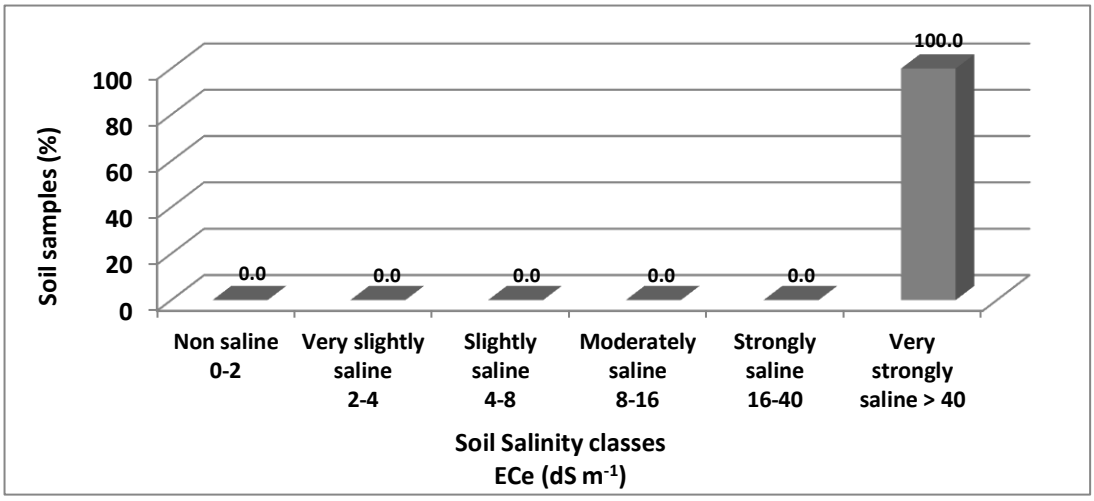

Figure 20: Frequency distribution of soil sample into different classes of salinity.

The salinities of the Arabian Gulf water are among the highest that have been measured in marine water, sometimes reaching as high as 57 dSm^{-1} (Bashitialshaaer et al., 2011). Interestingly, the salinity of mangrove soils in most sites exceeds the salinity of the marine water in the study area. This high concentration of the salts in the mangrove forest results from several factors including high frequency and duration of tidal inundation in the study area, very high temperature, high evaporation rate, and very low rainfall. According to Shahid et al. (2013), the climate of Abu Dhabi is extremely harsh and dry. In summer, the temperature is extremely high and rainfall is close to zero, while winter is warm with little rainfall. However, the evaporation rate for the entire year exceeds rainfall many times over. The ratio of mean yearly evaporation to mean yearly rainfall is nearly 45 to 1. Theses harsh environmental conditions show that *Avicennia marina* in Abu Dhabi have a very high salt-tolerance unlike many other mangrove species. Although most mangrove seedlings may require a low salinity level to survive, their salt

tolerance increases as they grow (Bhosale, 1994). Yet, *Avicennia marina* can adjust up to twice salinity of the ocean seawater (Cintron et al., 1978).

Mangroves, unlike most terrestrial plants, grow in a very harsh environment. They can survive the extreme salinity levels, hypoxic conditions, and sea wave currents. Special physiological functions, such as the respiration by pneumatophores (root system) under water logged conditions, the secretion of salts from glands, the absorption of high amount of water (succulence), and the lack of competition with other plants to live under such hostile saline environment, are the main advantages of mangroves in the coastline areas (Shahid 2012).

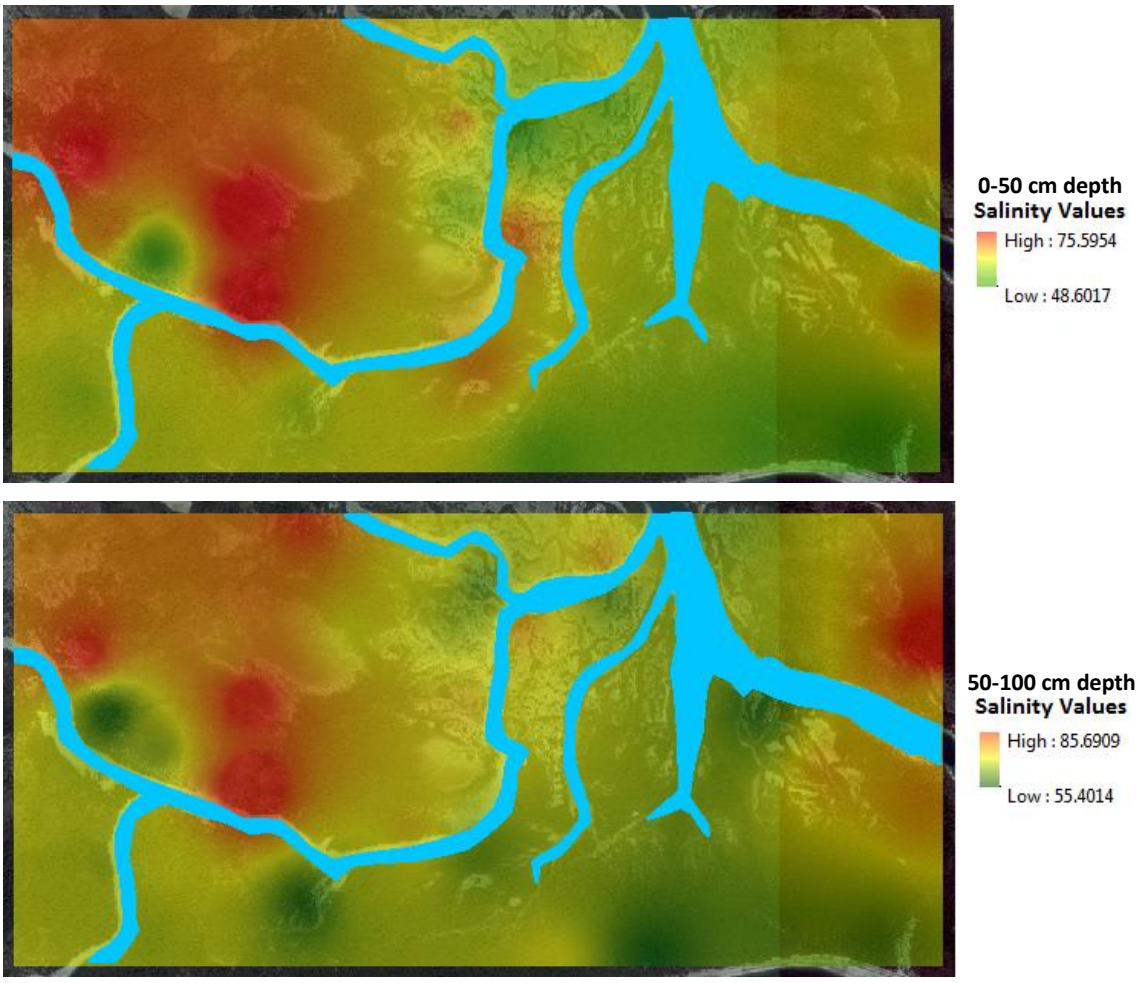

Figure 21: Soil salinity maps at 0 – 50cm and 50 – 100 cm layer depths created using IDW interpolation.

3. Soil pH

The results of soil pH analysis indicate that 86% of the soil samples are neutral and 14% of the samples were slightly alkaline as seen in Figure 22. The values of soil pH varied slightly among the sites. The maps in Figure 23 show the spatial variation of pH levels in the study area. There are not many differences between pH levels at the two layer depths. The pH values range from 6.78 to 7.72 with an average of 7.13 ± 0.02. Usually, soil pH values ranging from 6.7 to 7.3 are the most optimum values for the growth of mangrove trees. However, Lim et al. (2012) mentioned that mangrove seedlings and trees can grow at their maximum rate even with a soil pH range from 5.16 to 7.72 because they can adapt to survive harsh environmental conditions and low nutrient availability. Still, mangroves, especially in germination stage, cannot tolerate extreme pH conditions (outside the range of 5.16 - 7.72) because they will cause nutrients to be inaccessible to the plants. The neutral pH range of most of the soil samples can be related to the dominance of neutral salt (Na and Cl) in the solution chemistry of soils from the study area. Figure 24 clearly illustrates the relative availability of main nutrients critical for plant growth at different pH levels. Most nutrients are most available for plant uptake when the soil pH is neutral (6.6-7.3) to slightly acidic (6.1-6.5). Soils with high pH values can limit iron availability resulting in iron chlorosis. Other nutrients such as manganese, copper, and zinc are also less available at high pH levels (Cooper T., 2009).

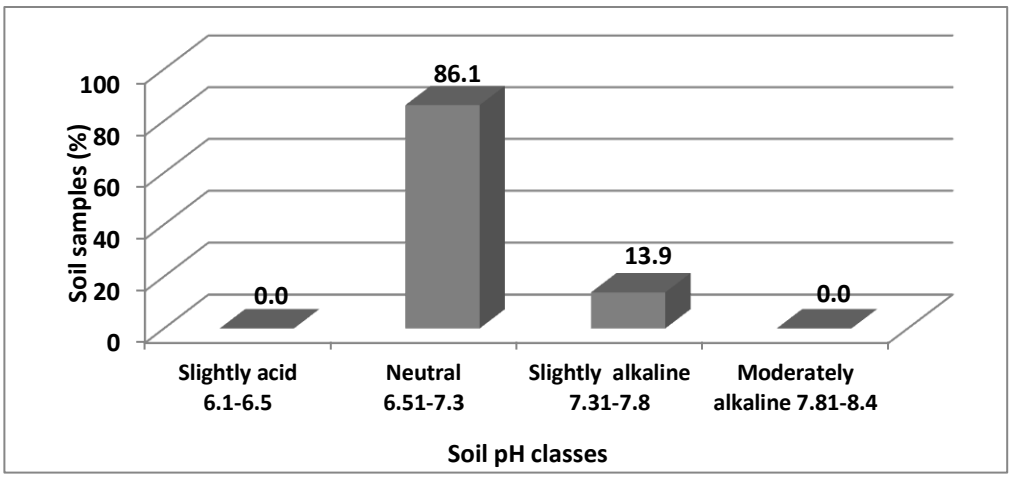

Figure 22: Frequency distribution of soil sample into different ranges of pH .

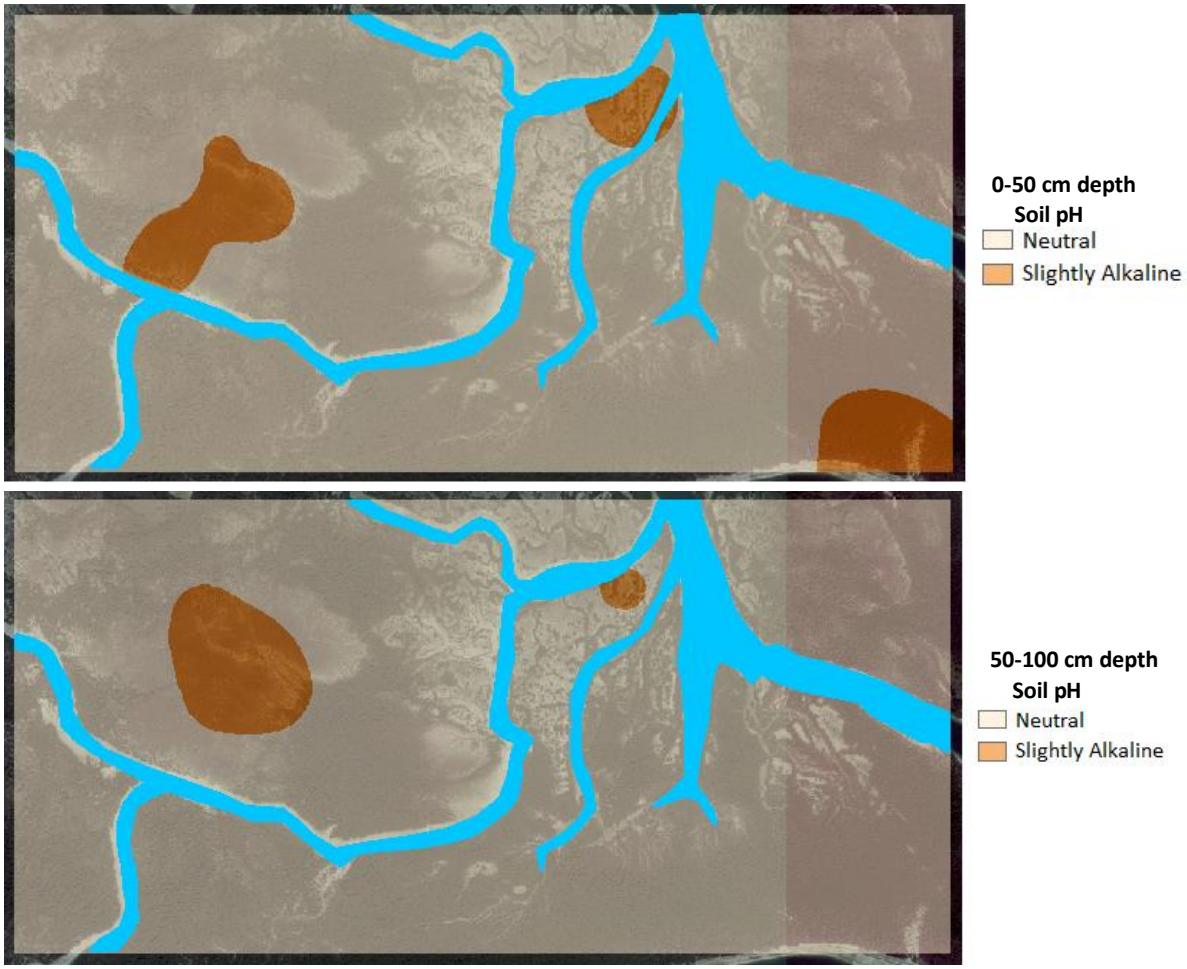

Figure 23: Soil pH maps at 0 – 50cm and 50 – 100 cm depths created using IDW interpolation.

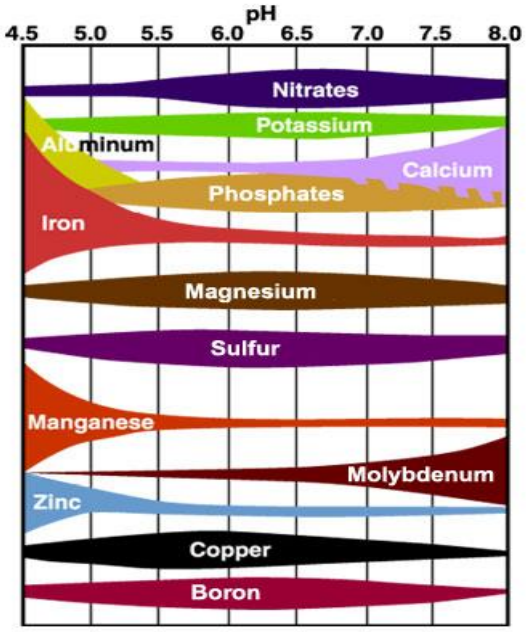

Figure 24: Effect of pH on nutrient availability to the plants. The band width shows the relative availability of each nutrient at different pH levels (Cooper T., 2009).

4. Soil SAR and ESP

The sodium adsorption ratio (SAR) and exchangeable sodium percentage (ESP) range from 53.57$(mmoles/\mathrm{L})^{0.5}$ to 80.69 $(mmoles/\mathrm{L})^{0.5}$ and 43.74% to 54.08%, with an average of 63.41 ± 0.7 and 47.89 ± 0.3%, respectively. Figure 25 and 26 shows the percentage of soil samples with different SAR and ESP values. Usually, soil with SAR levels higher than 13 and ESP levels higher than 15 is classified as sodic. Since mangrove soil in the study area is characterized by high levels of both soluble salts and sodium, then the soil is classified as saline-sodic soil (Figure 27).

In most sites, the values of SAR and ESP increase with depth. Figure 28 and 29 represent maps of the study area that shows the spatial variation in SAR and ESP amounts at two depths. Since SAR and ESP are measures of soil Na concentration relative to other soil cations (e.g. Ca, Mg, and K), the elevated values for SAR and ESP indicate high Na. This is due to the effect of

seawater which has greater Na than other cations. High values of SAR, ESP, and salts restrict the growth of many plants and affect properties of inland soils; however their affect is reduced under submerged conditions. *Avicennia marina* has a great tolerance and can accumulate higher concentration levels.

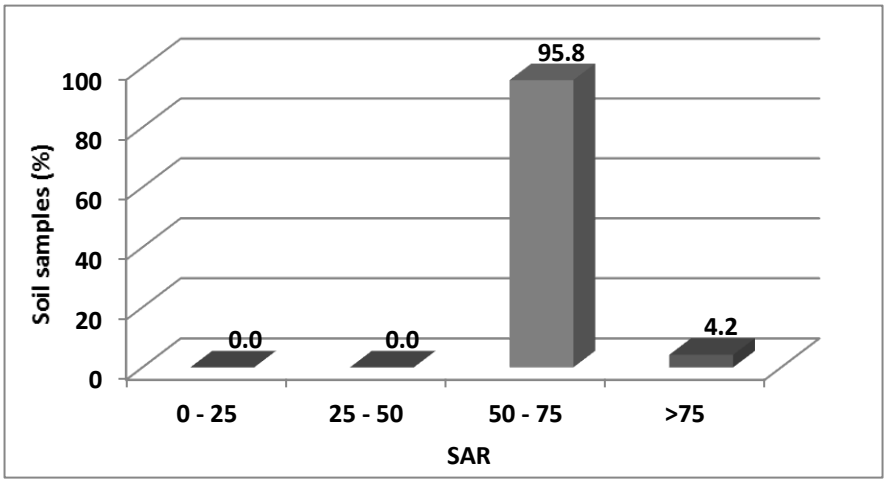

Figure 25: Sodium adsorption ratio of soil samples.

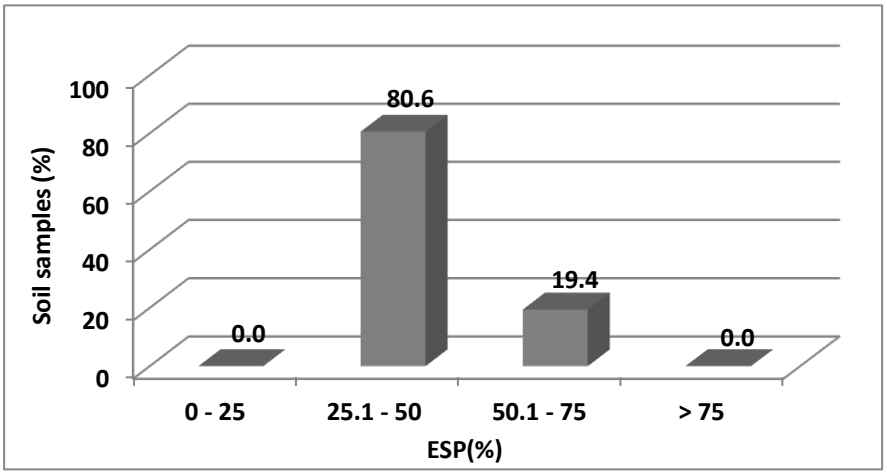

Figure 26: Exchangeable sodium percentage of soil samples.

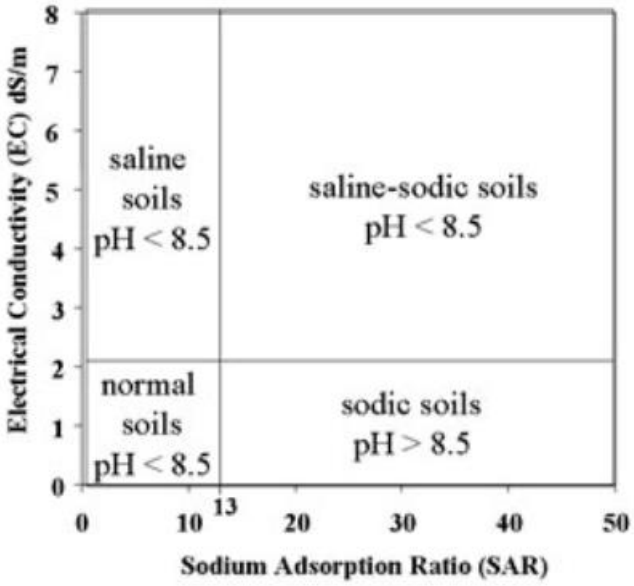

Figure 27: Classes of salt effected soils (Alberta Department of Agriculture and Rural Development, 2014).

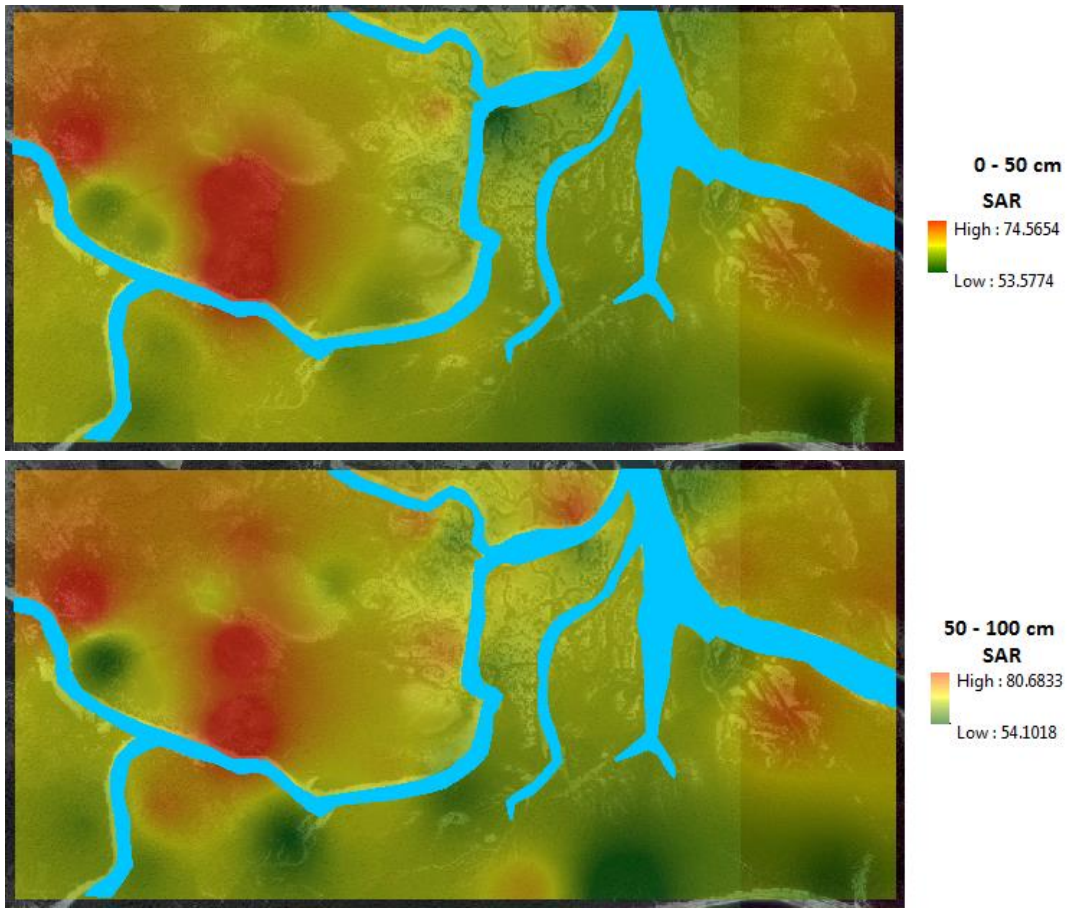

Figure 28: Soil SAR maps at 0 – 50cm and 50 – 100 cm depths created using IDW interpolation.

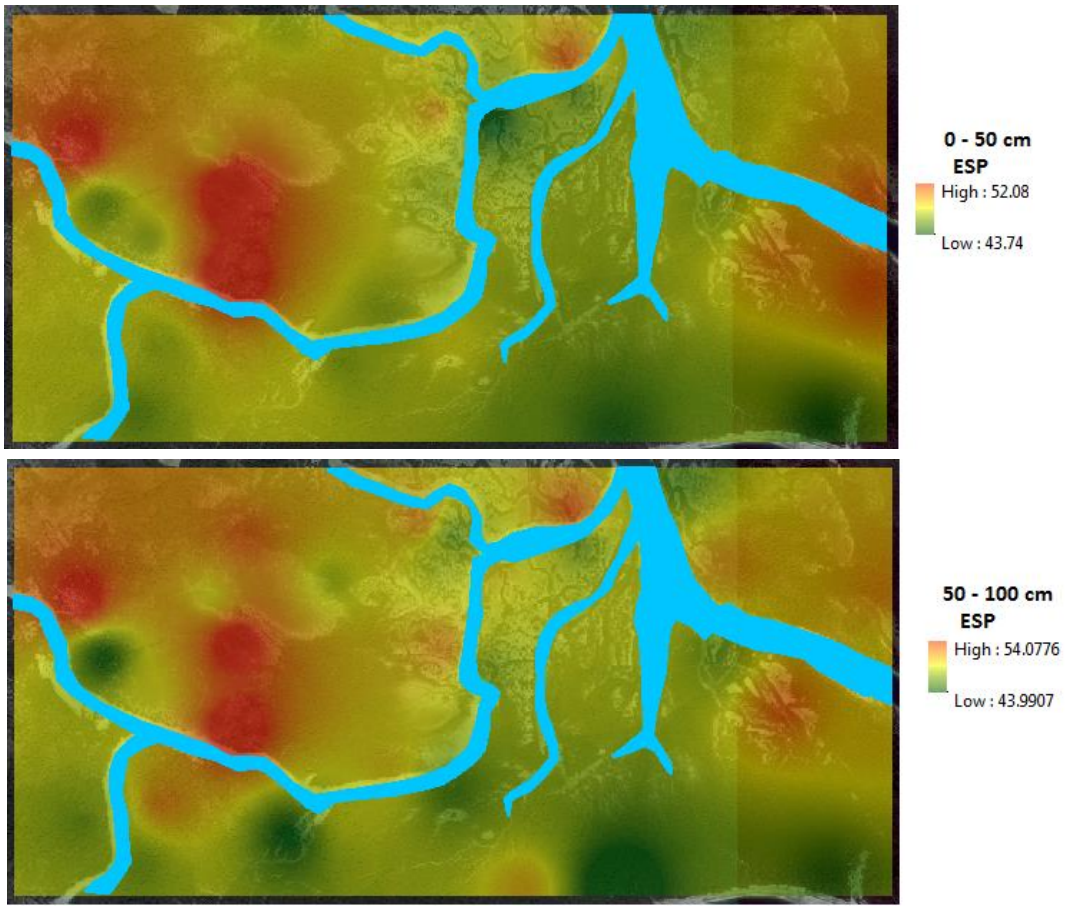

Figure 29: Soil ESP maps at 0 – 50cm and 50 – 100 cm depths created using IDW interpolation.

5. Calcium Carbonate Equivalents

The results show that the percentage of calcium carbonate equivalents (CCE) in the soil samples ranges from 68.40 to 88.30% with an average of 79.96 ± 0.49% (Figure 30). The percentage of CCE increases with depth in most sites. The maps in Figure 31 show the spatial variation in the percentage of CCE at two depths. The $CaCO_3$ amounts in the study area are extremely high due to the high presence of marine organisms' remains and sea shells as observed *in situ*. The high amounts of $CaCO_3$ result in high soil buffering capacity, which means that mangrove soils can absorb more acid without a major change in pH. The high buffering capacity, due to the presence of high $CaCO_3$ levels, stabilizes the pH above the optimum range

where most nutrients are available to plants. This limits the amounts of available essential nutrients to plants such as phosphorus. Additionally, the high amounts of $CaCO_3$ increase soil nitrogen (NH_4) losses through volatilization (Jones et al., 2007).

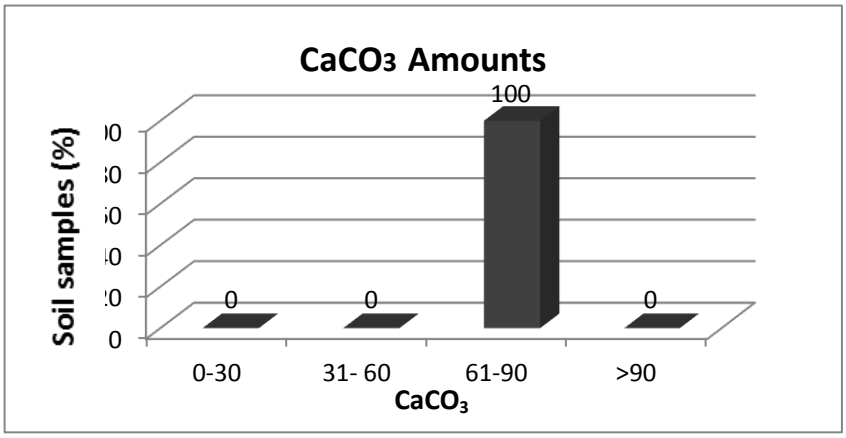

Figure 30: The percentage of calcium carbonate equivalents in the soil samples.

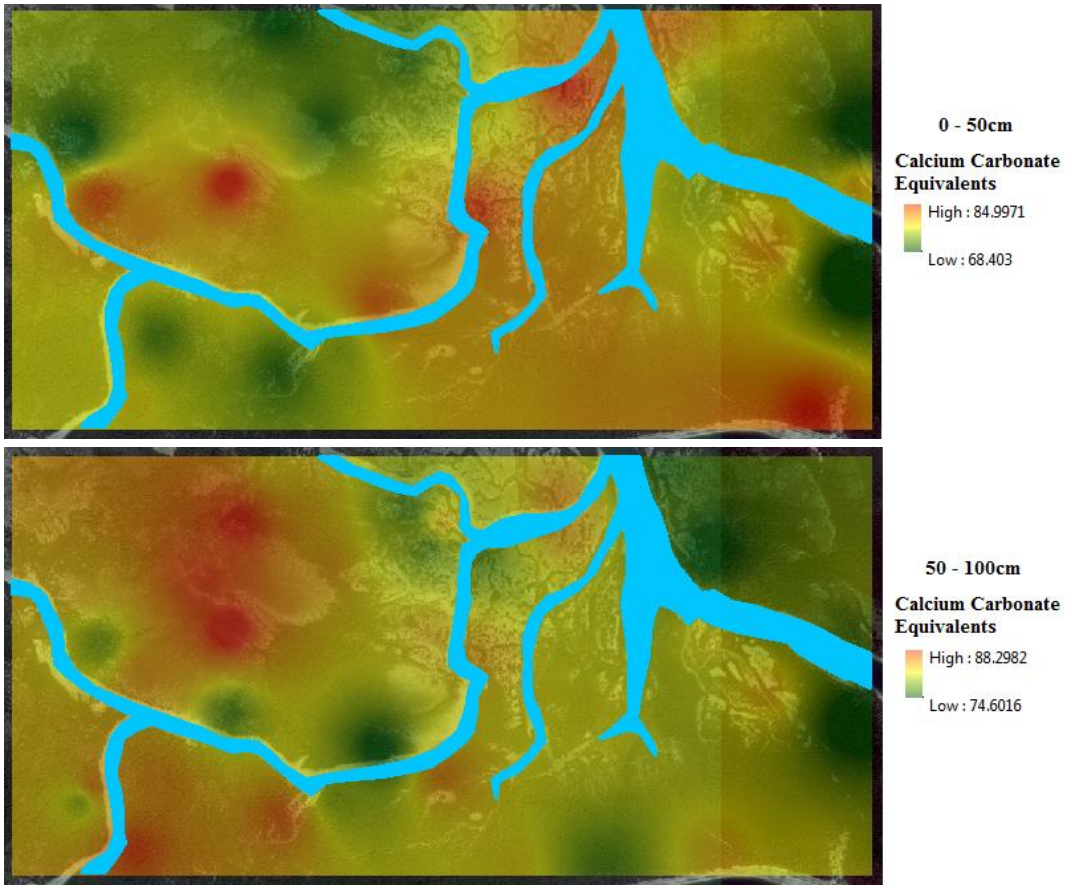

Figure31: Soil maps showing the percentage of CCE at 0 – 50cm and 50 – 100 cm depths created using IDW interpolation.

6. Nutritional Status

There are 16 essential nutrients required for plants in order to grow and develop properly. The three most vital nutrients are carbon (C), hydrogen (H) and oxygen (O_2), supplied from air and water (H_2O), while the other 13 nutrients are grouped into two main categories depending on the various amount needed for the plants. The first category is the macronutrients including N, P, K, S, Ca, and Mg, which are used in relatively large amounts. The second category is the micronutrients such as Zn, Cu, Fe, Mn, B, Cl, Mo, and Co, which are required in relatively small amounts. However, the micronutrients are just as important to plant development as the macronutrients. About 94% to 99.5% of fresh plant material is made up of the three essential nutrients C, H, and O_2, whereas the other nutrients make up the remaining 0.5% to 6%. In fact, nitrogen (N), phosphorus (P), and potassium (K) are the primary nutrients within the group of macronutrients (Barker & Pilbeam, 2006). Therefore, total N, available P, and available K are determined in the present study. Soluble K, which is dissolved in soil water, is also determined from soil saturation extract. Plants take up most of their potassium directly from soluble K.

The results show that the actual values of total nitrogen range from 34 to 1330 mg kg^{-1} (75 to 2926 kg ha^{-1}) with an average of 392 ± 34 mg kg^{-1}. In most sites, the amount of nitrogen increases with depth. Figure 32 shows the distribution of soil samples in different ranges of nitrogen quantities, while the maps in Figure 33 show the spatial variation of total nitrogen at different layer depths. The majority of the soil samples (83%) are distributed between 101-1000 mg kg^{-1} (222-2200 kg ha^{-1}). The high concentration of nitrogen can be related to organic rich mud (plants and animals based) developed over many years. Nitrogen (N) is essential for plant growth and is taken up primarily as nitrate (NO_3^-) or ammonium (NH_4^+) ions (Galitz, 1979). Plants utilize N to synthesize amino acids, which in turn form proteins. In fact, the protoplasm

of all living cells contains protein. It is a component of chlorophyll, which gives the green color to plants and is vital for photosynthesis. The higher concentration of N and its availability to mangroves keeps the mangroves plantation healthy even under stress conditions (Reef et al., 2010).

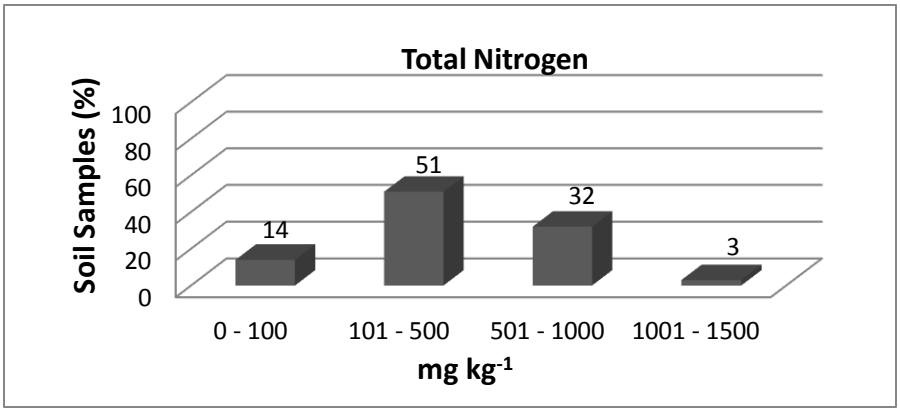

Figure32: Frequency distribution of soil sample into different ranges of total N.

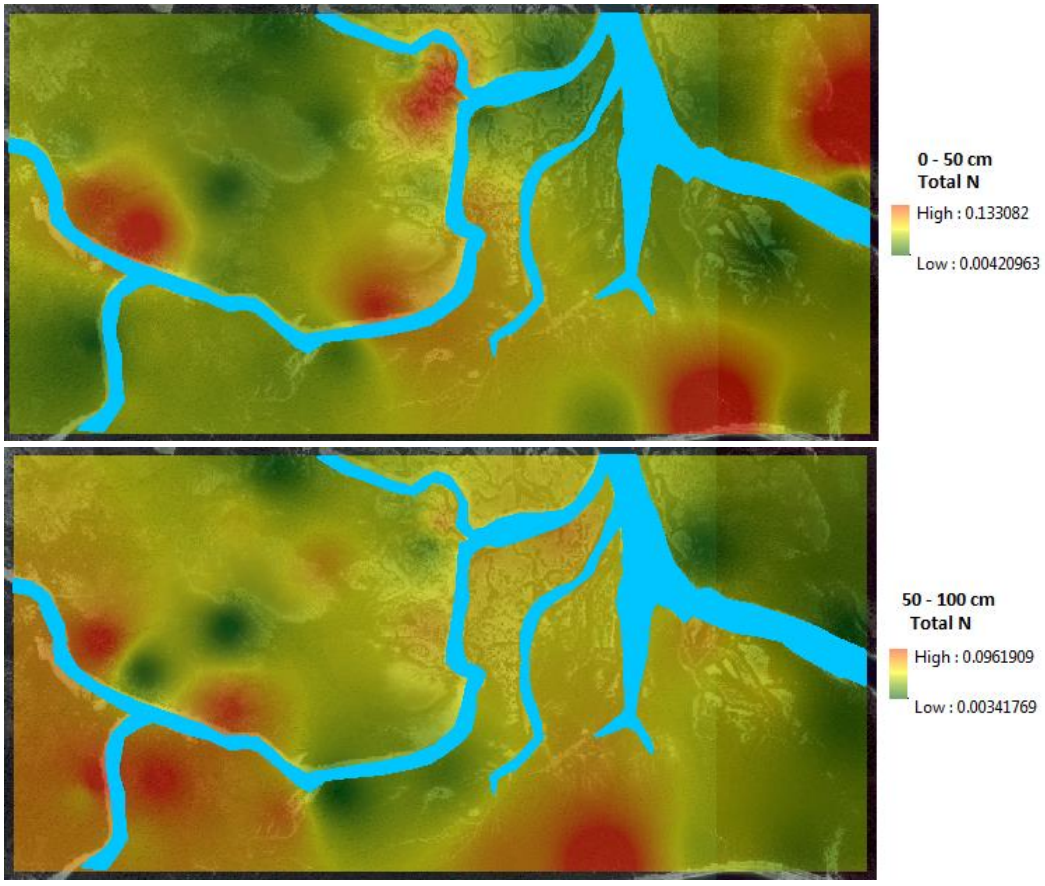

Figure33: Soil maps showing the spatial variation in nitrogen quantities at two layer depths created using IDW interpolation.

Phosphorus (P) plays a key role in different plant functions such as photosynthesis and transfer of energy. Phosphorus is also essential in stimulating early root formation and growth, which helps the plants to hasten maturity rates as well as seed production (Fageria, 2008). It is absorbed by plants as $H_2PO_4^-$, HPO_4^{2-} or PO_4^{3-}, depending upon soil pH. Compared to total N contents, available P is significantly low and occurs in the range of 11-74 mg kg^{-1} (24 to 163 kg ha^{-1}) with an average of 44 ± 1.75 mg kg^{-1}. As shown in Figure 34, about 87% of the soil samples are distributed in the range of 20-60 mg kg^{-1} (44 to 132 kg ha^{-1}). However, the amount of available P decreases with depth on most sites. The maps in Figure 35 show the spatial variation of available P at different layer depths. The low amount of available phosphorous is due to P fixation with high amount of calcium carbonates in the soil, resulting in low P availability and efficiency to the plants unless acidic conditions prevail to release the fixed P.

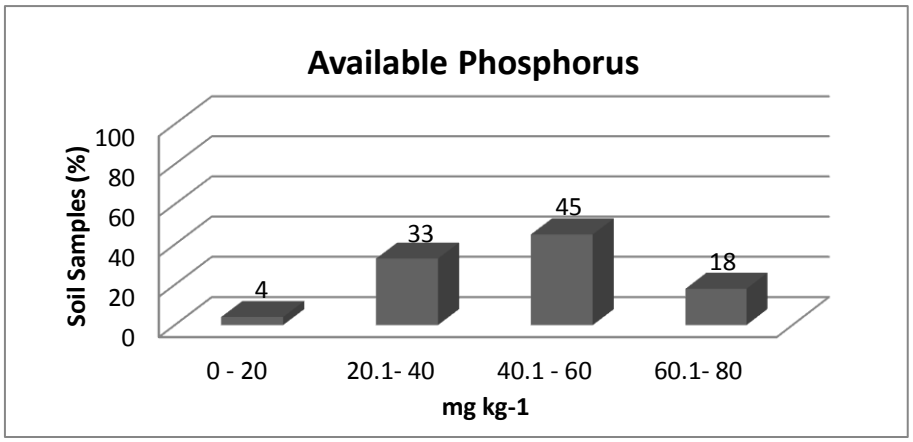

Figure34: Frequency distribution of soil sample into different ranges of available P.

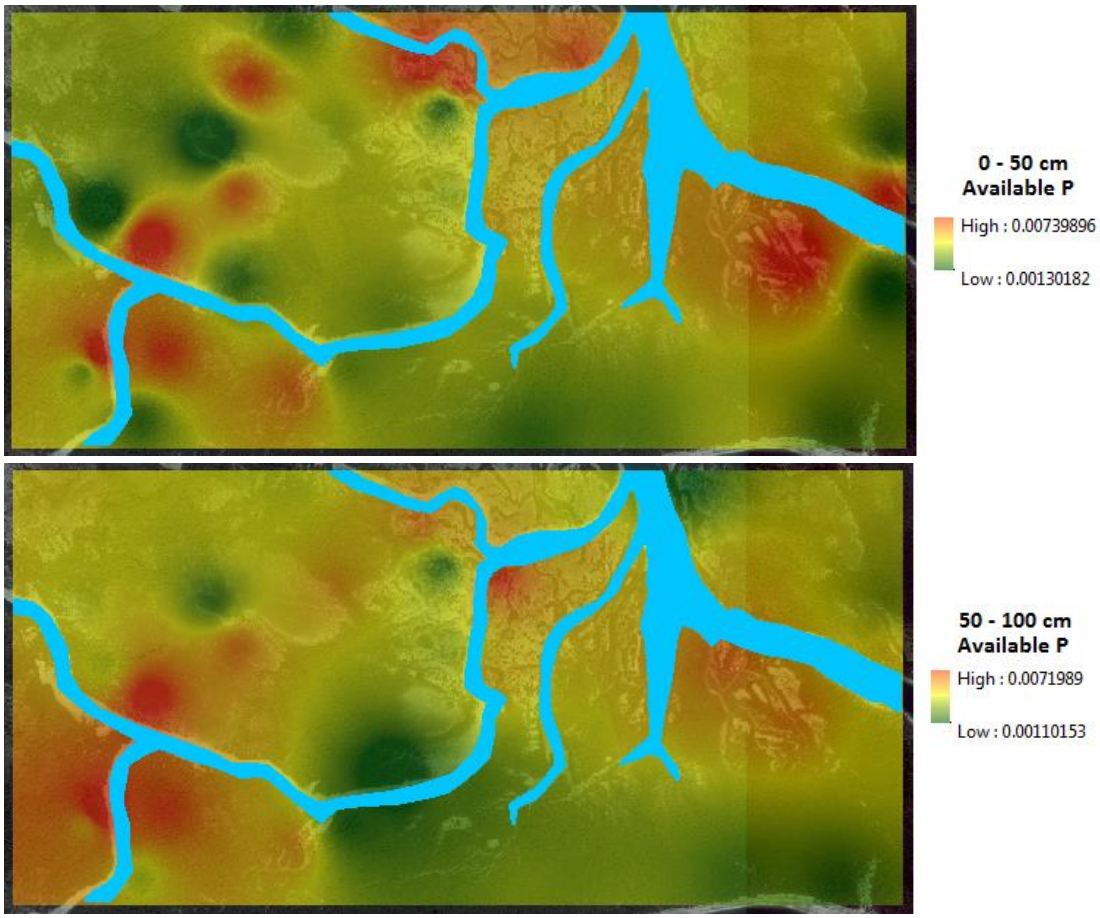

Figure35: Soil maps showing the spatial variation of available phosphorus at two layer depths created using IDW interpolation.

Potassium (K), taken up by plants as potassium ion (K^+), is vital in different plants' processes and functions. For example, K activates many enzyme systems, which play an important role in carbohydrate and protein synthesis. It also reduces respiration, prevents energy loss, improves the water regime of the plant, and increases its tolerance to salinity and drought. The plants are less affected by diseases, if they are well supplied with K (Fageria, 2008). The results of the soil tests reveal higher concentration of ammonium acetate extractable K ranging between 245-799 mg kg^{-1} (539 to 1757 kg ha^{-1}) compared to soluble K from soil saturation extract ranging between 156 to 198 mg kg^{-1} (343 to 436 kg ha^{-1}). Figure 36 shows that 75% of

the soil samples are distributed in the range of 201 to 600 mg kg^{-1} (442 to 1320 kg ha^{-1}). The results also indicate that the amount of K decreases with depth in most sites. The maps in Figure 37 show the spatial variation of available K in the area of study at different layer depths.

The high K concentration in the soil can be attributed to two main reasons. The first is the organic rich mud and decomposed organic matter accumulated over a period of time by the special root system of the forest (pneumatophores), which releases K into soil. Second, K is part of the crystal structure of minerals such as mica and K-feldspar, which release K through weathering. It is believed that the higher concentration of K together with N keeps the mangroves green and healthy without the application of NPK (Nitrogen, Phosphorous, and Potassium) fertilizers (Reef et al., 2010).

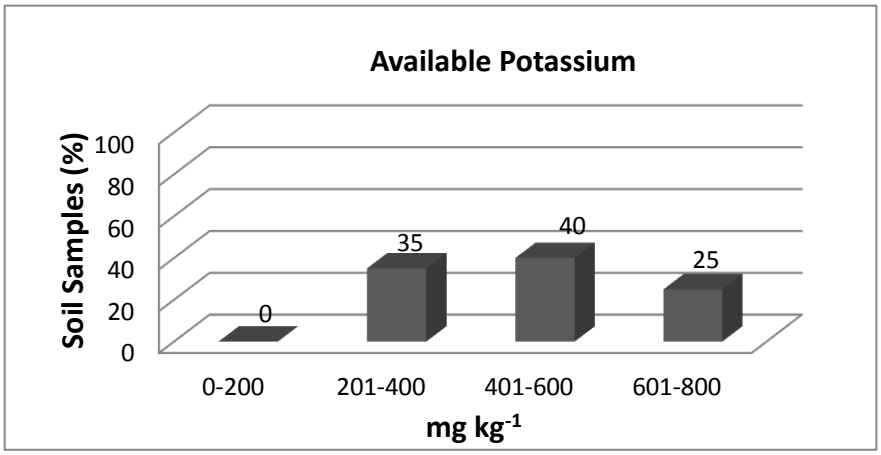

Figure36: Frequency distribution of soil sample into different ranges of available K.

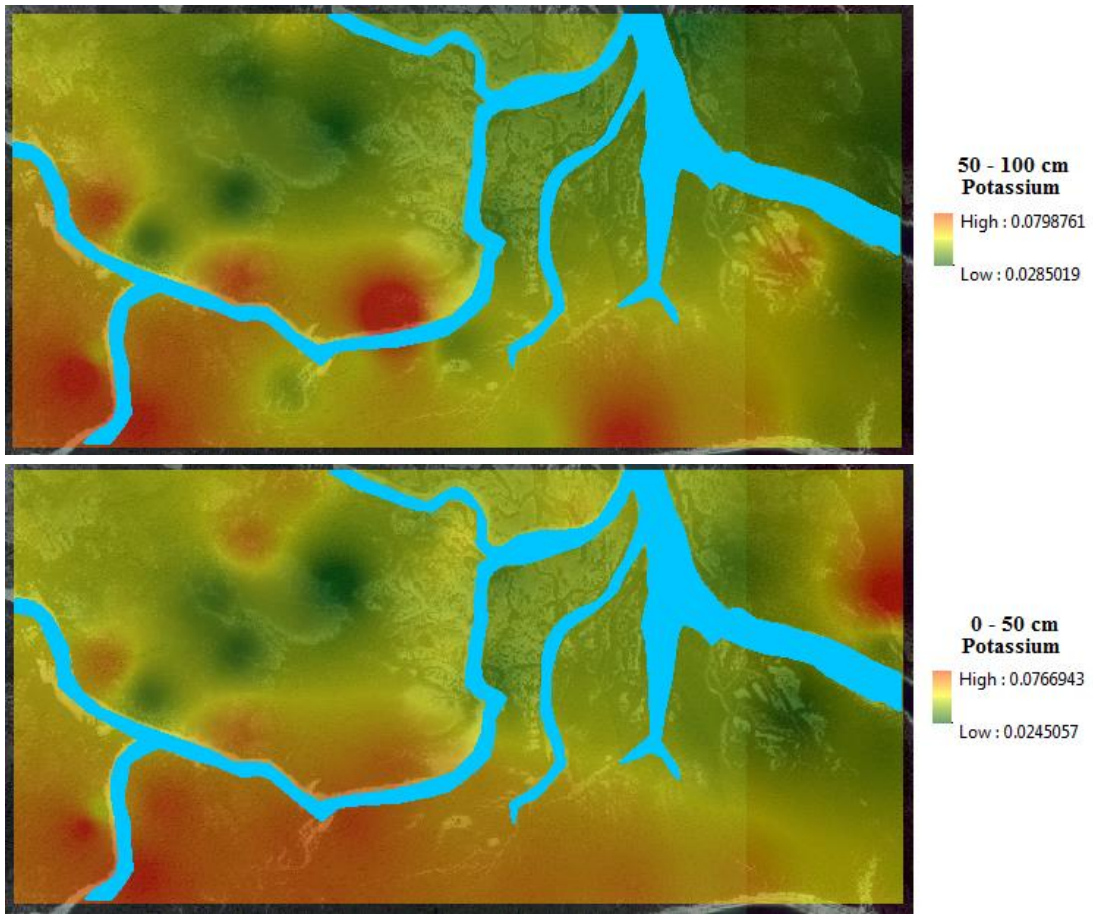

Figure37: Soil maps showing the spatial variation of available K at two layer depths created using IDW interpolation.

7. Soil Organic Matter

The results of the analysis indicate that mangrove soils are rich in organic matter content (Figure 38). The percentages of organic matter are high, ranging from 2.06 to 6.8% with an average of 3.56 ± 0.11%. There are significant differences in the amount of soil organic matter among the sites. The organic matter content also varies in different layer depths as seen in Figure 39. Some of the soils have higher OM% near the surface (0-50 cm), while other soils have a higher OM% at greater depth (50-100cm).

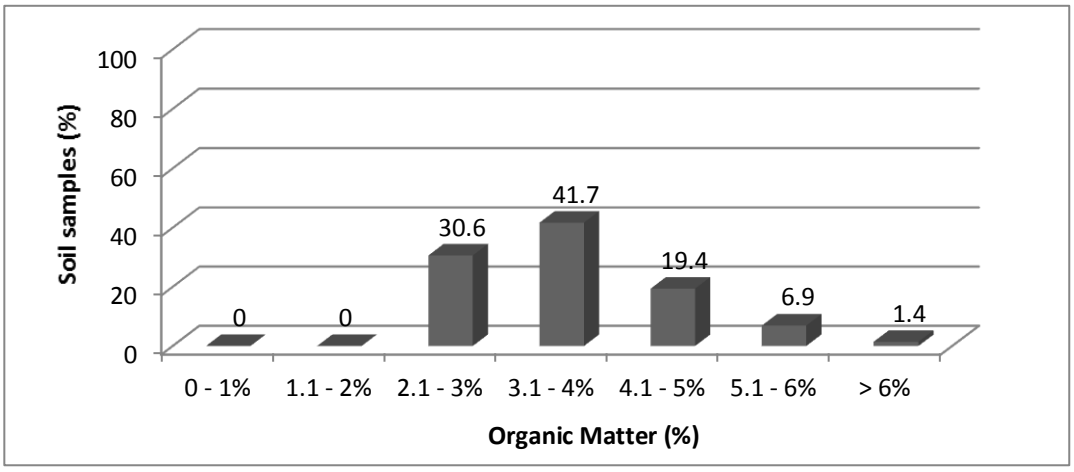

Figure 38: Frequency distribution of soil sample into different ranges of organic matter.

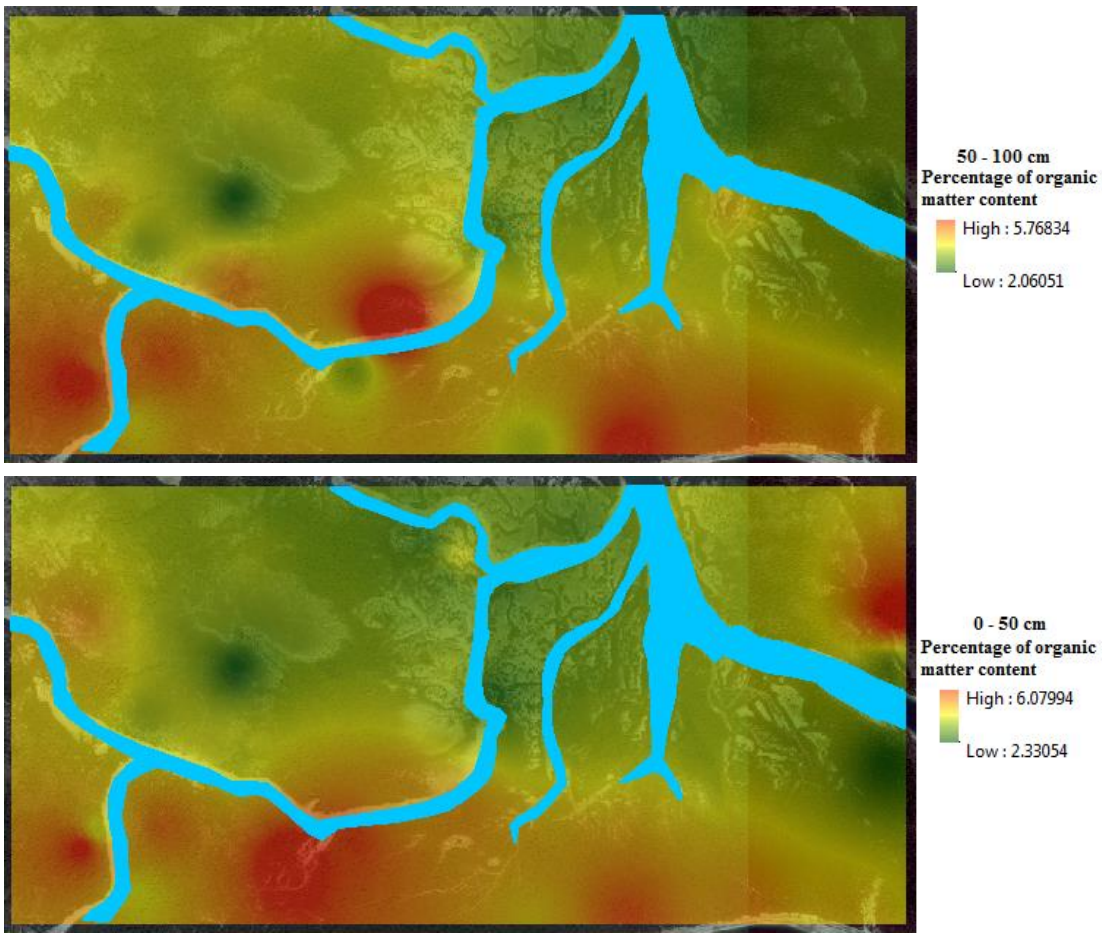

Figure 39: Soil maps showing the percentage of organic matter content in the soil at two depths created using IDW interpolation.

According to Shahid et al., (2013), the levels of organic matter in the soils of Abu Dhabi are generally very low due to the harsh arid environmental conditions. The amount of OM content in the soils of the most parts of Abu Dhabi is estimated to be about 0.2%. In contrast, as the results of the current work show, the soils of mangrove forests in Abu Dhabi have very high organic matter content. These high quantities of OM are due to the high densities of *Avicennia marina* (absolute total density was 143,896/ ha). Higher OM content present in the soils is decomposed mostly from litter fall (e.g. leaves, bark, twigs, branches, etc.) and soil micro-organisms. According to Sukardjo (1994), soils composed of rich OM and soft mud sediments of fine silt and clay are important to the flourishing of mangrove forests. Typically soils with rich organic matter have a darker brown to black color. However, the soils in the study area have a very light color due to the high amounts of calcium carbonate.

The relatively high concentration of organic matter in mangrove soils compared to that of inland desert allows mangrove soils to have high carbon sequestration capacity, and thus lower greenhouse gases. The coastal mangroves sequester more carbon than any other ecosystem in the world (Alongi, 2002; Lucas et al, 2007). In fact, mangroves have the capacity to store carbon five times more than any other tropical forests per hectare. According to Eng (2011), mangrove soil has more carbon than most tropical forests have in their soil and biomass together. Such a high carbon storing capacity is attributed partially to deep organic rich mud in which mangroves thrive. The special root system (pneumatophores) of mangrove trees slows down tidal waters, which capture the organic material by allowing it to settle into the sediment surface, where low oxygen conditions of the sediments under mangrove swamps inhibits the decay process and results in greater carbon amounts to accumulate in the soil.

E. Conclusions and Recommendations

This study indicates that the soils of Eastern Mangrove Lagoon National Park are fine in texture at the surface layer, but coarser in texture at the subsurface layer. The soils are classified as very saline-sodic due to the high levels of salinity, SAR and ESP, which may restrict the growth of many plants and affect soil properties. However, *Avicennia marina* have a very high salt-tolerance and can absorb higher concentrations of salts and exclude them through the leaves, tolerate high SAR and resultant ESP, and adapt to the harsh environmental conditions. Additionally, the soils are characterized with extremely high amounts of $CaCO_3$, which can increase soil buffering capacity and stabilize the pH above the optimum range, limiting the amounts of available essential nutrients to plants such as phosphorus. Conversely, the rich organic matter associated with soft mud sediments of fine silt and clay as well as the high availability of K and N supports mangrove forests' health and development. This study shows that there are significant spatial variations in soil chemical characteristics in addition to the amount of organic matter content and the essential nutrients among the sites in the study area. Interestingly, areas with the lowest mangrove population have the lowest organic matter content and the lowest N and K concentrations; the same areas have the highest $CaCO_3$ amounts, and the highest salinity and pH levels. These results indicate that soils' characteristics play a major role in the spatial distribution of *Avicenna marina* within the study area.

Good quality soil is needed for healthy growth and development of mangrove trees. Thus, ensuring that the three main nutrients (N, P, and K) are available to the plants is essential. Since the amount of P is low in the soils of study area, P fertilizer should be added to soils. Even though very few researchers claim that the low P amounts should not limit the growth of mangrove trees (Sukardio, 1994), several experiments indicate that the availability of P is

essential to the health of mangroves and that adding P to the soil has yielded increases in growth in mangroves (Neveu, 2013; Reef et. al.,2010).

Moreover, living organisms, bacteria, and fungus are critical to healthy soil. For example, arbuscular mycorrhizal (AM) fungi help plants to absorb more water and nutrients including P from the soil (Smith et al. 2003). However, highly saline soils affect the occurrence of AM fungi, which negatively influences the uptake of some essential nutrients and could possibly increase the susceptibility to toxic metals. Very few researchers have studied the existence of AM fungi in the soils of mangroves (Sengupta & Chaudhuri, 2002; Kothamasi et. al., 2006). Therefore, future studies should evaluate the occurrence and distribution of AM fungi and other soil organisms in order to improve the quality of mangrove soils.

V. Conclusion

A. Summary

Avicennia marina population structure, aboveground biomass, and soil properties in Eastern Mangrove Lagoon National Park in Abu Dhabi is researched. *In situ* measurements were used to assess *Avicennia marina* status, mortality rate (%), height (m), crown spread (m), stem number, DBH (cm), basal area (m), and aboveground biomass (t ha^{-1}). Aerial LIDAR data were used to estimate and map aboveground biomass density through employing LIDAR-derived height percentile statistics to segment the study area into structurally homogenous forested units. Then, regression relationships were developed using *in situ* reference data in machine learning environment. Mangrove canopy height of the study area was also created using classified LIDAR points. Furthermore, an *in situ* soil survey was conducted to examine mangrove soils' physical and chemical properties, fertility status, and organic matter. Then, soil maps were created to determine the key characteristics of soils and their influence on *Avicennia marina* spatial distribution.

B. Answering Research Questions

The main questions of this study, previously stated in chapter 1, are answered below.

1. What are the structural characteristics and the current status of mangrove vegetation in Eastern Mangrove Lagoon National Park?

As the results reveal in chapter 2 and 3, mangrove trees in the study area are generally healthy with a very low mortality rate of 0.02%. The percentage of adult trees is 49%, whereas the percentage of saplings and seedlings is 51%. The density of the trees varies significantly

among the sites and ranges from 9,090 trees ha^{-1} to 253,247 trees ha^{-1}. The frequency distribution of the trees height is positively skewed showing the presence of many small and few large trunks. The mean height of trees with DBH > 5cm is 2.47 ± 0.02 m, while the mean height of the trees in all sampling plots is 1.97 ± 0.02 m. The maximum trees height within the sites is 5.50 m. However, based on the canopy height model, created using LIDAR data, the average height in the entire study area is estimated to be 3.03m and the maximum height is 7.86 m.

The total basal area in all plots is 20.58 m^2, and the basal area varies significantly among the sites and ranges from 0.07 m^2 to 3.05 m^2. Some of the plots have a very high tree density but relatively low basal areas due to the high presence of young trees and saplings with small diameter size. The distribution of the trees' diameter classes reveals a typical reverse-J-shaped pattern, which indicates an uneven-aged stand structure with many regeneration seedlings and young trees. The mean diameter of the trees is 5.38 ± 0.14 cm. The distribution of the trees' average crown spread classes also reveals a typical reverse-J-shaped pattern very similar to diameter classes, showing a strong correlation between trees diameter and crown spread measurements ($R^2 = 0.72$). The average crown spread of all the trees is 0.79 ± 0.02 m, while the average crown spread of adult trees is 0.99 ± 0.02 m. The maximum crown spread in all sites is less than 6 m.

2. How applicable is the only available airborne LIDAR (collected in January 2013) for characterization of mangrove forests, including canopy height and stand biomass?

The only available aerial LIDAR data is successfully used to estimate mangrove canopy height and aboveground biomass. After processing the data, multiple percentile heights are calculated using a neighborhood algorithm. Then, image segmentation algorithm is employed to transform the LIDAR-derived image into structurally homogeneous units. Additionally,

aboveground biomass of the sampling plots calculated from *in situ* measurements are incorporated into a machine learning algorithm to produce a regression-tree model for aboveground biomass estimation per segment of the entire study area. Based on *in situ* measurements, aboveground biomass of the sampling plots ranges from 0.103 to 4.279 (kg/m^2), while aboveground biomass of the entire study area calculated using LIDAR data is estimated to be 14,850.26 kg. The biomass map created using LIDAR data indicates that 49% of the study area has relatively low biomass density (≤ 4.15 kg/m^2), 23% of the study area has a relatively moderate biomass density (ranging from 4.16 - 8.01 kg/m^2), and 28% of the study area has a relatively high biomass density (ranging from 8.02 - 13.17 kg/m^2). A canopy height model created using LIDAR data shows that the maximum canopy height is 7.86 m, the average height is 3.03 m, and the minimum height is 0.12m.

3. What are the key characteristics of mangrove forest soils, and how do soil properties influence the spatial distribution of mangrove trees?

The soil test as described in chapter 4 indicates that mangrove soils are clayey on the surface and sandy beneath. The salinity levels are extremely high and even exceeded the salinity of seawater in some locations. The soil pH levels are neutral for 86% of the soil samples and slightly alkaline for 14% of the soil samples. The SAR and ESP values are high, indicating high Na due to the effect of seawater. The high $CaCO_3$ amounts, reaching up to 88% in some locations, increases the buffering capacity of the soil and limits the amounts of available nutrients to the plants. However, the rich OM content associated with soft mud sediments of fine silt and clay supports the development of the forest. The values of N are high compared to values of available P. The low P availability and uptake efficiency to the plants is attributed to P fixation with high $CaCO_3$ quantities in the soil. The soil tests show higher concentration of

ammonium acetate extractable K compared to soluble K from soil saturation extract. The high amounts of K and N can be attributed to organic rich mud and decomposed OM accumulated over years by the mangrove root system, which releases K and N into soil to maintain the health of mangroves even in harsh environments. Areas with high mangrove populations are rich in organic matter content and high in nutrient concentrations, whereas areas with low mangrove population have very high $CaCO_3$ quantities, salinity levels, SAR, and ESP. This indicates that soil properties affect the spatial distribution of *Avicennia marina*.

C. Discussing Research Hypotheses

The research hypotheses are discussed below.

1. There are strong positive correlations among mangrove structural parameters including DBH, basal area, height, crown spread, and aboveground biomass.

This research hypothesis is accepted. As seen in chapter 2, Pearson correlation coefficients and coefficients of determination are calculated between mangrove aboveground biomass and structural parameters including height, DBH, basal area, and crown spread. The correlation coefficients vary from 0.518 to 0.981, which shows a strong positive correlation between the structural variables. In fact, aboveground biomass has the strongest correlations, with basal area explaining 96% of the variance.

2. The available airborne LIDAR data can derive high resolution 3D map products of mangrove canopy height.

This research hypothesis is accepted. The canopy height map seen in chapter 3 is created using LIDAR data in ArcScene (10.2) with 1 m pixel resolution. After filtering and removing

noise points, LIDAR points are classified to ground points and vegetation points. The forest canopy heights are derived by subtracting the bare ground elevations from those for the canopy.

3. Image segmentation of LIDAR canopy height metrics can be used in a machine learning environment to accurately estimate and map aboveground biomass density of *Avicennia marina*.

This research hypothesis is accepted. As seen in chapter 3, aboveground biomass density is estimated and mapped by utilizing LIDAR-derived height percentile statistics to segment the forest into structurally homogenous units and to develop regression relationships between remote sensing data and *in situ* reference data using a machine learning approach. However several factors affect the accuracy of the model performance such as neighborhood window size, and the number of percentile layers. The following statistics represent the accuracy of the model used to estimate biomass in this study: RMSE= 10.16713, R= 0.8722238, and R^2= 0.7597432.

4. Variations in soil characteristics play a major role in the spatial distribution of *Avicennia marina*.

This research hypothesis is accepted. Based on the soil maps created in chapter 4, it is clear that soil plays a major role in the spatial distribution of *Avicennia marina*. Areas with the lowest mangrove population have the lowest organic matter content and the lowest N and K concentrations; the same areas have the highest $CaCO_3$ quantities, highest SAR and ESP values, and highest salinity and pH levels. On the other hand, Areas with the highest mangrove population have the highest organic matter content and the highest N and K concentrations; the same areas have the lowest $CaCO_3$ quantities, lowest SAR and ESP values, and lowest salinity and pH levels.

5. The soil conditions of the study area are ideal to the growth of mangrove trees, and no urgent actions are needed to increase soil fertility.

This research hypothesis is rejected. The very harsh saline-sodic soil conditions of the study area are not ideal, especially with the recorded extreme high amount of salinity, SAR, ESP, and $CaCO_3$. Even though *Avicennia marina* can survive and adapt to these harsh conditions, actions should be taken to enhance the soil of the forest in order to maintain the health of the trees. The information presented in this research diagnoses the areas of poor soil conditions, so actions can be taken to enhance the properties of the soils within these areas. It is important to ensure the application of enough fertilizer while taking the advantage of nutrients already present in the soil. As mentioned in chapter 4, P concentrations, which are one of the essential nutrients to the survival of the trees, are extremely low. Therefore, P fertilizer should be added to the soils to maintain the growth of mangroves. However adding P fertilizer to the soils with such high $CaCO_3$ quantities may not be very effective, and thus increasing specific type of bacteria, and fungus such arbuscular mycorrhizal (AM) can play an important role to help the trees to absorb more water and nutrients including P from the soil.

D. Future Work

1. *Avicennia marina* is the only mangrove species that grows widely in UAE and in similar arid countries. However, no studies have developed allometric equations to accurately estimate aboveground biomass of *Avicennia marina* in UAE. Such equations can be developed in future studies by measuring the oven-dry-weight of different trees of all sizes for accurate biomass estimation.

2. *In situ* measurements including status, height (m), crown spread (m), stem number, DBH (cm), basal area (m), mortality rate (%) and aboveground biomass (t ha^{-1}) are collected from the sampling plots to study *Avicennia marina* biophysical characteristics. However, LIDAR data is only used to estimate canopy height and above ground biomass of the entire study area. Thus, available Worldview-2 satellite imagery, collected in 2013, should be used in future studies to estimate the other biophysical characteristics of the forest such as crown spread and basal area. The advantage of using the high spatial resolution 8 multispectral bands (2 m) and the 50 cm panchromatic band enables the discrimination of fine details. Object-based image analysis (OBIA) approach can be employed to segment mangrove features and discriminate them. This approach has the ability to combine several scales in the analysis through multi-scale segmentation process, which support the analysis of multi-scale features in mapping mangroves.

3. LIDAR-derived elevation data, digital terrain model (DTM), can be used for studies related to sea level rise associated with climate change. A sea level model can be created in future studies to detect areas of mangrove forests that are susceptible to sea level rise at different levels, so that mangrove inundation zones can be mapped.

VI. References

Aardt J. V., Wynne R. H., Scrivani. J. A., (2008). Lidar-based Mapping of Forest Volume and. Biomass by Taxonomic Group Using. Structurally Homogenous Segments. *Photogrammetric Engineering and Remote Sensing.* Vol. 74 (8). pp. 1033-1044.

Abdelfattah M.A., & Shahid S.A., (2006). Characterization and Classification of Soils in the Coastline of Abu Dhabi Emirate. *Proceedings of the 5th International Agroenviron Symposium titled "Agricultural Constraints in the Soil-Plant-Atmosphere Continuum*", 4-7 September 2006, Ghent, Belgium. Pp. 347-354.

Abdelfattah, M.A., & Shahid, S.A., (2007). A Comparative Characterization and Classification of Soils in Abu Dhabi Coastal Area in Relation to Arid and Semi-Arid Conditions using USDA and FAO Soil Classification Systems, *Arid Land Research and Management*, Vol. 21 (3), 245 – 271.

Aguilar, F.J., Mills J.P., (2008). *Accuracy Assessment of LiDAR-derived Digital Elevation Models*. Photogrammetric Record, 23 (122), 148-169.

Aheto D. W., Aduomih A. A. O., and Obodai E. A., (2011). Structural parameters and above-ground biomass of mangrove tree species around the Kakum river estuary of Ghana. *Annals of Biological Research*, 2(3):504-514.

Al Ashram, Omar. (2008). Wastes and Pollution Sources of Abu Dhabi Emirate, United Arab Emirates. *Published by the Environmental Agency*- Abu Dhabi (EAD).

Alberta Department of Agriculture and Rural Development (2014), Retrieved from: http://www1.agric.gov.ab.ca/$department/deptdocs.nsf/all/agdex13200.

Al Habshi A., Youssef T., Aizpuru M., & Blasco F., (2007). New Mangrove Ecosystem Data Along the UAE Coast Using Remote Sensing. *Aquatic Ecosystem Health and Management*. Vol.10 (3), 309-319.

Alongi, D. M., (2002). *Present and future of the world's mangrove forests*, Environ. Conserv., 29(3), 331–349.

American Society for Photogrammetry and Remote Sensing- ASPRS, (2013). LAS Specification Version 1.4 – R13. Bethesda, Maryland.

Aschbacher, J. K., Ofren, R. B., Delsol, J. P., Suselo, T. B., Vibulsresth, S. K. and T. K. Charrupat., (1995). *An Integrated Comparative Approach to Mangrove Vegetation Mapping Using Advanced Remote Sensing and GIS Technologies*; Preliminary Results. Hydrobiologia, 295:285-294.

Ashton, E.C. and D.J. Macintosh., (2002). *Preliminary Assessment of the Plant Diversity and Community Ecology of the Sematan Mangrove Forest, Sarawak, Malaysia*. Forest Ecology and Management, Volume 166, No 1, p.111-129.

Aspinall S., (2001). *Environmental Development and Protection in the UAE*. In:Al-Abed,I., Hellyer,P. (Eds). United Arab Emirates: A New Perspective. Trident Press, Book Craft, UK. pp. 227-304.

Baatz M., Schape A., (2000). Multiresolution Segmentation: an optimization approach for high quality multi-scale image segmentation. *In: Strobl, J., Blaschke T., Griesebner G. (eds.), Angewandte Geographische Informations verarbeitung XII*. Wichmann-Verlag, Heidelberg, pp 12-23.

Barker A. V. & Pilbeam D. J., (2006). Handbook of Plant Nutrition. CRC Press. ISBN: 978-0-8247-5904-9.

Bashitialshaaer R., Persson K., Aljaradin M., (2011). Estimated Future Salinity in the Arabian Gulf, the Meditterean Sea and the Red Sea Consequences of Brine Discharge from Desalination. *International Journal of Academic Research*. Vol. 3(1).

Bast, L., Warncke. D., & Christenson D., (2011). Facts about soil acidity and lime. Retrieved from: http://www.oakgov.com/msu/Documents/publications/e1566_soil_acidity.pdf.

Bettinger B., Boston K., Siry J., & Grebner D. (2009). Forest Management and Planning. Academic Press, New York.Bhosale L.J., (1994). Propagation techniques for regeneration of mangrove forests-A new asset. *Journal of Non-timber Forest Products,* 1:119-122.

Brady, N.C., & Weil, R.R., (1999). *The nature and properties of soils*. Prentice Hall,Inc., Upper Saddle River, NJ.

Boer, B. & Aspinall. S., (2009). Life in the Mangroves. *The Emirates - A Natural History*. Published by the Environmental Agency- Abu Dhabi (EAD), 132-136.

Bombelli A., Avitabile V., Balzter H., Belelli Marchesini L., Bernoux M., Brady M., Hall. R., Hansen M., Henry M., Herold M., Janetos A., Law B.E, Manlay R., Marklund L.G., Olsson. H., Pandey D., Saket M., Schmullius C., Sessa R., Shimabukuro Y.E., Valentini R.,. Wulder M., (2009). Assessment of the status of the development of the standards for the Terrestrial Essential Climate Variables: BIOMASS. GTOS 67, AFO, Global Terrestrial Observing System. Rome.

Boto, K., & Wellington J., (1984). Soil Characteristics and Nutrient Status in a Northern Australian Mangrove Forest. *Estuaries.*Vol.7 (1), 61-69.

Burt R. (Ed.), (2004). Soil Survey Laboratory Methods Manual. *Investigation Report No42. USDA NRCS*. National Soil Survey Center, Lincoln, NE.

Carter, M.R., & Gregorich, E.G., (2006). Soil Sampling and Methods of Analysis, Second Ed. Taylor and Francis Group, LLC. ISBN-13: 978-0-8493-3586-0.

Chadwick, D.J., (2011). *Integrated LiDAR and IKONOS multispectral imagery for mapping mangrove distribution and physical properties*, International Journal of Remote Sensing, DOI 10.1080/01431161.2010.512944, 1-17.

Chong, V. C. (2006). Sustainable utilization and Management of Mangrove Ecosystems of Malaysia. *Aquatic Ecosystem Health & Management*, 9(2): 249-260.

Cintron, G., A.E. Lugo, D.J. Pool & G. Morris, (1978). Mangroves of Arid Environments in Puerto Rico and Adjacent Islands. Biotropica 10:2: 110-121.

Cintron, G., A.E. Lugo, and R. Martinez., (1985). Structural and functional properties of mangrove forests. *In: The botany and Natural History of Panama*. W.G. Darcy and M.D. Correa, eds.), Monogr. Syst. Bot., Vol. 10, 53-66.

Comley, B. W. T. and McGuinness, K. A., (2005). Above- and below-ground biomass, and allometry, of four common northern Australian mangroves. Aust. J. Bot. 53:431-436.

Cooper T. H. & Regents of the University of Minnesota,(2009). Chapter 5: Significance of Soil pH. retrieved from: http://www.swac.umn.edu/classes/soil2125/doc/s12ch5.htm.

Dahle, G.A., & Grabosky J.C., (2009). Review of Pertinent Literature on the Allometric Relationships in Tree Stems and Branches. *Arboriculture and Urban Forestry* 35:311-320.

Dittmar, T., Hertkorn, N., Kattner, G. and Lara, R.J., (2006). *Mangroves, a Major Source of Dissolved Organic Carbon to the Oceans*. Global Biogeochemical Cycles 20 (1), GB1012, doi:10.1029/1005GB002570.

Edwards J.H., C.W. Wood, D.L. Thurlow, & M.E. Ruf. (1999). Tillage and crop rotation effects on fertility status of a Hapludalf soil. *Soil Sci. Soc. Am. J*. 56:1577-1582.

Edward A. Keller (2007). Introduction to Environmental Geology. Prentice Hall, Inc. 4th Edition. ISBN13: 978-0132251501.

Empi Rambok, Seca G., Osumanu H.A. and Nik M.A. (2010): Comparison of Selected Soil Chemical Properties of Two Different Mangrove Forests in Sarawak. *American Journal of Environmental Sciences*. ISSN 1553-345X. Vol. 6 (5), 2010: 438 – 441.

Eng S. (2011), Mangroves among the Most Carbon-Rich Forests in the Tropics; Coastal trees key to lowering greenhouse gases. USDA Forest Service, Pacific Southwest Research Station. Retrieved from: http://www.fs.fed.us/psw/news/2011/110403_mangroves.shtml.

English, S., Wilkinson, C and Baker, V., (1997). Survey manual for tropical marine resources, *Chapter3 Mangrove Survey, Australian Institute of Marine Science, Townsville*, 119-196.

Environmental Atlas of Abu Dhabi Emirate. Abu Dhabi Environment Agency (EAD), (2011). Retrieved from http://www.environmentalatlas.ae.

Fageria N. K., (2008). The Use of Nutrients in Crop Plants Hardcover. CRC Press. ISBN-10: 1420075101.

Fatoyinbo, T., Armstrong, A., (2010). *Remote Characterization of Biomass Measurements: Case Study Of Mangrove Forests Biomass.* Sciyo Publishing.

Feller, I. C., D. F. Whigham, K. M. McKee and J.P. O'Neill. (2002). Nitrogen vs. phosphorus limitation across an ecotonal gradient in a mangrove forest. *Biogeochemistry* 62:145:175.

Food and Agriculture Organization of the United Nations - FAO's, (2007). Mangrove Assessment Study. The World's Mangroves 1980-2005. *FAO Forestry Paper 153, Rome, Italy.*

Frazer, G.W.; Magnussen, S.; Wulder, M.A.; Niemann, K.O., (2011). Simulated Impact of Sample Plot Size and Co-registration Error on the Accuracy and Uncertainty of LiDAR-Derived Estimates of Forest Stand Biomass. *Remote Sensing of Environment* 115(2):636–649.

Fromard, F., Puig, H., Mougin, E., Marty, G., Betoulle, J. L., and Cadmuro, L., (1998). Structure, above-ground biomass and dynamics of mangrove ecosystems: new data form French Guiana. *Oecologia* 115:39-53.

Fry, B. & Cormier, N. (2011). Chemical Ecology of Red Mangroves, Rhizophora mangle, in the Hawaiian Islands. *Pacific Science,* 65(2): 219-234.

Galitz, D. S., (1979). Uptake and Assimilation of Nitrogen by Plants. Farm Research: Vol. 37, No. 3.

Gillespie, T. W., Brock, J. & Wright, C. W., (2004). *Prospects for quantifying structure, floristic composition and species richness of tropical forests*. International Journal of Remote Sensing, Vol.25, No.4, pp.707-715, ISSN: 1366-5901.

Gilman, E.L., et al., (2008). Threats to Mangroves from Climate Change and Adaptation Options. doi:10.1016/*j.aquabot*.2007.12.009.

Giri, C., Ochieng, E., Tieszen, L. L., Zhu, Z., Singh, A., Loveland, T., Masek, J. and Duke, N., (2011). Status and distribution of mangrove forests of the world using earth observation satellite data. *Global Ecology and Biogeography*, 20: 154–159. doi: 10.1111/j.1466-8238.2010.00584.x.

Gobakken, T.; Næsset, E., (2009). Assessing Effects of Laser Point Density, Ground Sampling Intensity, and Field Sample Plot Size on Biophysical Stand Properties Derived from Airborne Laser Scanner Data. *Canadian Journal of Forest Research* 38(5):1095–1109.

Goerndt M., Monleon V., Temesgen H., (2010), Relating Forest Attributes and Area-based LiDAR Canopy Height, Density, and Intensity Metrics for Western Oregon. *Western Journal of Applied Forestry*. Vol. 25 Issue 3, 105.

Goetz, S.J., Baccini, A., Laporte, N.T., Johns,T., Walker,W., Kellndorfer, J., Houghton, R. A., and Sun, M., 2009. *Mapping and monitoring carbon stocks with satellite observations: a comparison of methods*. Carbon Balance and Management.

Hazelton, P.A., Murphy, B.W., (2007). Interpreting Soil Test Results: What Do All The Numbers Mean?. CSIRO Publishing: Melbourne.

Herweg K., (1996). Assessment of current erosion damage. Center for Development and Environment, University of Bern, Switzerland, 69 p.

Houghton, J., Ding, Y., Griggs, D., Noguer, M., van der Linden, P., Dai, X., Maskell, K., Johnson, C. (Eds.), (2001). *Climate Change 2001: The Scientific Basis (Published for the Intergovernmental Panel on Climate Change)*. Cambridge University Press, Cambridge, United Kingdom, and New York, NY, USA.

Houghton A., (2005). Aboveground Forest Biomass and the Global Carbon Balance. *Global Change Biology*. Vol. 11, Issue 6, 945–958.

Houngton, R.A. Hall, F.G. Goetz, S.J., (2009) The importance of biomass in the global carbon cycle. *Journal of Geophysical Research* – Biogeosciences. 114(G2).

Howari F., Jordan B., Bouhouche N., and Sandy Wyllie-Echeverria. 2009. Field and Remote-Sensing Assessment of Mangrove Forests and Seagrass Beds in the Northwestern Part of the United Arab Emirates. *Journal of Coastal Research*. VOL.25, NO.1, pp.48–56, West Palm Beach, Florida.

Hurni, H., (1986). Soil Conservation in Ethiopia. Center for Development and Environment, University of Bern, Switzerland, 69 p.

Inoue, T., Nohara, S., Matsumoto, K. & Anzai, Y. (2011). What Happens to Soil Chemical Properties after Mangrove Plants Colonize? *Plant & Soil*, 346: 259-273.

Jensen, John R., (2005). Introductory Digital Image Processing, 3rd Ed. New Jersey. Prentice Hall: Upper Saddle River.

Jones, C. A., R. T. Koenig, J. W. Ellsworth, B. D. Brown, *and* G. D. Jackson *(*2007*)*, Management of urea fertilizer to minimize volatilization, *Ext. Bull. 173, Mont. State Univ.*, Bozeman.

Kothamasi D., Kothamasi S., Bhattacharyya A., Kuhad R., Babu C., (2006). Arbuscular mycorrhizae and phosphate solubilising bacteria of the rhizosphere of the mangrove ecosystem of Great Nicobar island, India. Biol. Fertil. Soils;42:358-361.

Laba, M., S.D. Smith, and S.D. Degloria, (1997). *Landsat-based land cover mapping in the lower Yuna River watershed in the Dominican Republic*, International Journal of Remote Sensing, 18(14):3011–3025.

Lacerda L. D., (2002). Mangrove Ecosystems: Function and Management. Springer. Verlag, Berlin.

Lim Zhi Kai, Genevieve Ngoh Hwee Peng, Goh Ming Min, Loh Tze Yuan Ken, (2012). Investigating the Effect of Soil pH on the Germination of *Avicennia alba* seedlings. *Natural Society*. Singapore.

Lim K. S., Treitz P. M., (2004). Estimation of Above Ground Forest Biomass From Airborne Discrete Return Laser Scanner Data Using Canopy-based Quintile Estimators. *Scandinavian Journal of Forest Research*, 19(6):558-570.

Lucas, R.M. ; Sch. of Geogr. Sci., Bristol Univ., UK ; Milne, A.K. ; Mitchell, A. ; Donnelly, B., (2000). Use of stereo aerial photography for assessing changes in the extent and height of mangrove canopies in tropical Australia. *IGRASS Proceedings, 5: 1880 - 1882*

Lucas, R.M., et al., (2007). The potential of L-band SAR for quantifying mangrove characteristics and change: case studies from the tropics. *Aquatic Conservation: Marine and Freshwater Ecosystems*, 17, 245.

Lucian D., Tiede D., Levick S. R., (2010). ESP: a tool to estimate scale parameter for multiresolution image segmentation of remotely sensed data. *International Journal of Geographical Information Sciences.* Vol. 24 No. 6. pp 859- 871.

Lu D., Chen Q., Wang G., Moran E., Batistella M., Zhang M., Laurin G.V., and Saah D., (2012). Aboveground Forest Biomass Estimation with Landsat and LiDAR Data and Uncertainty Analysis of the Estimates. *International Journal of Forestry Research.* Volume 2012, Article ID 436537, 16 pages.

Mariappan, M. Lingava, S. Murugaiyan, R. Kolanuvada, S.R. Thirumeni, R.S.L., (2012). Carbon Accounting of Urban Forest in Chennai City using Lidar Data. *European Journal Of Scientific Research.* 81(3):314-328.

Marshall, N., (19*94)*. Mangrove conservation in relation to overall environmental considerations. *Hydrobiologia* , 285, 303-309.

McGarrigle, E.; Kershaw, J.A.; Lavigne, M.B.; Weiskittel, A.; Ducey, M., (2011). Predicting the Number of Trees in Small Diameter Classes Using Predictions from a Two-parameter Weibull Distribution. *Forestry* 84: 431-439.

McGaughey R. J., (2014). FUSION/LDV: Software for LIDAR Data Analysis and Visualization. United States Department of Agriculture (USDA). Forest Service. Pacific Northwest Research Station. FUSION Version 3.42.

McKee, K.L. (1993). Soil physicochemical patterns and mangrove species distribution - reciprocal effects? *J,Ecol*.81:477-487.

McKee K. L. (2004). Global Change Impacts on Mangrove Ecosystems. *U.S. Geological Survey (USGS). National Wetlands, Research Center*, Lafayette, LA, p. 1- 3.

McLeod, E. and R.V. Salm, (2006). *Managing Mangroves for Resilience to Climate Change.* IUCN, Gland, Switzerland. 64p.

Mitchard E. T. A., Saatchi S. S.,Woodhouse I. H., Nangendo G., Ribeiro N.S., Williams M., Ryan C.M., Lewis S.L., Feldpausch T.R. , Meir P., (2009). Using satellite radar backscatter to predict above-ground woody biomass: A consistent relationship across four different African landscapes. *Geophysical Research Letters*, vol. 36.

Miyazaki R., Yamamoto M., Hanamoto E., Izumi H., Harada K., (2014). A line-based approach for precise extraction of road and curb region from mobile mapping data. *ISPRS Annals of Photogrammetry, Remote Sensing and Spatial Information Sciences*, Volume II-5, 2014, pp.243-250.

Næsset, E.; Okland, T., (2002). Estimating Tree Height and Tree Crown Properties Using Airborne Scanning Laser in a Boreal Nature Reserve. *Remote Sensing of Environment* 79(1):105–115.

National Oceanic and Atmospheric Administration (NOAA) Coastal Services Center, (2012). Lidar 101: An Introduction to Lidar Technology, Data, and Applications. Revised. Charleston, SC: *NOAA Coastal Services Center*.

Neveu, D. E., (2013) Growth and Herbivory of the Black Mangrove, *Avicennia germinans*, Along a Salinity Gradient. *M.S. Thesis, University of South Florida,* Retrieved from: http://search.proquest.com/docview/1476438551.

Parvaresh H., Parvaresh E., Zahedi G., (2012). Establishing Allometric Relationship Using Crown Diameter for the Estimation of above-Ground Biomass of Grey Mangrove, Avicennia. *J. Basic Appl. Sci. Res*. 2(2):1763-1769.

Powell, N. & Osbeck, M. (2010). Approaches for Understanding and Embedding Stakeholder Realities in Mangrove Rehabilitation Processes in Southeast Asia: Lessons Learnt from Mahakam Delta, East Kalimantan. *Sustainable Development*, 18: 260-270.

Proisy, C., Gratiot, N., Anthony, E. J. Gardel, A., Fromard, F., Heuret, P., (2009). Mud bank colonization by opportunistic mangroves: a case study from French Guiana using lidar data. *Continental Shelf Research*, 29(3): 632-641.

Ramsey III, E., and J. Jensen, (1996). Remote sensing of mangroves: relating canopy spectra to site-specific data. *Photogrammetric Engineering and Remote Sensing*, 62(8):939-948.

Rasolofoharinoro et al., (1998). A remote sensing based method for mangrove studies in Madagascar. *Int. J. of Remote Sensing* . 19 (10) : 1873-1886.

Reef R., Feller I., and Lovelock C., (2010). Nutrition of Mangroves. *Oxford Journals.* Science & Mathematics. *Tree Physiology*. Vol. 30, Issue 9. P1148-1160.

Reganold, J.P., & Harsh, J.B., (1985). Expressing cation exchange capacity in milliequivalents per 100 grams and SI units. *Journal of Agronomic Education* 14:84-90.

Riggins J.J., Tullis J.A. & Stephen F.M., (2009) Per-segment aboveground forest biomass estimation using LIDAR-derived height percentile statistics. *GIScience & Remote Sensing* 46: 232-24.

Sengupta A., Chaudhuri S. (2002). Arbuscular mycorrhizal relations of mangrove plant community at the Ganges river estuary in India. *Mycorrhiza*;12:169-174.

Shahid S.A., (2012). Mangroves – Adaptation and occurrence, climate change and coastline protection. *Farming Outlook* Volume 11 No 3, p. 26-31.

Shabbir S. A., Abdelfattah M. A., Othman Y., Anil Kumar,. Taha F. K., Kelley J. A. and. Wilson M. A., (2013). Developments in Soil Classification, Land. Use Planning and Policy Implications: Innovative Thinking for Sustainable Use of Terrestrial Resources in Abu Dhabi Emirate through Scientific Soil Inventory and Policy Development. Springer Science. DOI 10.1007/978-94-007-5332-7-1.

Shahid S. A., Abdelfattah M. A., Wilson M.A., Kelley J. A.., Chiaretti J., (2014). *United Arab Emirates Keys to Soil Taxonomy.* Springer. ISBN 978-94-007-7420-9.

Skurikhin A. N., (2009). Hierarchal Image Feature Extraction by an Irregular Pyramid of Polygonal Partitions. ASPRS Annual Conference, Baltimore, MD.

Simard, M., Zhang, K., Rivera-Monroy, V.H., Ross, M., Ruiz, P., Castaneda-Moya, E., Rodriguez, E., Twilley, R., (2006). Mapping mangrove height and estimate biomass in the Everglades using SRTM elevation data. *Photogrammetric Engineering and Remote Sensing*, 72 (3):299-311.

Smith S.E., Smith F.A., Jakobsen I. (2003). Mycorrhizal fungi can dominate phosphate supply to plants irrespective of growth responses. *Plant Physiol*.;133:16-20.

Snedkar S. C. & Snedkar J. K. (1984) (Eds.). The Mangrove Ecosystem: Research Methods. Unesco.

Soil Survey Division Staff. (1993). Soil survey manual. Chapter 3, selected chemical properties.". Soil Conservation Service. U.S. Department of Agriculture Handbook 18. Retrieved 2011-03-12.

Soil Survey - Alameda Area, California (1966). United States Department of Agriculture (USDA). Series 1961 No. 41.

Song C., (2013). Optical remote sensing of forest leaf area index and biomass. Progress in *Physical Geography*, vol. 37, 1: pp. 98-113.

Stahl R., Abou Bakr Ramadan A.B., (2011). Qalubeya Drain System / Egypt Environmental Studies on Water Quality. KIT Scientific Publishing.

Storer D.A., (1984). A simple high sample volume procedure for determination of soil organic matter. *Communications in Soil Science and Plant Analysis*.15: 752:759.

Sukardjo S., (1994). Soils in the mangrove Forests of Apar Nature Reserve, Tanah Grogot, East Kalimantan, Indonesia. *Southwest Asian Studies*, Vol.32 (3).

Tam, N. F. Y., and Wong, Y. S., (1998). Variations of soil nutrient and organic matter content in a subtropical mangrove ecosystem. *Water Air Soil Pollut*. 103:245-261.

Thomas, V.; Oliver, R.D.; Lim, K.; Woods, M., (2008). LiDAR and Weibull Modeling of Diameter and Basal Area. *The Forestry Chronicle* 84(6):866–875.

Troeh, F.R., & Thompson, L.M., (2005). Soils and Soil Fertility. 6th Ed. Ames, Iowa: Blackwell Pub.

Upadhyay, V.P, Ranjan, R., Singh, J.S. (2002). Human-mangrove Conflicts: The way out. *Current Science*, Vol 83, No II pp1328-1336.

Valiela, I., J. L. Bowen, and J. K. York. (2001). Mangrove Forests: One of the World's Threatened Major Tropical Environments. *BioScience*. 51(10): 807-815.

Vistro, N. (2010). Manual for Raising Mangrove Container Plants Nurseries and Mangrove Plantations in the United Arab Emirates, *Published by Environmental Research and Wildlife Development Agency - Abu Dhabi (ERWDA)*.

Wannasiri W., Nagai M., Honda K., Santitamnont P., Miphokasap P., (2013). *Extraction of Mangrove Biophysical Parameters Using Airborne LiDAR*. Remote Sensing 04/2013; 5(4):1787-1808. DOI:10.3390/rs5041787.

White, J.C.; Wulder, M.A.; Varhola, A.; Vastaranta, M.; Coops, N.C.; Cook, B.D.; Pitt, D.; Woods, M., (2013). Best Practices Guide for Generating Forest Inventory Attributes from Airborne Laser Scanning Data Using an Area-based Approach. *Natural Resources Canada, Canadian Forest Service, Canadian Wood Fibre Centre, Victoria, BC*.

Wulder, M. A.; White, J.C.; Nelson, R.F.; Næsset, E.; Orka, H.O.; Coops, N.C.; Hilker, T.; Bater, C.W.; Gobakken, T., (2012). Lidar Sampling for Large-area Forest Characterization: a review. *Remote Sensing of Environment* 121:196–209.

Yagoup M. M., Kolan G. R., (2006). Monitoring Coastal Zone Land Use and Land Cover Changes of Abu Dhabi Using Remote Sensing, *Journal of the Indian Society of Remote Sensing*, Vol. 34, No. 1.

Zenner, E.K., Hibbs, D.E., (2000). A new method for modeling the heterogeneity of forest structure. *Forest Ecology and Management,* 129(1):75-87.

Zhao, K., S. C. Popescu, & R.F. Nelson, (2009). Lidar remote sensing of forest biomass: A scale-invariant estimation approach using airborne lasers. *Remote Sensing of Environment* 113(1): 182-196.

Zhao F., Guob Q., Kelly M., (2012). Allometric equation choice impacts lidar-based forest biomass estimates: A case study from the Sierra National Forest, CA. *Agricultural and Forest Meteorology* 165:64-72.